UC Santa Cruz

UC Santa Cruz Previously Published Works

Title

Simultaneous measurements of the $t\bar{t}$, W+W-, and $Z/\gamma^* \rightarrow \tau\tau$ production cross-sections in pp collisions at s=7 TeV with the ATLAS detector

Permalink

https://escholarship.org/uc/item/3qh6w83h

Journal

Physical Review D, 91(5)

ISSN

2470-0010

Authors

Aad, G

Abbott, B

Abdallah, J

et al.

Publication Date

2015-03-01

DOI

10.1103/physrevd.91.052005

Copyright Information

This work is made available under the terms of a Creative Commons Attribution License, available at https://creativecommons.org/licenses/by/4.0/

Peer reviewed

eScholarship.org Powered by the California Digital Library
University of California

Simultaneous measurements of the $t\bar{t}$, W^+W^-, and $Z/\gamma^* \to \tau\tau$ production cross-sections in pp collisions at $\sqrt{s} = 7$ TeV with the ATLAS detector

G. Aad *et al.*[*]
(ATLAS Collaboration)

(Received 2 July 2014; published 6 March 2015)

Simultaneous measurements of the $t\bar{t}$, W^+W^-, and $Z/\gamma^* \to \tau\tau$ production cross-sections using an integrated luminosity of 4.6 fb^{-1} of pp collisions at $\sqrt{s} = 7$ TeV collected by the ATLAS detector at the LHC are presented. Events are selected with two high transverse momentum leptons consisting of an oppositely charged electron and muon pair. The three processes are separated using the distributions of the missing transverse momentum of events with zero and greater than zero jet multiplicities. Measurements of the fiducial cross-section are presented along with results that quantify for the first time the underlying correlations in the predicted and measured cross-sections due to proton parton distribution functions. These results indicate that the correlated next-to-leading-order predictions for $t\bar{t}$ and $Z/\gamma^* \to \tau\tau$ underestimate the data, while those at next-to-next-to-leading-order generally describe the data well. The full cross-sections are measured to be $\sigma(t\bar{t}) = 181.2 \pm 2.8^{+9.7}_{-9.5} \pm 3.3 \pm 3.3$ pb, $\sigma(W^+W^-) = 53.3 \pm 2.7^{+7.3}_{-8.0} \pm 1.0 \pm 0.5$ pb, and $\sigma(Z/\gamma^* \to \tau\tau) = 1174 \pm 24^{+72}_{-87} \pm 21 \pm 9$ pb, where the cited uncertainties are due to statistics, systematic effects, luminosity and the LHC beam energy measurement, respectively. The W^+W^- measurement includes the small contribution from Higgs boson decays, $H \to W^+W^-$.

DOI: 10.1103/PhysRevD.91.052005 PACS numbers: 13.85.Lg, 14.65.Ha, 14.70.Fm, 14.70.Hp

I. INTRODUCTION

Proton collisions at the LHC have large cross-sections for the production of top quark pairs, W boson pairs, and Z bosons. The cross-section for each of these processes is predicted to a high precision within the standard model (SM) of particle physics. In this article, a global test of these SM predictions is presented through the study of a common final state including an oppositely charged electron and muon pair ($e\mu$ events). Specifically, a simultaneous measurement of the cross-sections of the pair production of top quarks ($t\bar{t}$), W bosons (W^+W^-, written as WW), and tau leptons via the Drell-Yan mechanism ($Z/\gamma^* \to \tau\tau$) is performed. These processes are considered in a two-dimensional parameter space spanned by the missing transverse momentum, $E_{\mathrm{T}}^{\mathrm{miss}}$, and jet multiplicity, N_{jets}, where they are naturally well separated, allowing the simultaneous extraction of their cross-sections. Events from $t\bar{t}$ production tend to have large $E_{\mathrm{T}}^{\mathrm{miss}}$ and large N_{jets}, whereas WW events tend to have large $E_{\mathrm{T}}^{\mathrm{miss}}$ and small N_{jets}, and $Z/\gamma^* \to \tau\tau$ events are characterized by small $E_{\mathrm{T}}^{\mathrm{miss}}$ and even smaller N_{jets}.

This analysis of $e\mu$ events allows a broader test of the SM than that given by dedicated cross-section measurements, and provides a first simultaneous measurement of the production cross-sections for the processes of interest at the LHC. This simultaneous measurement unifies the definitions of fiducial region, physics object and event selections, and estimation of uncertainties for each signal measurement. In particular these measurements offer a new window on the effects of the parton distribution functions (PDF) through consideration of the correlations between pairs of production cross-sections, induced by the use of common PDF predictions. An improved understanding of these processes can improve the theoretical calculations and methods used in their study, and thereby more precisely constrain background predictions for future new physics searches at the LHC.

The measurement technique used here was first used by the CDF experiment at the Tevatron [1] using the $p\bar{p}$ collision data at a center-of-mass energy, $\sqrt{s}$, of 1.96 TeV. In this paper the results are obtained from $\sqrt{s} = 7$ TeV pp collision data collected by the ATLAS detector [2] at the LHC corresponding to an integrated luminosity of 4.6 fb^{-1} [3]. Furthermore the measurement of WW includes the small contribution from Higgs boson decays, $H \to W^+W^-$. Previous dedicated measurements of these cross-sections in the dilepton channel were performed by ATLAS using data samples of 4.6 fb^{-1} for $t\bar{t}$ [4] and WW [5], and 36 pb^{-1} for $Z/\gamma^* \to \tau\tau$ [6]. Other dedicated measurements in the dilepton channel were also performed by the CMS collaboration, namely for $t\bar{t}$ using 2.3 fb^{-1} [7], for WW using 4.9 fb^{-1} [8], and for $Z/\gamma^* \to \tau\tau$ [9] using 36 pb^{-1}.

[*]Full author list given at the end of the article.

Published by the American Physical Society under the terms of the Creative Commons Attribution 3.0 License. Further distribution of this work must maintain attribution to the author(s) and the published articles title, journal citation, and DOI.

 © 2015 CERN, for the ATLAS Collaboration

This paper is organized as follows. Section II provides an overview of the ATLAS detector. Section III describes the data sample and summarizes the Monte Carlo simulation used for the key SM processes relevant to this study, while Sec. IV details the reconstruction of the final-state objects, the $e\mu$ event selection, as well as the full definition of the $E_{\mathrm{T}}^{\mathrm{miss}}$–$N_{\mathrm{jets}}$ parameter space. Section V covers the data-driven estimation of backgrounds from misidentified and nonprompt leptons. The template fitting method used to extract the results is discussed in Sec. VI along with the treatment and evaluation of systematic uncertainties. Results obtained for the cross-sections of the three processes of interest are presented and compared to predictions and other measurements in Sec. VII, and conclusions are presented in Sec. VIII.

II. THE ATLAS DETECTOR

ATLAS [2] is a multipurpose particle physics detector with forward-backward symmetric cylindrical geometry. The inner detector (ID) system is immersed in a 2 T axial magnetic field and provides tracking information for charged particles in the pseudorapidity range $|\eta| < 2.5$ [10]. It consists of a silicon pixel detector, a silicon microstrip detector, and a transition radiation tracker (TRT).

The calorimeter system covers the range $|\eta| < 4.9$. The highly segmented electromagnetic calorimeter consists of lead absorbers with liquid argon (LAr) as active material and covers the range $|\eta| < 3.2$. In the region $|\eta| < 1.8$, a presampler detector using a thin layer of LAr is used to correct for the energy lost by electrons and photons upstream of the calorimeter. The hadronic tile calorimeter is a steel/scintillator-tile detector and is situated directly outside of the electromagnetic calorimeter. The barrel section of this sampling calorimeter provides a coverage of $|\eta| < 1.7$. The endcap hadronic calorimeters have LAr as the active material and copper absorbers covering the range $1.5 < |\eta| < 3.2$. They cover the region between the barrel and the forward calorimeter with a small overlap with each of them. The forward calorimeter uses LAr as active material and copper and tungsten as absorber materials. It extends the calorimeter coverage out to $|\eta| = 4.9$.

The muon spectrometer (MS) measures the deflection of muons in the magnetic field produced by the large superconducting air-core toroid magnets. It covers the range $|\eta| < 2.7$ and is instrumented with separate trigger and high-precision tracking chambers. A precision measurement of the track coordinates in the bending direction of the toroidal magnetic field is provided by drift tubes in the range $|\eta| < 2.7$. Within the region $2.0 < |\eta| < 2.7$, cathode strip chambers with higher granularity are used in the innermost tracking layer. The muon trigger system, which covers the range $|\eta| < 2.4$, consists of resistive plate chambers in the barrel ($|\eta| < 1.05$) and thin gap chambers in the endcap regions ($1.05 < |\eta| < 2.4$).

A three-level trigger system is used to select events for offline analysis. The level-one trigger is implemented in hardware and uses a subset of the detector information to reduce the event rate to its design value of at most 75 kHz. This is followed by two software-based trigger levels, level two and the event filter, which together reduce the event rate to an average of 400 Hz during the 2011 data-taking period.

III. DATA AND MONTE CARLO SAMPLES

The data sample used in this measurement consists of proton-proton collision events at a center-of-mass energy $\sqrt{s} = 7$ TeV recorded by ATLAS in 2011. Only data collected during stable beam conditions and with the relevant ATLAS subsystems being operational are used. In particular, the inner detector, the electromagnetic and hadronic calorimeters, and the muon spectrometer must deliver data of high quality to ensure that electrons, muons, jets, and missing transverse momentum are measured accurately. The data selected for this study were collected using single-lepton triggers (e or μ). In the case of the electron trigger, a threshold is applied to the transverse energy (E_{T}) of the electron while for the muon trigger a threshold is applied to the transverse momentum (p_{T}) of the muon. Due to the increases in luminosity achieved by the LHC during the 2011 run, the value of the electron E_{T} threshold applied changed during the course of the year. Thresholds employed by the electron trigger were either 20 or 22 GeV while the muon trigger threshold remained constant at 18 GeV. The data collected correspond to an integrated luminosity of 4.6 fb^{-1}, after applying data quality requirements, with an uncertainty of 1.8% [3].

Monte Carlo simulated events are generated at $\sqrt{s} =$ 7 TeV and processed through a detector simulation [11] based on GEANT4 [12]. In these samples, all particle masses are taken from 2010 values published by the Particle Data Group [13] with the exception of the top quark mass, which is taken to be 172.5 GeV and the Higgs boson mass which is set to 125 GeV. The simulation includes modeling of additional pp interactions in the same and neighboring bunch crossings, referred to as pileup. These events are subsequently reweighted such that the distribution of the number of interactions per bunch crossing in simulation matches that of data. Corrections to the selection efficiency of electrons and muons are applied to simulated events, and the detector simulation is tuned to reproduce the energy and momentum measurements and resolution observed in data.

Unless otherwise specified, common attributes between the Monte Carlo samples are the generation of the underlying event (UE), which is performed by PYTHIA v. 6.425 [14] or JIMMY v. 4.31 [15] (included as part of the HERWIG v. 6.520 [16] software package), and the choice of PDFs, which is the next-to-leading-order (NLO) CT10 set [17]. An exception is the ALPGEN [18] generator configurations which use the leading-order set CTEQ6L1 [19].

The cross-sections for the different processes obtained from a range of event generators are always normalized to the best available theoretical calculations, as discussed below.

A. $t\bar{t}$ production

Simulation of $t\bar{t}$ production is performed using the NLO generator MC@NLO v4.01 [20] interfaced to HERWIG and JIMMY. The $t\bar{t}$ cross-section has been calculated at next-to-next-to-leading-order (NNLO) in QCD, including resummations of next-to-next-to-leading logarithmic soft gluon terms with TOP++2.0 [21–26]. The resulting cross-section is calculated to be $\sigma_{t\bar{t}} = 177^{+10}_{-11}$ pb for a top quark mass of 172.5 GeV [27]. The uncertainty due to the choice of PDF and α_s is calculated using the PDF4LHC prescription [28] that includes the MSTW2008 68% C.L. NNLO [29,30], CT10 NNLO [17,31] and NNPDF2.3 5f FFN [32] PDF sets. This is added in quadrature to the scale uncertainty.

Additional samples are provided using POWHEG [33] version powheg-hvq4 interfaced to the PYTHIA and HERWIG parton shower (PS) generators, to compare PS and fragmentation models, and to assign a generator modeling uncertainty.

To estimate uncertainties due to modeling of QCD initial- (ISR) and final-state radiation (FSR) in the $t\bar{t}$ system (discussed in Sec. VI), ALPGEN interfaced to the PYTHIA PS generator is used. The uncertainty is evaluated using two different generator tunes with increased or reduced rates of QCD radiation.

B. WW production

The simulation of WW signal production is based on samples of $q\bar{q} \to WW$, $gg \to WW$ and $gg \to H \to WW$ events, which are generated with MC@NLO, GG2WW [34], and POWHEG respectively. The Higgs resonance sample is interfaced to PYTHIA and the nonresonant samples are interfaced to HERWIG. A combined WW sample is formed from cross-section weighted contributions, where cross-sections of $44.7^{+2.1}_{-1.9}$ pb, $1.3^{+0.8}_{-0.5}$ pb and 3.3 ± 0.3 pb are assumed for $q\bar{q} \to WW$, $gg \to WW$ and $gg \to H \to WW$, respectively [35,36].

Alternative WW samples are produced with the POWHEG generator interfaced to PYTHIA and HERWIG PS generators for comparison of PS and fragmentation models and to assess a generator modeling uncertainty. ALPGEN samples are used to estimate uncertainties due to modeling of additional QCD radiation.

C. Drell-Yan lepton pair production

The only Drell-Yan process whose final states include a prompt e and μ is the production of a pair of tau leptons. For $Z/\gamma^* \to \tau\tau$, the SHERPA v. 1.4.0 [37] generator is used. SHERPA handles the full generation of the event, including a fixed-order matrix element calculation, parton showering, hadronization, and underlying event. The cross-section for inclusive Z/γ^* production is calculated at NNLO in FEWZ [38] with MSTW2008 NNLO PDFs to be $\sigma^{Z/\gamma^* \to \tau\tau}_{\mathrm{NNLO}} = 1070 \pm 54$ pb. This calculation is performed for $m_{\tau\tau} > 40$ GeV, and includes contributions from $\gamma^* \to \tau\tau$.

D. Single top quark production

The associated production of a single top quark and a W boson, referred to as the Wt channel, is simulated with MC@NLO interfaced to HERWIG and JIMMY. Single top production through the s and t channels is not considered here, since only the Wt channel is a source of prompt $e\mu$ pairs. These are considered a background in the analysis. During event generation a diagram removal scheme is implemented [39,40] to remove overlaps between the single top and $t\bar{t}$ final states. The cross-section for the Wt channel calculated at approximate NNLO is $\sigma^{Wt}_{\mathrm{theory}} = 15.7 \pm 1.1$ pb [41].

E. WZ and ZZ production

In the analysis, prompt $e\mu$ events originating from diboson samples, such as WZ and ZZ, are considered part of the background. These are generated with ALPGEN interfaced to HERWIG and JIMMY. The NLO cross-sections for these processes are calculated with MCFM v5.8 [42] with MSTW2008 NLO PDFs [29], and found to be $\sigma^{WZ}_{\mathrm{NLO}} = 17.8 \pm 1.3$ pb and $\sigma^{ZZ}_{\mathrm{NLO}} = 5.9 \pm 0.3$ pb for $m_Z > 60$ GeV.

IV. OBJECT AND EVENT SELECTION

The high-precision tracking of the ATLAS ID provides efficient reconstruction of multiple inelastic pp collisions that take place in a single bunch crossing. The primary vertex is selected as the one with the largest sum of squared transverse momenta of associated ID tracks. Contamination due to poorly reconstructed vertices is reduced by requiring that the primary vertex has at least five associated tracks with $p_{\mathrm{T}} > 0.4$ GeV.

Electron candidates are formed by an electromagnetic energy cluster with an associated track in the ID. They must fulfil $|\eta| < 2.47$ with an exception of $1.37 < |\eta| < 1.52$ to exclude the transition region between the barrel and end-caps of the calorimeter. The candidates are required to have a transverse energy of $E_{\mathrm{T}} > 25$ GeV and meet the tight selection criteria [43] optimized for the 2011 data-taking period. These criteria are based on the quality of the position and momentum association between the extrapolated track and the calorimeter energy cluster, the consistency of the longitudinal and lateral shower profiles with those expected for an incident electron, and the observed transition radiation in the TRT. To suppress background from photon conversions, the electron track is required to have a hit in the innermost layer of the tracking system.

Muon candidates are reconstructed by combining the information from pairs of stand-alone ID and MS tracks to form a single track [44,45]. The candidates are required to have $p_{\mathrm{T}} > 20$ GeV and be located within the central region of the detector ($|\eta| < 2.5$).

The longitudinal impact parameter of each lepton with respect to the primary vertex is required to be less than 2 mm in order to suppress the nonprompt production of leptons. To suppress the contribution from hadronic jets misidentified as leptons, electron and muon candidates are required to be isolated in both the ID and the calorimeter. Specifically, two measures of isolation are used: the sum of transverse energies of all calorimeter energy cells around the lepton but not associated with the lepton within a cone of size $\Delta R \equiv \sqrt{(\Delta\phi)^2 + (\Delta\eta)^2} = 0.2$, denoted $E_{\mathrm{T}}^{\mathrm{cone20}}$, and the scalar sum of the transverse momenta of all tracks with $p_{\mathrm{T}} > 1$ GeV that originate from the primary vertex and are within a cone of size $\Delta R = 0.3$ around the lepton track, denoted $p_{\mathrm{T}}^{\mathrm{cone30}}$. For electrons the maximum allowed values for $E_{\mathrm{T}}^{\mathrm{cone20}}$ and $p_{\mathrm{T}}^{\mathrm{cone30}}$ are chosen as a function of the cluster η so that the efficiency for the requirement measured in a $Z \to ee$ control sample is 90% across the detector. These values are also adjusted to account for pileup conditions and energy leakage from the calorimeter. The isolation requirement applied to the muons, $E_{\mathrm{T}}^{\mathrm{cone20}} <$ 4 GeV and $p_{\mathrm{T}}^{\mathrm{cone30}} < 2.5$ GeV, has an overall efficiency of 96% determined using a $Z \to \mu\mu$ control sample. The combination of cone sizes and efficiency working points was studied and optimized to find a requirement that reduces dependence on the pileup conditions of the event.

Jets are reconstructed using the anti-k_t algorithm [46] with a radius parameter of $R = 0.4$. The inputs to the jet algorithm are topological clusters of calorimeter cells. These topological clusters are seeded by calorimeter cells with energy $|E_{\mathrm{cell}}| > 4\sigma$, where σ is the cell-by-cell RMS of the noise (electronics plus pileup). Neighboring cells are added if $|E_{\mathrm{cell}}| > 2\sigma$ and topological clusters are formed through an iterative procedure. In a final step, all remaining neighboring cells are added to the topological cluster. The baseline calibration for these topological clusters calculates their energy using the electromagnetic energy scale [47]. This is established using test-beam measurements for electrons and muons in the electromagnetic and hadronic calorimeters [48,49]. Effects due to noncompensation, energy losses in the dead material, shower leakage, as well as inefficiencies in energy clustering and jet reconstruction are also taken into account. This is done by associating calorimeter jets with simulated jets in bins of η and E, and is supplemented by an *in situ* calibration. This jet energy scale calibration is thoroughly discussed in Ref. [50].

To count a jet in the context of this analysis, it needs to fulfil the following kinematic requirements: $p_{\mathrm{T}} > 30$ GeV and $|\eta| < 2.5$. A cut on the jet vertex fraction (JVF) is applied to minimize the number of jets originating from pileup. The JVF is defined as the ratio of the sum of the p_{T} of charged particle tracks that are associated with both the jet and the primary vertex, to the sum of the p_{T} of all tracks belonging to the jet. Its value must be greater than 75%.

To further remove nonprompt leptons that are likely to have originated from heavy-quark decays, leptons within a distance of $\Delta R = 0.4$ from a reconstructed jet with $p_{\mathrm{T}} >$ 25 GeV and JVF > 0.75 are vetoed.

The second discriminating variable of the parameter space is the imbalance of the transverse momentum measured in each event due to the presence of neutrinos. The reconstruction of the direction and magnitude ($E_{\mathrm{T}}^{\mathrm{miss}}$) of the missing transverse momentum vector is described in Ref. [51]. It is calculated from the vector sum of the transverse momenta of all jets with $p_{\mathrm{T}} > 20$ GeV and $|\eta| < 4.5$, the transverse momenta of electron and muon candidates, and finally from all calorimeter energy clusters not belonging to a reconstructed object.

Events are required to contain exactly one selected electron and one selected muon of opposite charge. Events with an electron and muon of same-sign charge are used as a control sample for background studies. Some properties of the electrons, muons, and jets belonging to events that satisfy the criteria described in this section are shown in Figs. 1 and 2, where signal and background prompt processes are normalized to theory predictions and the fake and nonprompt backgrounds are obtained as described in Sec. V. The data and simulation agree within the uncertainties associated with the theoretical predictions.

V. BACKGROUND ESTIMATED FROM DATA

Background contributions that include events where one or both of the leptons are fake or nonprompt are challenging to model with Monte Carlo simulation. These events include a lepton from a heavy-flavor quark decay, a jet misidentified as a lepton, or an electron from a photon conversion. These background contributions are difficult to estimate from simulation due to the potential mismodeling and limited knowledge of the relative composition of the background. Additionally, the probability of accepting an event is small enough that the statistical uncertainty on the simulated sample becomes a serious concern. The analysis therefore relies on auxiliary measurements in data to obtain a robust estimate of background contributions shown in Table I, using the matrix method described in Ref. [52].

A. Matrix method

The matrix method utilizes data where the standard object selection requirements (referred to as tight criteria; see Sec. IV) on either electron or muon or both candidates are relaxed (referred to as loose criteria). The premise of this approach is that lepton candidates satisfying looser requirements have a higher chance of being fake or nonprompt than those satisfying tight requirements. This information

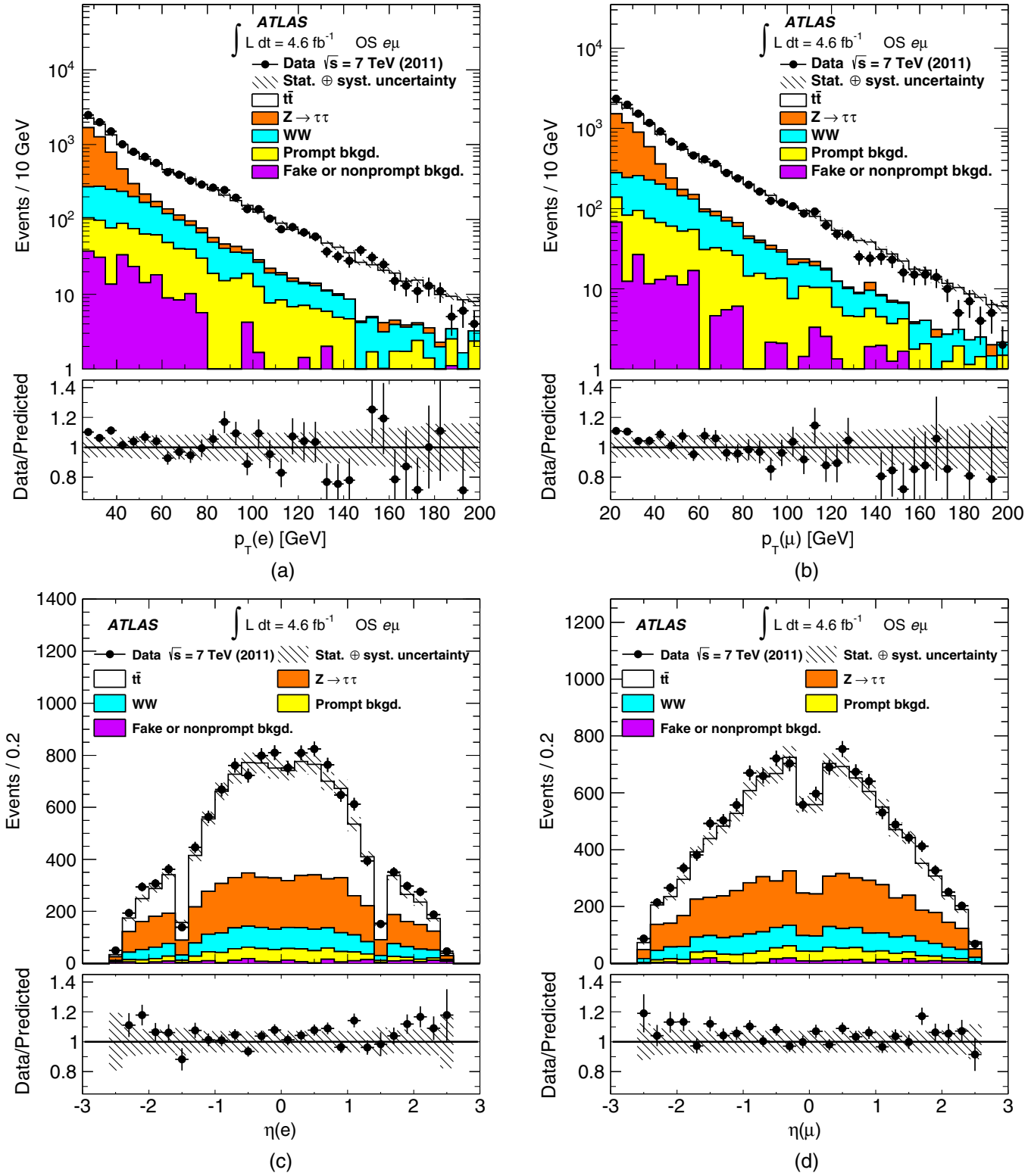

FIG. 1 (color online). Comparison between data and Monte Carlo samples (including the data-driven fake described in Sec. V and nonprompt backgrounds described in Sec. III) normalized to their theoretical cross-sections for an integrated luminosity of 4.6 fb^{-1}: (a) electron and (b) muon candidate p_T distributions and, (c) and (d), their respective η distributions for events producing one electron and one muon of opposite-sign (OS) charge. The electron and muon satisfy the signal region selection criteria presented in Sec. IV. A bin by bin ratio between the data and simulated events is shown at the bottom of each comparison. The hatched regions represent the combination of statistical and systematic uncertainties as listed in Table II (except for shape uncertainties) and described in Sec. VI together with the full theoretical cross-section uncertainties for the $t\bar{t}$, WW, and $Z/\gamma^* \to \tau\tau$ signal processes.

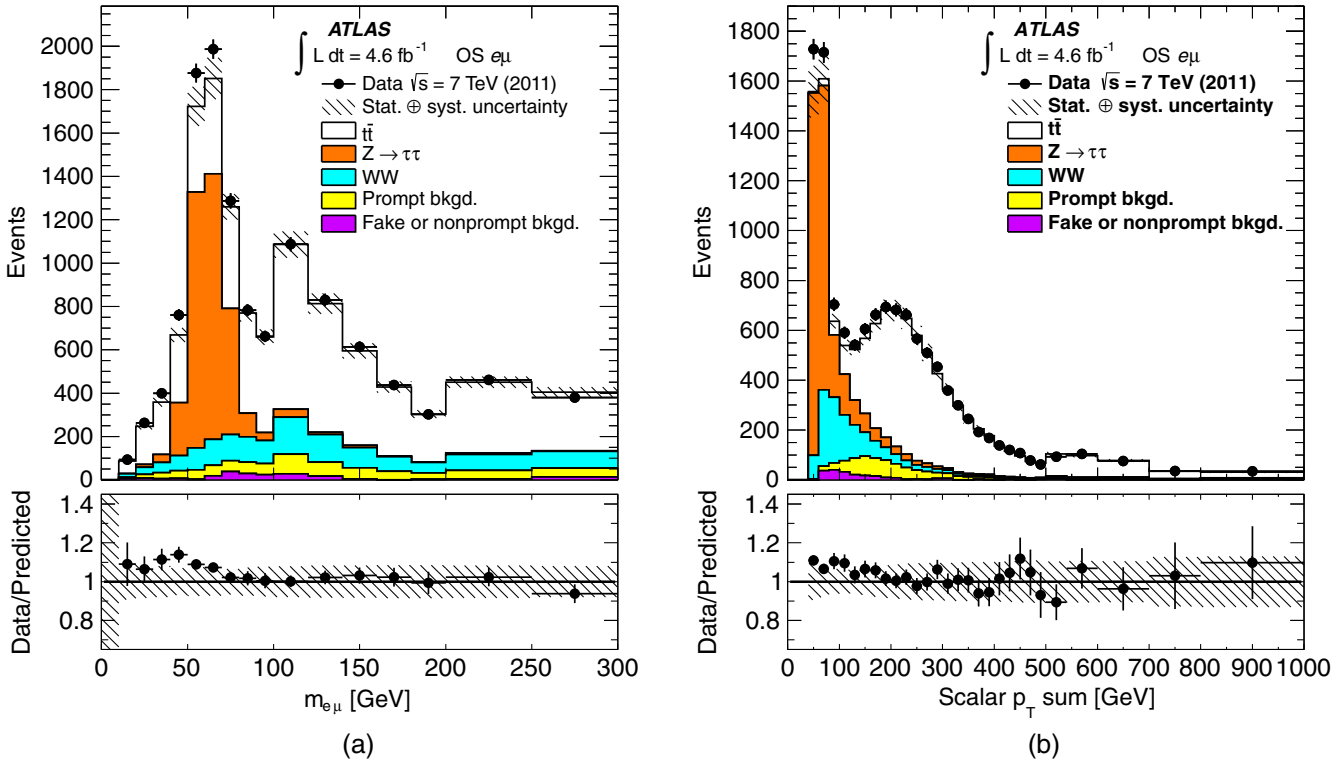

FIG. 2 (color online). Comparison between data and Monte Carlo samples (including the data-driven fake described in Sec. V and nonprompt backgrounds described in Sec. III) normalized to their theoretical cross-sections for an integrated luminosity of 4.6 fb^{-1}: (a) invariant mass distribution of electron and muon pairs and (b) distribution of the scalar sum of the transverse momenta of the selected electron, muon and jets. The electron and muon of OS charge satisfy the signal region selection criteria presented in Sec. IV. A bin by bin ratio between the data and simulated events is shown at the bottom of each comparison. The hatched regions represent the combination of statistical and systematic uncertainties as listed in Table II (except for shape uncertainties) and described in Sec. VI together with the full theoretical cross-section uncertainties for the $t\bar{t}$, WW, and $Z/\gamma^* \to \tau\tau$ signal processes.

combined with inputs of the probability that a real lepton or fake or nonprompt lepton meeting the loose criteria also satisfies the tight criteria is used to arrive at a background estimate. For loose electrons, the isolation requirements are dropped, and electron identification criteria as defined in Ref. [43] are used, where the requirements on particle identification in the TRT and on the calorimeter energy to track momentum ratio E/p are relaxed. For loose muons, the isolation requirements are dropped.

For a given selected event, the matrix method, by solving a set of linear equations, implements a change of basis from observed data regions into event categories. The data regions comprise the signal region that is defined by a tight electron and a tight muon, denoted "TT"; and control regions, containing events that produce a tight electron and a loose and not tight muon, denoted "TL"; a loose and not tight electron and a tight muon, denoted "LT"; and a loose and not tight electron and a loose and not tight muon, denoted "LL". Event categories are denoted "RR," "RF," "FR" and "FF," where "R" refers to a true prompt electron or muon, and "F" refers to a fake or nonprompt electron or muon.

For a given event in a data region, the array **w** contains the weights assigned to the event in question and specifies to which category the event belongs. This array is made up of four components, denoted w_{RR}, w_{FR}, w_{RF} and w_{FF} and is calculated as

$$\begin{pmatrix} w_{\mathrm{RR}} \\ w_{\mathrm{RF}} \\ w_{\mathrm{FR}} \\ w_{\mathrm{FF}} \end{pmatrix} = \mathcal{M}^{-1} \begin{pmatrix} \delta_{\mathrm{TT}} \\ \delta_{\mathrm{TL}} \\ \delta_{\mathrm{LT}} \\ \delta_{\mathrm{LL}} \end{pmatrix}, \tag{1}$$

where δ equals unity when the event falls in the given signal or control region, and zero otherwise. The matrix $\mathcal{M}$ is written in terms of $r_{e(\mu)}$, the probability for a real loose electron (muon) to meet the tight criteria, and $f_{e(\mu)}$, the probability for a fake or nonprompt loose electron (muon) to meet the tight criteria, and is calculated as

$$\mathcal{M} = \begin{pmatrix} r_e r_\mu & r_e f_\mu & f_e r_\mu & f_e f_\mu \\ r_e \bar{r}_\mu & r_e \bar{f}_\mu & f_e \bar{r}_\mu & f_e \bar{r}_\mu \\ \bar{r}_e r_\mu & \bar{r}_e f_\mu & \bar{f}_e r_\mu & \bar{f}_e f_\mu \\ \bar{r}_e \bar{r}_\mu & \bar{r}_e \bar{f}_\mu & \bar{f}_e \bar{r}_\mu & \bar{f}_e \bar{f}_\mu \end{pmatrix}, \tag{2}$$

TABLE I. Fake or nonprompt background estimates in the OS and SS electron-muon samples. Overall data yields are given for the control (LL, LT and TL) and signal (TT) regions, together with the estimates of the backgrounds ($\sum^{\text{Bins}}\sum^{\text{Events}} W$). The events from the control regions are used to produce the background estimate after applying the appropriate weights from Eq. (3). Backgrounds are shown with their statistical, electron-related, and muon-related systematic uncertainties.

Region	Event yields	
	OS	SS
LL	3560	1623
LT	4744	896
TL	1137	499
TT	12224	407
	Estimated fake or nonprompt background	
$\sum^{\text{Bins}}\sum^{\text{Events}} W$	$210 \pm 20 \pm 150 \pm 50$	$240 \pm 10 \pm 120 \pm 10$

where $\bar{x} \equiv 1 - x$ for $x = f$ or r. Given that the matrix method probabilities, as detailed later, are parametrized as a function of event characteristics such as lepton kinematics and the number of jets, **w** is calculated on an event-by-event basis, allowing an improved determination of the background, and therefore the matrix method as described here is a generalization of that presented in Ref. [52]. The estimated background contribution to the signal region due to a given event is given by

$$W = r_e f_\mu w_{\text{RF}} + f_e r_\mu w_{\text{FR}} + f_e f_\mu w_{\text{FF}}. \quad (3)$$

The background in a given $E_{\text{T}}^{\text{miss}}$–$N_{\text{jets}}$ bin is given by the sum of W over all events in that bin. The respective event yields in the opposite-sign and same-sign lepton samples, are shown separately in Table I for the various classes of events used in the matrix method, together with the results, expressed as estimated fake or nonprompt background yields in the two samples, integrated over $E_{\text{T}}^{\text{miss}}$ and N_{jets}.

B. Measurement of matrix method probabilities

The probabilities r_μ for real muons and r_e for real electrons which pass both the loose and tight selection cuts are determined with high-purity samples of $Z \to \mu\mu$ and $Z \to ee$ decays, respectively, using a tag and probe method.

The values of r_μ are measured as a function of muon η and jet multiplicity and vary from 0.94 to 0.97. The values of r_e are measured as a function of electron η and p_{T} for events without jets, and also as a function of the angular distance ΔR between the electron and nearest jet otherwise. For events containing two or more jets, r_e is corrected to better match the expected efficiency in $t\bar{t}$ events. The correction is calculated from comparisons of $t\bar{t}$ and $Z \to ee$ simulated events. The complexity of parametrization for the electrons with respect to muons is due to the greater sensitivity of electron identification to jet activity. The values of r_e vary from 0.77 to 0.81 from lowest to highest electron p_{T}, from 0.75 to 0.81 from low to high $|\eta|$, and from 0.70 to 0.81 from low to high ΔR separation between the electron and the nearest jet. Uncertainties on r_e (1%–2%) and r_μ (1%–4%) reflect both statistics and variations observed in their determination derived from changes in the modeling of signal and background components in $Z \to ee$ and $Z \to \mu\mu$ invariant mass distributions.

The probabilities for jets to be misidentified as muons or for nonprompt muons, f_μ, are measured in a data sample dominated by multijet events selected by requiring low $E_{\text{T}}^{\text{miss}}$. The measurement method employs fits to the transverse impact parameter significance distribution of the candidate muon to disentangle the fake or nonprompt component. Over the muon range $|\eta| < 2.5$, f_μ varies from 0.13 to 0.18 and shows less variation with the number of jets, only shifting by about 0.02 within any particular η bin. An uncertainty on f_μ is assigned based on the difference with measurements made using an alternative method, in which specific selection criteria are relied upon to provide a pure sample of muon candidates from fake or nonprompt sources. Measured as a function of muon η and the p_{T} of the jet with the highest p_{T}, f_μ varies from 0.18 to 0.28. The difference in predicted net background yield from these two f_μ measurements is taken as the uncertainty on the background estimate, which amounts to about 24%.

The probabilities for jets to be misidentified as electrons or for nonprompt electrons, f_e, are determined in samples dominated by multijet events and parametrized in the same way as r_e. In order to assign a central value and uncertainty for f_e, separate criteria are imposed on the multijet events, to enhance the presence of either fake electrons from jets or electrons from photon conversions in light-flavor quark jets, yielding $f_e^{\text{jets}} \approx 0.15$ and $f_e^{\text{conv}} \approx 0.30$, respectively. From data samples enriched in light or heavy quark (b or c) jets, it is found that the probability f_e is very similar between the two categories. As the relative composition of fake or nonprompt electrons is not known *a priori*, a simple average of f_e^{jets} and f_e^{conv} is performed in each p_{T} and η bin to give the f_e values. The uncertainty in each bin is determined as half of the difference between f_e^{jets} and f_e^{conv}. In the opposite-sign signal region, the contribution from electrons and muons with mismeasured charge in the inner detector is estimated to be very small and is not accounted for in this analysis.

C. Validation of background estimate

The estimate of the background in the signal region was validated using an event sample defined by selection criteria that are the same as those just described, with the exception that a same-sign (SS) $e\mu$ pair is required. Figure 3 shows the jet multiplicity and $E_{\text{T}}^{\text{miss}}$ distributions in

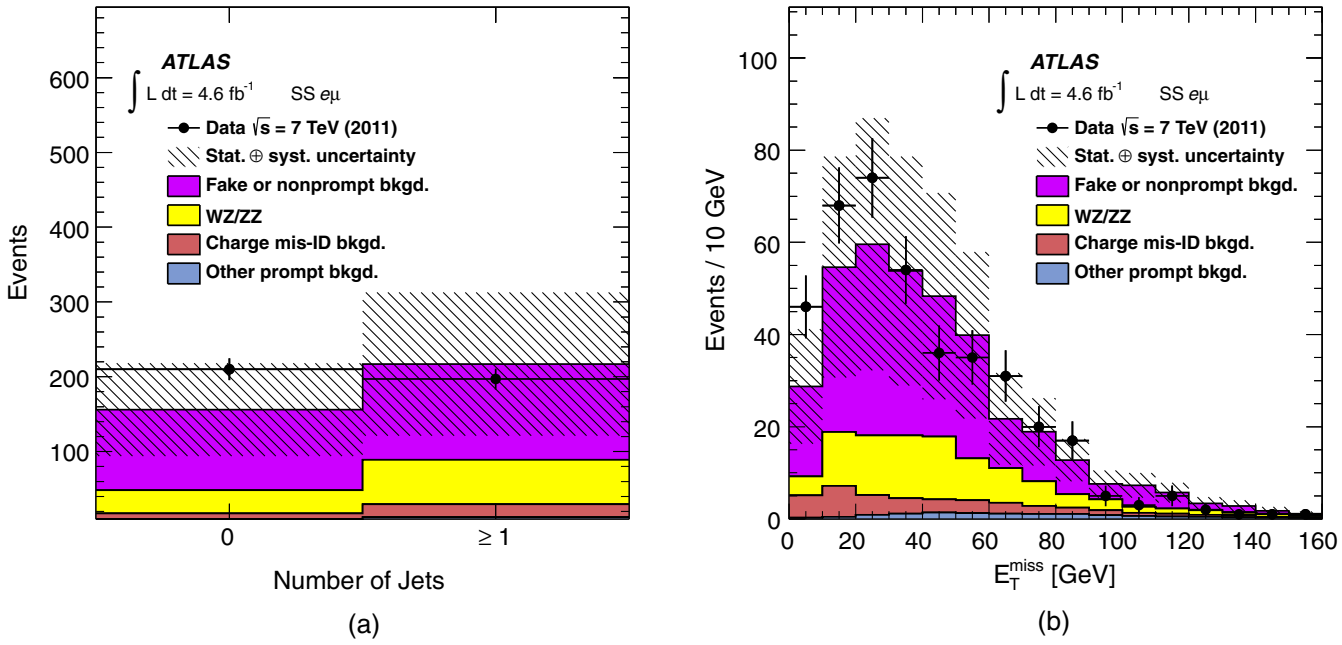

FIG. 3 (color online). (a) Jet multiplicity spectrum and (b) missing transverse momentum spectrum for events producing one electron and one muon of SS charge. The electron and muon candidates and events fulfil the same selection criteria required on the OS charge sample. The hatched regions represent the combination of statistical uncertainty and rate uncertainties on the fake or nonprompt background, as well as uncertainties on the acceptance, efficiency, theoretical cross-sections, and modeling of the processes. The other prompt lepton background category includes contributions from $t\bar{t}W$, $t\bar{t}Z$, and same-sign $W^{\pm}W^{\pm}jj$ processes.

the SS data sample. This sample is dominated by fake and nonprompt lepton events along with a contribution of prompt leptons from WZ and ZZ, and also small contributions from $t\bar{t}W$, $t\bar{t}Z$, and same-sign $W^{\pm}W^{\pm}jj$ processes, which are collectively denoted as "other prompt bkgd." in Fig. 3. Opposite-sign events where electron charge is misidentified, predominantly because of bremsstrahlung in the ID material followed by photon conversion, provide a significant contribution. This same-sign sample is expected to marginally differ in the exact composition of fake or nonprompt leptons from that of the OS sample. For example, the $W + c$ process preferentially yields a nonprompt lepton with opposite charge to that of the prompt lepton from the W decay.

A closure test of the matrix method was performed using a collection of simulated samples for processes that could contribute to this background category in the opposite-charge $e\mu$ final state. This included $W/Z +$ jets (including heavy flavor), $W\gamma +$ jets, top- or W-pair production where at least one of the W bosons decays hadronically, Drell-Yan τ-pair production where one τ decays hadronically, and s- and t-channel single top production. Probabilities were measured using generator-level information in simulated samples of $Z +$ jets and multijet production. The results of calculating the background contribution using the matrix method were compared to those derived from generator-level information and were found to agree within uncertainties.

D. Results

Table I lists event yields from data in the signal and control regions and the resulting estimation and associated uncertainty of the fake or nonprompt background in both the OS and the SS sample. Signal processes that dominate the OS sample are absent in the SS sample, and the contribution of fake or nonprompt leptons is dominant in the SS event yield as noted previously. The estimated background in the OS (SS) signal region is 210 ± 160 (240 ± 120) events, where the uncertainty is derived from alternative estimates of the background made by varying the electron input probabilities by their associated errors, as well as using muon input probability estimates from the alternative measurement method. An N_{jets} versus $E_{\text{T}}^{\text{miss}}$ distribution is made for each configuration of matrix method probabilities and later used as input in the likelihood fit in order to assign systematic uncertainties on the signal yields returned in the default fit.

VI. FIT METHOD AND UNCERTAINTIES

Templates in the $E_{\text{T}}^{\text{miss}}$–$N_{\text{jets}}$ parameter space are produced for signal processes ($t\bar{t}$, WW, $Z/\gamma^{*} \to \tau\tau$) and backgrounds ($Wt$, WZ/ZZ, fake and nonprompt) by applying the object and event selection described above. These templates are employed in a fit to data. The parameter space is divided into two bins of jet multiplicity, $N_{\text{jets}} = 0$ and $N_{\text{jets}} \geq 1$, counting reconstructed jets with

$p_T \geq 30$ GeV. The E_T^{miss} distribution is divided into twenty bins from $0 < E_T^{miss} < 200$ GeV in increments of 10 GeV, with the bins bordering 200 GeV also containing the overflow of events with $E_T^{miss} \geq 200$ GeV. Studies using simulated samples found the choices of two jet multiplicity bins and of a jet threshold $p_T \geq 30$ GeV to be optimal in terms of minimizing statistical and systematic uncertainties, such as those arising from jet energy scale effects and $t\bar{t}$ modeling.

Normalized templates for signal and background components are used to construct a binned likelihood function that is maximized in the fit to data. The normalization parameters of the $t\bar{t}$, WW and $Z/\gamma^* \to \tau\tau$ templates are treated as free parameters in the fit, whereas the normalization parameters of the Wt and WZ/ZZ templates are constrained to their expected values. The template for background involving at least one fake or nonprompt lepton candidate is constrained to the estimate derived from data as described previously in Sec. V. The templates for $t\bar{t}$ and WW include electrons and muons from tau-lepton decays.

The fiducial region in this analysis is defined by particle level quantities chosen to be similar to the selection criteria used in the fully reconstructed sample. Electrons must have transverse energy $E_T > 25$ GeV and pseudorapidity $|\eta| < 2.47$, excluding the transition region $1.37 < |\eta| < 1.52$. Muons are required to have transverse momentum $p_T > 20$ GeV and pseudorapidity $|\eta| < 2.5$. All selected electron or muon particles must originate from a W boson decay from the hard scattering process, or from tau-lepton decays that themselves are from a W boson or Z boson decay. A further correction applied to leptons, to include the momenta contribution of photons from narrow-angle QED FSR, is the addition of the momenta of all photons within a cone of $\Delta R = 0.1$ around the lepton to its momentum.

Fitted event yields are used to extract fiducial and full cross-sections for the signal processes. The former is desirable because it is a quantity that is closer to what is measured by the detector and does not suffer from theoretical extrapolation errors. The two cross-sections are calculated as

$$\sigma_X^{fid} = \frac{N_X^{fid}}{\mathcal{C} \cdot \mathcal{L}}, \tag{4}$$

$$\sigma_X^{tot} = \frac{N_X^{tot}}{\mathcal{A} \cdot \mathcal{C} \cdot B(X \to e\mu + Y) \cdot \mathcal{L}} \tag{5}$$

respectively, where $\mathcal{L}$ corresponds to the integrated luminosity of the data sample; $\mathcal{A}$ is the kinematic and geometric acceptance of the fiducial region as a fraction of the complete phase space; $\mathcal{C}$ is the ratio of the number of events fulfilling the offline selection criteria to the number of events produced in the fiducial region estimated from simulation; N_X^{tot} (N_X^{fid}) is the number of events attributed to the specified process by the fit using systematic uncertainties that affect $\mathcal{A} \cdot \mathcal{C}$ ($\mathcal{C}$ only); and $B(X \to e\mu + Y)$ is the branching fraction to inclusive $e\mu$ final states for the decay channel under consideration taking into account the branching fractions of tau-lepton decays to electrons and muons.

Systematic uncertainties are estimated by examining their effects on the nominal templates. These effects are broadly broken up into two categories, those affecting normalization and those affecting the shape of predicted templates, which are calculated using Monte Carlo pseudoexperiments. Each source of uncertainty considered may affect both template normalization and shape, with the exception of integrated luminosity and LHC beam energy uncertainties, which affect only template normalization. Uncertainties associated with the fake or nonprompt background and parton distribution function modeling are handled differently as special cases, described in detail below. The dominant sources of systematic uncertainties are listed in Table II for the signal processes. For background templates, most of the uncertainties listed in Table II are applied with the exception of Monte Carlo model uncertainties, LHC beam energy, and PDF uncertainties.

A. Template normalization uncertainties

Systematic uncertainties affecting the acceptance, efficiency and background cross-sections are incorporated as Gaussian constrained parameters in the likelihood function. The Gaussian probability distributions for each systematic uncertainty parameter multiply the likelihood, thus profiling the uncertainty. These terms penalize the likelihood if the parameters move away from their nominal values during the minimization procedure.

B. Template shape uncertainties

Monte Carlo pseudoexperiments are performed to estimate uncertainties on event yields due to systematic uncertainties affecting template shapes. For a given source of systematic uncertainty, S, sets of modified E_T^{miss}–N_{jets} signal and background templates are produced in which S is varied up and down by its expected uncertainty, while the template normalization remains fixed to its assumed standard model expectation. Pseudoexperiments are performed by fitting these modified templates to "pseudodata" randomly drawn according to the nominal (i.e., no systematic effects applied) templates.

Pseudodata are constructed for each pseudoexperiment using the expected number of events, $\bar{N}_X$, and E_T^{miss}–N_{jets} shape for each process X. For each pseudoexperiment the following procedure is carried out. The expected number of events for process X is sampled from a Gaussian distribution of mean $\bar{N}_X$ and width determined by the uncertainty

TABLE II. Summary of dominant systematic uncertainties. Uncertainties expressed as a percentage are shown for each signal process, broken down into normalization effects on $\mathcal{C}$ (the factor relating the measured events to the fiducial phase space) and $\mathcal{A}\cdot\mathcal{C}$ (the factor relating the measured events to the full phase space), and template shape effects. The normalization uncertainties on $\mathcal{A}\cdot\mathcal{C}$ and $\mathcal{C}$ are symmetrized. The reconstruction uncertainties are applied to $\mathcal{C}$ and affect both the fiducial and full cross-section measurements. The theoretical uncertainties due to template shape are applied to both the fiducial and full cross-section measurements as well. Uncertainties on the fake and nonprompt background, luminosity, and LHC beam energy, which are not divided into normalization and shape components, are listed together.

	Process								
	Systematic uncertainties (%)								
	$t\bar{t}$			WW			$Z/\gamma^* \to \tau\tau$		
Source	$\mathcal{C}$	$\mathcal{A}\cdot\mathcal{C}$	Shape	$\mathcal{C}$	$\mathcal{A}\cdot\mathcal{C}$	Shape	$\mathcal{C}$	$\mathcal{A}\cdot\mathcal{C}$	Shape
ISR/FSR + scale	±1.1	±0.4	$+1.0(-1.5)$	±1.0	±0.8	$+4.7(-3.5)$	±1.1	±0.4	$+0.7(-1.0)$
Generator	±0.7	±0.8	$+0.2(-0.0)$	±0.6	±0.5	$+4.5(-0.4)$			$+0.0(-0.7)$
PS modeling	±0.9	±0.6	$+0.0(-0.1)$	±0.5	±1.0	$+3.5(-0.0)$			$+0.0(-0.6)$
$Z/\gamma^* \to \tau\tau$ PS Modeling			$+0.0(-0.5)$			$+0.0(-0.6)$	±1.8	±3.3	$+0.5(-0.0)$
PDF	±0.6	±1.7	±0.5	±0.1	±0.7	±1.6	±0.2	±1.3	±0.8
e reconstruction, ID, isolation	±3.2		$+0.0(-0.1)$	±3.2		$+0.3(-0.3)$	±3.3		$+0.0(-0.8)$
μ reconstruction	±0.8		$+0.0(-0.0)$	±0.8		$+0.0(-0.0)$	±0.8		$+0.0(-0.0)$
$E_{\mathrm{T}}^{\mathrm{miss}}$ cellout	±0.0		$+0.4(-0.2)$	±0.0		$+8.1(-9.9)$	±0.0		$+2.3(-0.2)$
$E_{\mathrm{T}}^{\mathrm{miss}}$ pileup	±0.0		$+0.1(-0.1)$	±0.0		$+3.7(-4.5)$	±0.0		$+1.0(-1.7)$
Jet energy scale	±0.8		$+1.4(-1.4)$	±0.6		$+0.5(-4.8)$	±0.5		$+1.4(-3.1)$
Jet energy resolution	±0.2		$+0.3(-0.0)$	±0.2		$+0.0(-2.6)$	±0.2		$+0.0(-0.1)$
Jet vertex fraction	±0.8		$+0.1(-0.0)$	±0.3		$+0.0(-1.7)$	±0.2		$+0.0(-0.3)$
	$t\bar{t}$			WW			$Z/\gamma^* \to \tau\tau$		
Fake or nonprompt background	±0.8			±5.6			±0.7		
Luminosity	±1.8			±1.8			±1.8		
LHC beam energy	±1.8			±1.0			±0.8		

on $\bar{N}_X$. This number is then Poisson fluctuated to determine the number of events, N_X, for process X. The shape of process X in the $E_{\mathrm{T}}^{\mathrm{miss}}$–$N_{\mathrm{jets}}$ parameter space is then used to define a probability distribution function from which to sample the N_X events contributing to the pseudodata for the pseudoexperiment. This is repeated for all processes to construct the pseudodata in the $E_{\mathrm{T}}^{\mathrm{miss}}$–$N_{\mathrm{jets}}$ parameter space as the input to the pseudoexperiment. The pseudoexperiment is then performed by fitting the pseudodata to the modified templates and extracting the number of events for each signal process, N_{sig}. This procedure is repeated one thousand times to obtain a well-defined distribution of N_{sig} values.

The difference, ΔN_{sig}, between the mean value of this distribution and $\bar{N}_X$ is taken as the error due to template shape effects. To obtain the final template shape uncertainty, each positive $\Delta N_{\mathrm{sig}}/N_{\mathrm{sig}}$ value is added in quadrature to obtain the total positive error, and each negative value is added likewise to obtain the total negative error.

C. Fake or nonprompt background uncertainties

To evaluate the uncertainty on the fake or nonprompt background contribution, the matrix method input probabilities are varied; the background templates are then rederived and the measurement is repeated. The observed maximum deviation of the signal parameters measured from templates where electron probabilities are varied is assigned as an uncertainty. Similarly the deviation observed when using the alternative set of muon probabilities is assigned as an uncertainty. The net uncertainty is calculated as a quadratic sum of both uncertainties.

D. PDF uncertainties

The uncertainties associated with the choice of parton distribution functions are evaluated using a number of different PDF sets. The envelope of uncertainty bands from the CT10 [17], MSTW2008 [29] and NNPDF 2.3 [32] sets is determined using the procedure prescribed for LHC studies [28]. There are two PDF-related uncertainties defined, which are the intra-PDF uncertainty and the inter-PDF uncertainty. The former is the uncertainty within a given PDF set originating from uncertainties on various inputs to the PDF calculation or other uncertainties assigned by the particular PDF set authors. The latter is the variation observed when comparing one PDF to another. The comparison is made using the central value of each PDF set and measuring the variation of the observable. The full PDF set uncertainty combines the inter- and intra-PDF uncertainties by taking the envelope of

the minimum and maximum of these values. Uncertainties associated with the parton distribution functions are not profiled in the fit. Shape uncertainties are measured by fitting the varied templates to data while variations between calculated $\mathcal{A}$ and $\mathcal{C}$ values are used to assign acceptance uncertainties. Fitting the templates with different PDF sets to data results in yield uncertainties, the envelope of which is taken as the PDF shape uncertainty. The PDF set uncertainties, shown in Table II, are computed in this way to avoid the complexity that would otherwise be introduced into the fit if they were to be profiled.

E. LHC luminosity and beam energy

The uncertainty in the measured integrated luminosity is 1.8%, which affects both the fitted yields and the calculated cross-sections for signal and background templates, while the uncertainty associated with the center-of-mass collision energy, $\sqrt{s}$, affects the production cross-sections. The beam energy can be calibrated using the revolution frequency (RF) difference between protons and lead ions. The RF is different for lead ions and protons due to their different ratio of charge to rest mass, and depends on the LHC dipole field setting. The calibration can be performed because the proton beam momentum is proportional to the square root of the proton's RF divided by the frequency difference [53]. The nominal beam energy at $\sqrt{s} = 8$ TeV was calibrated to be $3988 \pm 5 \pm 26$ GeV during $p+\mathrm{Pb}$ runs in early 2013 [53] and corresponds to a relative uncertainty of 0.66%, which is assumed to be the same for $\sqrt{s} = 7$ TeV. Both of these sources of uncertainty affect template normalization but have no effect on template shape, unlike other uncertainties which affect both normalization and shape.

F. Summary of systematic uncertainties

Table II lists the sources and effects of the most significant systematic variations on the acceptance correction factors and on the event yields derived from the fit. The first group of entries in the table is the theoretical uncertainties. To determine the uncertainty due to the choice in the modeling of a particular aspect of the event, comparisons are made between Monte Carlo samples featuring alternative choices to the default ones. The uncertainty on the modeling of additional QCD radiation on $t\bar{t}$ and WW is evaluated by comparing MC@NLO to ALPGEN where the default scales are varied simultaneously by factors of 2 and 0.5. The uncertainty due to the choice of Monte Carlo generator is determined for $t\bar{t}$ and WW by comparing the default generators to POWHEG while the uncertainty due to the modeling of the parton shower and fragmentation is evaluated by interfacing the default generators to PYTHIA. In the case of $Z/\gamma^* \to \tau\tau$, the theoretical uncertainties are calculated by comparing SHERPA to the appropriate ALPGEN sample interfaced to HERWIG. The evaluation of the uncertainty due to the choice of PDF has been described in Sec. VI D.

The second group of entries in Table II corresponds to the experimental uncertainties. The uncertainties associated with Monte Carlo modeling of the lepton trigger, reconstruction and identification efficiencies are evaluated by studying $Z \to ee/Z \to \mu\mu$ and $W \to e\nu/W \to \mu\nu$ events selected from data as well as $Z \to ee/Z \to \mu\mu$, $W \to e\nu/W \to \mu\nu$, and $t\bar{t}$ events from simulation [43]. The dominant experimental uncertainties on template normalization stem from electron reconstruction, identification, and isolation. These uncertainties are large due to the difference in efficiency of the isolation cut between the $Z+$ jets region where the efficiency is measured and the rest of the signal region.

The main contributors to the uncertainty on $E_{\mathrm{T}}^{\mathrm{miss}}$ originate from calorimeter cells not associated with any physics object ($E_{\mathrm{T}}^{\mathrm{miss}}$-cellout term) and the pileup correction factors. In fact the former is responsible for the single largest contribution and results, in the WW measurement, in shape uncertainties in excess of 10% which is a dominant source of uncertainty on the full and fiducial cross-section values.

The uncertainty on the jet energy scale also leads to relatively large template shape uncertainties for all signal processes. In the central region of the detector ($|\eta| < 1.7$) the jet energy scale uncertainty varies from 2.5 to 8% as a function of jet p_{T} and η [54], as estimated from *in situ* measurements of the detector response. This uncertainty estimate includes uncertainties from jet energy scale calibration, calorimeter response, detector simulation, and the modeling of the fragmentation and UE, as well as other choices in the Monte Carlo event generation. Intercalibration of forward region detector response from the central regions of the detector also contributes to the total uncertainty on jet energy scale. Additional uncertainties due to pileup and close-by jet effects are also included. The uncertainty introduces distortions in the template shapes including effects propagated to the calculation of $E_{\mathrm{T}}^{\mathrm{miss}}$. To obtain an estimate of this source of uncertainty, the jet energy scale is broken into sixteen independent components. Each component is individually shifted up and down within its uncertainties for a total of 32 variations in the evaluation of shape uncertainties, the results of which are combined and shown as a single entry in Table II.

The jet energy resolution has been found to be well modeled by simulation. It is measured from calorimeter observables by exploiting the transverse momentum balance in events containing jets with large p_{T}. Two independent *in situ* methods sensitive to different sources of systematic uncertainties are used to measure the resolution which the Monte Carlo simulation describes within 10% for jets whose p_{T} ranges from 30–500 GeV [55]. The uncertainty due to the JVF is determined from studies of $Z \to ee/\mu\mu +$ jets events.

The last group of entries on Table II includes uncertainties on fake or nonprompt backgrounds, the measurement of integrated luminosity, and the determination of the LHC beam energy. The uncertainty due to modeling of the fake or nonprompt background, whose evaluation is described in Sec. VI C, has the greatest effect on the WW measurement. The uncertainty in the integrated luminosity is dominated by the accuracy of the beam separation scans and the resulting uncertainty of 1.8% is assigned to each signal process. The uncertainty of 0.66% on the beam energy is found to vary the prediction for $t\bar{t}$ production, calculated at NNLO plus next-to-next-to-leading logarithm by TOP++ [26], by 1.8%. Similarly, for WW and $Z/\gamma^* \to \tau\tau$, an equivalent study was performed with predictions at NLO from MCFM v6.6 [42], resulting in variations of 1.0 and 0.8% respectively. These variations are assigned as uncertainties to the measured cross-sections as shown in the last item of Table II.

Overall since the WW and $Z/\gamma^* \to \tau\tau$ signals overlap in the 0-jet bins, most of the significant shape uncertainties involve the wrong assignment of events to one of these two samples. Very few effects can move a WW or $Z/\gamma^* \to \tau\tau$ event into the ≥ 1 jet bin, so generally small shape uncertainties on $t\bar{t}$ are observed, where interference from the other processes is minimal. This event assignment uncertainty affects WW approximately three times more than $Z/\gamma^* \to \tau\tau$ due to the larger yield of $Z/\gamma^* \to \tau\tau$ events.

The main contributions to the uncertainty on $\mathcal{A} \cdot \mathcal{C}$, as shown in Table II, are the PDF for $t\bar{t}$ and the PS modeling for WW and $Z/\gamma^* \to \tau\tau$. The theoretical uncertainties on the correction factors $\mathcal{C}$ are small. No individual source of theoretical uncertainty on $\mathcal{C}$ exceeds the uncertainty due to experimental effects (dominated by those associated with electron scale factors and luminosity). One effect observed from this table is that there is apparent anticorrelation between uncertainties on $\mathcal{A}$ and $\mathcal{C}$, leading to an uncertainty on their product that is smaller than that on the multiplicands, e.g. the ISR/FSR + scale uncertainty. Uncertainties on branching ratios [56] used in the cross-section calculations are negligible relative to experimental uncertainties and not included in Table II.

Within the fiducial region, uncertainties on $\mathcal{C}$ come mainly from experimental sources and template shape uncertainties. The dominant source varies between signals; template shape uncertainties are dominant in the WW measurement, where the likelihood fit is sensitive to variation in the scale of $E_{\mathrm{T}}^{\mathrm{miss}}$-cellout terms. The uncertainty on the fiducial $t\bar{t}$ cross-section is dominated by the electron reconstruction, identification and isolation. In the $Z/\gamma^* \to \tau\tau$ channel, leading uncertainties derive from PS modeling and the jet energy scale measurement.

VII. RESULTS

A. Event yields

Comparisons between data and Monte Carlo predictions together with event yields before the application of the fitting procedure are displayed in Fig. 4 and Table III. The Monte Carlo predictions are normalized to the values given in Sec. III. These comparisons are shown in the signal region and subdivisions thereof based on jet multiplicity calculated for jets above the 30 GeV p_{T} threshold and on events with reconstructed $E_{\mathrm{T}}^{\mathrm{miss}}$ below and above 30 GeV. The events shown here satisfy the OS and tight identification criteria specified in Sec. IV. The inclusive yields represent the sum of the binned yields in the $E_{\mathrm{T}}^{\mathrm{miss}}$–$N_{\mathrm{jets}}$ parameter space, which provide the templates used in the fit to the data. The data yield is observed to be in good overall agreement with the prediction.

The same comparisons are shown after the fitting procedure in Fig. 5 and Table IV for the signal region and for subdivisions thereof, based on the classification defined above. In Fig. 5 the error bands are smaller in general than in Fig. 4 since they do not include the uncertainties on the theoretical cross-sections for the three signal processes that are included in the prefit results. As expected, yields for the signal processes given by the fit rise with respect to the prefit normalization to better fit the observed yield in data. Furthermore, good agreement is observed within each of the categories shown in Table IV, indicating that the background estimation and signal template shapes provide a good description of the data.

In Table V, the fitted yields are shown together with the acceptance correction factors $\mathcal{A}$ and $\mathcal{C}$ introduced in Sec. VI, the branching ratios $\mathcal{B}$, and the fiducial and full cross-sections calculated using Eqs. (4)–(5). For these branching ratios, the most precise available measurements are used [56], including the best theoretical prediction of the W leptonic branching ratio, $B(W \to \ell\nu) = 0.1082$ with 0.07% uncertainty. A fiducial cross-section, for which electrons and muons from tau-lepton decays in $t\bar{t}$ and WW are removed, is also quoted along with a ratio, $R_{\mathcal{C}}$, that translates between the two fiducial region definitions. This additional fiducial definition is implemented to allow comparisons with predictions for $t\bar{t}$ and WW fiducial cross-sections that do not include tau-lepton decays to electrons and muons. Such a redefinition of the fiducial region does not alter the product $\mathcal{A} \cdot \mathcal{C}$ or the relative uncertainties on the fiducial cross-sections. Also shown are the full uncertainties accompanied by a breakdown of the systematic uncertainty into its three main components (discussed in Sec. VI, namely those arising from normalization, shape, and the fake or nonprompt backgrounds). For the $t\bar{t}$ and $Z/\gamma^* \to \tau\tau$ processes, which have higher production rates, the normalization uncertainty is dominant while the shape uncertainty is dominant for the lower-rate WW process. This shape uncertainty is not shown in Figs. 4–5, leading to some underestimate of the error bands at high values of $E_{\mathrm{T}}^{\mathrm{miss}}$ in Figs. 4(c) and 5(c), where the WW process is dominant.

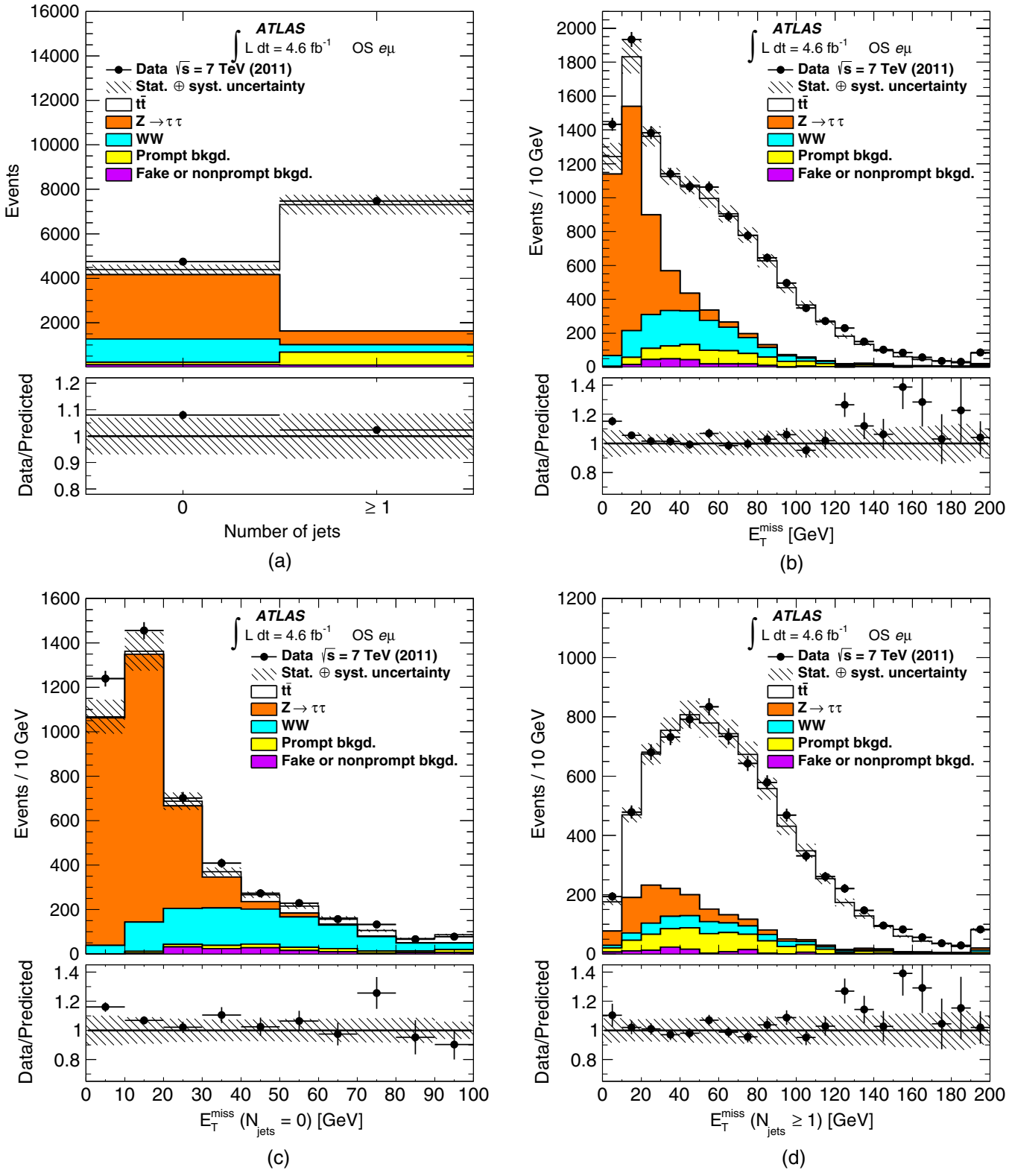

FIG. 4 (color online). Comparison between data and Monte Carlo samples (including the data-driven fake or nonprompt background) normalized to their theoretical cross-sections for an integrated luminosity of 4.6 fb^{-1} for events producing one electron and one muon of OS charge: (a) N_{jets}, with bins corresponding to zero jets and ≥ 1 jet; (b) missing transverse momentum spectrum, $E_{\text{T}}^{\text{miss}}$; (c) $E_{\text{T}}^{\text{miss}}$ for $N_{\text{jets}} = 0$ and (d) $E_{\text{T}}^{\text{miss}}$ for $N_{\text{jets}} \geq 1$. The electron and muon satisfy the signal region selection criteria presented in Sec. IV. The hatched regions represent the combination of statistical and systematic uncertainties as described in Table II (except for shape uncertainties) together with the full theoretical cross-section uncertainties for the $t\bar{t}$, WW, and $Z/\gamma^* \to \tau\tau$ signal processes. The last bins in (b), (c) and (d) contain overflow events.

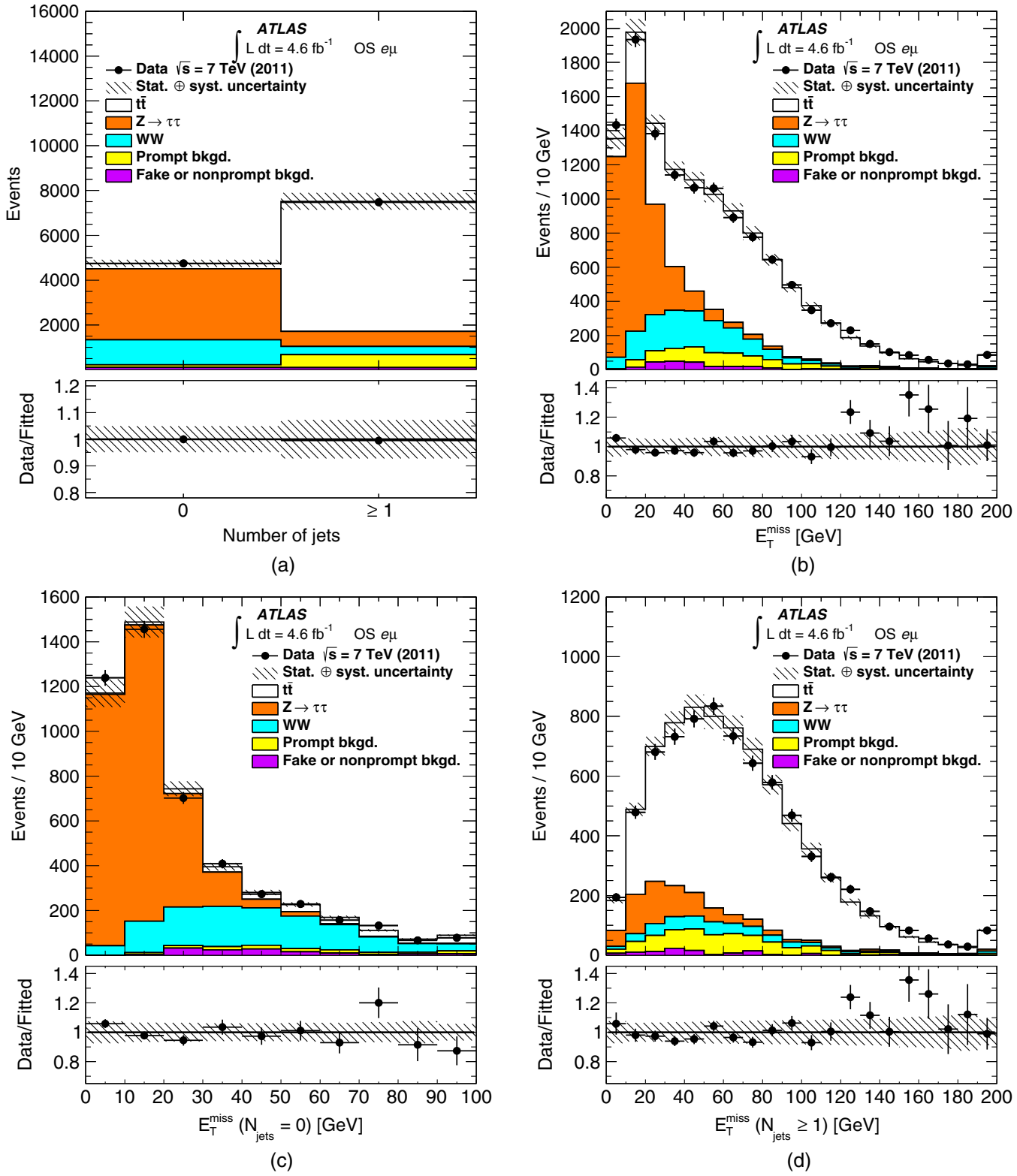

FIG. 5 (color online). Comparison between data and Monte Carlo samples (including the data-driven fake or nonprompt background) after fitting signal processes to data corresponding to an integrated luminosity of 4.6 fb^{-1} for events producing one electron and one muon of OS charge: (a) N_{jets}, with bins corresponding to zero jets and ≥ one jet; (b) missing transverse momentum, $E_{\text{T}}^{\text{miss}}$; (c) $E_{\text{T}}^{\text{miss}}$ for $N_{\text{jets}} = 0$ and (d) $E_{\text{T}}^{\text{miss}}$ for $N_{\text{jets}} \geq 1$. The electron and muon satisfy the signal region selection criteria presented in Sec. IV. The hatched regions represent the combination of statistical and systematic uncertainties as described in Table II (except for shape uncertainties). The last bins in (b), (c) and (d) contain overflow events.

TABLE III. Expected and observed inclusive yields for events producing one electron and one muon of OS electric charge in an integrated luminosity of 4.6 fb^{-1} at $\sqrt{s} = 7$ TeV. The total yields are given followed by the yields subdivided into events producing zero jets and events producing one or more jets with $p_{\mathrm{T}} > 30$ GeV. In the final two columns the total yields are subdivided into events that produce $E_{\mathrm{T}}^{\mathrm{miss}} < 30$ GeV and events that produce $E_{\mathrm{T}}^{\mathrm{miss}} \geq 30$ GeV. Uncertainties are a quadratic sum of statistical and systematic (including theoretical cross-section) uncertainties, but do not include shape systematic uncertainties. The net predicted yields are calculated using unrounded contributions.

Process	Total	$N_{\mathrm{jets}} = 0$	$N_{\mathrm{jets}} \geq 1$	$E_{\mathrm{T}}^{\mathrm{miss}} < 30$ GeV	$E_{\mathrm{T}}^{\mathrm{miss}} \geq 30$ GeV
$t\bar{t}$	5900 ± 500	230	5670	860	5100
WW	1400 ± 100	1030	360	420	970
$Z \to \tau\tau$	3500 ± 250	2900	610	3000	520
Single top	590 ± 50	80	510	90	500
WZ/ZZ	90 ± 40	30	60	30	60
Fake or nonprompt	210 ± 170	110	100	50	160
Predicted	11700 ± 600	4400	7300	4400	7300
Observed	12224	4744	7480	04750	7474

B. Comparison to previous ATLAS measurements

This analysis is the first simultaneous measurement of the $t\bar{t}$, WW, and $Z/\gamma^* \to \tau\tau$ cross-sections at $\sqrt{s} = 7$ TeV. Measured cross-sections are summarized and compared to previous measurements and predictions in Table VI. The $t\bar{t}$ cross-section obtained from the simultaneous measurement is in agreement with the dedicated $t\bar{t}$ cross-section measurement in the dilepton channel [4] at $\sqrt{s} = 7$ TeV with identical integrated luminosity. The dedicated measurement benefits from a more optimized electron identification which reduces the overall systematic uncertainty associated with the measurement. Both measurements assume a top quark mass of 172.5 GeV; in the simultaneous measurement the dependence of the measured cross-section on the assumed mass is found to be -0.8 pb/GeV.

In the WW channel, the dedicated analysis at $\sqrt{s} = 7$ TeV [5] with an integrated luminosity of 4.6 fb^{-1} has significantly greater precision as a result of large shape uncertainties in the simultaneous measurement. As the smallest of the three measured signals, WW is the one subject to the largest relative variations in the simultaneous fit and has large uncertainties.

Finally, the $Z/\gamma^* \to \tau\tau$ simultaneous measurement shows smaller uncertainties than the dedicated measurement [6] at $\sqrt{s} = 7$ TeV with an integrated luminosity of 36 pb^{-1}. Statistical and luminosity uncertainties are substantially smaller due to the larger data sample with a more precise luminosity determination.

The measurements presented here include the effect of the uncertainty on the LHC beam collision energy, which was not evaluated in prior measurements. Overall, the comparisons show that each simultaneous cross-section measurement is consistent with its corresponding dedicated ATLAS measurement.

C. Comparison to theoretical calculations

Figures 6–7 show the best-fit cross-section values with likelihood contours obtained from the simultaneous fit, overlayed with theoretical cross-section predictions. These do not include the contribution from leptonically decaying

TABLE IV. Fitted and observed inclusive yields for events producing one electron and one muon of OS electric charge in an integrated luminosity of 4.6 fb^{-1} at $\sqrt{s} = 7$ TeV. The total yields are given followed by the yields subdivided into events producing zero jets and events producing one or more jets with $p_{\mathrm{T}} > 30$ GeV. In the final two columns the total yields are subdivided into events that produce $E_{\mathrm{T}}^{\mathrm{miss}} < 30$ GeV and events that produce $E_{\mathrm{T}}^{\mathrm{miss}} \geq 30$ GeV. Uncertainties are a quadratic sum of statistical and systematic uncertainties. The net fitted yields are calculated using unrounded contributions.

Process	Total	$N_{\mathrm{jets}} = 0$	$N_{\mathrm{jets}} \geq 1$	$E_{\mathrm{T}}^{\mathrm{miss}} < 30$ GeV	$E_{\mathrm{T}}^{\mathrm{miss}} \geq 30$ GeV
$t\bar{t}$	6050 ± 350	240	5810	880	5170
WW	1480 ± 220	1120	360	450	1030
$Z \to \tau\tau$	3840 ± 300	3170	670	3280	560
Single top	590 ± 50	80	510	90	500
WZ/ZZ	90 ± 40	30	60	30	60
Fake or nonprompt	210 ± 170	110	100	50	160
Fitted	12260 ± 540	4750	7510	4780	7480
Observed	12224	4744	7480	4750	7474

TABLE V. Summary of fitted yields (unrounded), acceptance correction factors, and cross-section measurements. The acceptance correction factors, $\mathcal{A}\cdot\mathcal{C}$ and $\mathcal{C}$, are extracted from simulated events. The branching ratios are taken from the best theoretical calculations or experimental measurements [56]. The fiducial and full cross-sections are calculated using Eqs. (4) and (5) and accompanied by statistical uncertainties, systematic uncertainties, and uncertainties associated with the luminosity and LHC beam energy. Also given is a breakdown of the systematic uncertainty including template normalization uncertainties, template shape uncertainties, and uncertainties attributed to the estimation of the fake or nonprompt background. Fiducial cross-sections for $t\bar{t}$ and WW where leptons from τ decays are excluded from the definition of the fiducial region are also given along with the ratio, $R_{\mathcal{C}}$, used to translate to the fiducial region that includes leptons from τ decays. The factor $R_{\mathcal{C}}$ is defined as the ratio between the acceptance when τ decays are included in the definition and when τ decays are not.

Process	$t\bar{t}$	WW	$Z/\gamma^* \to \tau\tau$
Fitted yield N_{fit}	6049	1479	3844
$\mathcal{C}$	0.482	0.505	0.496
$R_{\mathcal{C}}$	1.150	1.133	
$\mathcal{A}\cdot\mathcal{C}$	0.224	0.187	0.0115
Branching ratio B	0.0324	0.0324	0.0621
σ_X^{fid} [fb]	2730	638	1690
Statistical	±40	±32	±35
Systematic	±140	+88(−95)	+89(−116)
Luminosity	±50	±11	±30
LHC beam energy	±50	±6	±14
σ_X^{fid} (excluding $\tau \to \ell\nu\nu$) [fb]	2374	563	
Statistical	±37	±28	
Systematic	±120	+78(−84)	
Luminosity	±43	±10	
LHC beam energy	±43	±6	
Uncertainties (%)			
Statistical	1.5	5.0	2.0
Systematic	5.1	+13.7(−14.9)	+5.5(−7.0)
Luminosity	1.8	1.8	1.8
LHC beam energy	1.8	1.0	0.8
Total	5.9	15.9	7.5
Breakdown of systematic uncertainty (%)			
Normalization	+4.6(−4.3)	4.3(−3.8)	+4.2(−3.9)
Shape	+1.8(−2.4)	+11.7(−13.2)	+3.0(−5.6)
Fake or nonprompt background	±0.8	±5.6	±0.7
σ_X^{tot} [pb]	181.2	53.3	1174
Statistical	±2.8	±2.7	±24
Systematic	+9.7(−9.5)	+7.3(−8.0)	+72(−88)
Luminosity	±3.3	±1.0	±21
LHC beam energy	±3.3	±0.5	±9
Uncertainties (%)			
Statistical	1.5	5.0	2.1
Systematic	+5.4(−5.3)	+13.8(−14.9)	+6.1(−7.5)
Luminosity	1.8	1.8	1.8
LHC beam energy	1.8	1.0	0.8
Total	6.1	15.9	8.0
Subdivision of systematic uncertainty (%)			
Normalization	+4.7(−4.3)	+4.2(−3.7)	+5.1(−4.6)
Shape	+1.8(−2.4)	+11.7(−13.2)	+3.0(−5.6)
Fake or nonprompt background	±0.8	±5.6	±0.7

taus. The numerical correlation values from the likelihood fit are given in Table VII for each pair of signal processes. These values give the correlations between the numbers of fitted events in the fiducial region.

NLO fiducial and NLO full cross-section predictions were computed using MCFM v6.6 [42] except for the $Z/\gamma^* \to \tau\tau$ fiducial cross-section, which was computed with MC@NLO interfaced to HERWIG, TAUOLA and PHOTOS. The computed WW cross-section does not include the contribution from $gg \to H \to WW$, which is expected to contribute roughly 5% of the total WW cross-section as discussed in Sec. III B. Fiducial calculations are performed

TABLE VI. Comparisons of the total $t\bar{t}$, WW, and $Z/\gamma^* \to \tau\tau$ cross-sections as measured simultaneously in this analysis with symmetrized uncertainties to previous dedicated ATLAS measurements and to the most accurate predictions from QCD. The NLO QCD prediction for WW presented here is the sum of the $qq \to WW$, $gg \to WW$, and $gg \to H \to WW$ cross-sections. The ATLAS dedicated $Z/\gamma^* \to \tau\tau$ production cross-section was measured in the fiducial region where 66 GeV $< m_{\tau\tau} <$ 116 GeV and so is corrected by a factor 1.1 to compare it directly with the $Z/\gamma^* \to \tau\tau$ cross-section measured here in the fiducial region $m_{\tau\tau} > 40$ GeV.

Process	Source	σ_X^{tot}	Uncertainties					$\int \mathcal{L} dt$	Reference
		[pb]	Statistic	Systematic	Luminosity	Beam	Total	[fb^{-1}]	
$t\bar{t}$	Simultaneous	181	3	10	3	3	11	4.6	
	Dedicated	183	3	4	4	3	7	4.6	[4]
	NNLO QCD	177					11		[25]
WW	Simultaneous	53.3	2.7	7.7	1.0	0.5	8.5	4.6	
	Dedicated	51.9	2.0	3.9	2.0		4.9	4.6	[5]
	NLO QCD	49.2					2.3		[35]
$Z/\gamma^* \to \tau\tau$	Simultaneous	1174	24	80	21	9	87	4.6	
	Dedicated ($e\mu$)	1170	150	90	40		170	0.036	[6]
	NNLO QCD	1070					54		[38] [29]

for the region excluding electrons or muons from tau-lepton decays.

Theoretical predictions were calculated for the following PDF sets: ABM11 [57], MSTW2008CPdeut [58], CT10, HERAPDF15 [59], NNPDF2.3 [32], JR09 [60] (for NNLO calculations) and epWZ [61] (for NNLO calculations). In both figures, the markers represent the cross-sections calculated for a pair of processes using a specific central PDF with its error bars depicting the uncertainty due to the choice of renormalization (μ_R) and factorization (μ_F) scales. No attempt is made to treat these scale choices in a correlated way between processes. The asymmetric scale uncertainty is obtained from the maximum upper and lower deviation from the central value (μ_R and μ_F) found in a process-specific grid composed of seven cross-sections. These were calculated by independently varying values of μ_R and μ_F by factors of 1/2, 1 and 2 (while ignoring the cases where μ_R is doubled and μ_F is halved and vice versa). The central values of μ_R and μ_F are set to process-specific values: m_t for $t\bar{t}$, m_W for WW, and m_Z for $Z/\gamma^* \to \tau\tau$.

The theory contours shown in Fig. 6 correspond to the 68% C.L. regions around each cross-section prediction calculated from the error sets associated with each specific PDF (intra-PDF uncertainties, defined in Sec. VI). The derived uncertainties from different PDF sets are scaled so that all the contours reflect a 68% C.L. and are constructed using prescribed recipes (in the case of the HERAPDF15 the contour displays asymmetrical errors).

The fiducial cross-sections provide the most direct comparison between theory and experiment. Since the fiducial region is chosen to correspond to the sensitive volume of the detector, the theoretical uncertainties are small on the measured values of the fiducial cross-sections. The uncertainty regions in the fiducial measurements in Fig. 6 suggest that the NLO predictions underestimate all three cross-sections, especially in the case of $Z/\gamma^* \to \tau\tau$ versus $t\bar{t}$, irrespective of the PDF model. The WW fiducial measurement, however, is consistent with predictions from each PDF model considered, especially considering the fact that the theory predictions in Fig. 6 do not account for the $gg \to H \to WW$ contribution and therefore underestimate the fiducial cross-section by approximately 5% (see Sec. III C).

Full cross-section measurements are shown in Fig. 7 accompanied by 68 and 90% C.L. contours calculated for the case where the fit only includes the theoretical uncertainty (inner contours) and the case when the full uncertainty is included (outer contours). Although larger acceptance uncertainties clearly reduce the separation power with respect to the fiducial measurements, here the full theoretical calculations at NNLO in QCD can be used for $Z/\gamma^* \to \tau\tau$ versus $t\bar{t}$, as shown in Fig. 7(d). As described in Sec. III, the software packages FEWZ and TOP ++ were used to calculate the cross-sections to NNLO. Figure 7(d) (NNLO case) in contrast to Fig. 7(c) (NLO case) shows good overlap between the experimental measurement and most of the NNLO theoretical predictions and corresponding PDF sets for $Z/\gamma^* \to \tau\tau$ versus $t\bar{t}$ where they are available. Also notable is the difference in the uncertainties in theoretical predictions: in the NLO case scale uncertainties are dominant, while in the NNLO case the PDF model provides the dominant uncertainty. Theory contours using ABM11 and JR09 PDFs, however, do not overlap with the measurements. For the former, one significant reason for a lower $t\bar{t}$ cross-section lies in the value of α_s employed in its calculation. At NNLO its value is 0.113, which is substantially lower than the range of 0.117 to 0.118 employed by most of the other PDF models here. In the case of JR09, which is only considered in the comparison of NNLO calculations, the 5% difference in the $Z/\gamma^* \to \tau\tau$ cross-section is consistent with what is reported elsewhere [60].

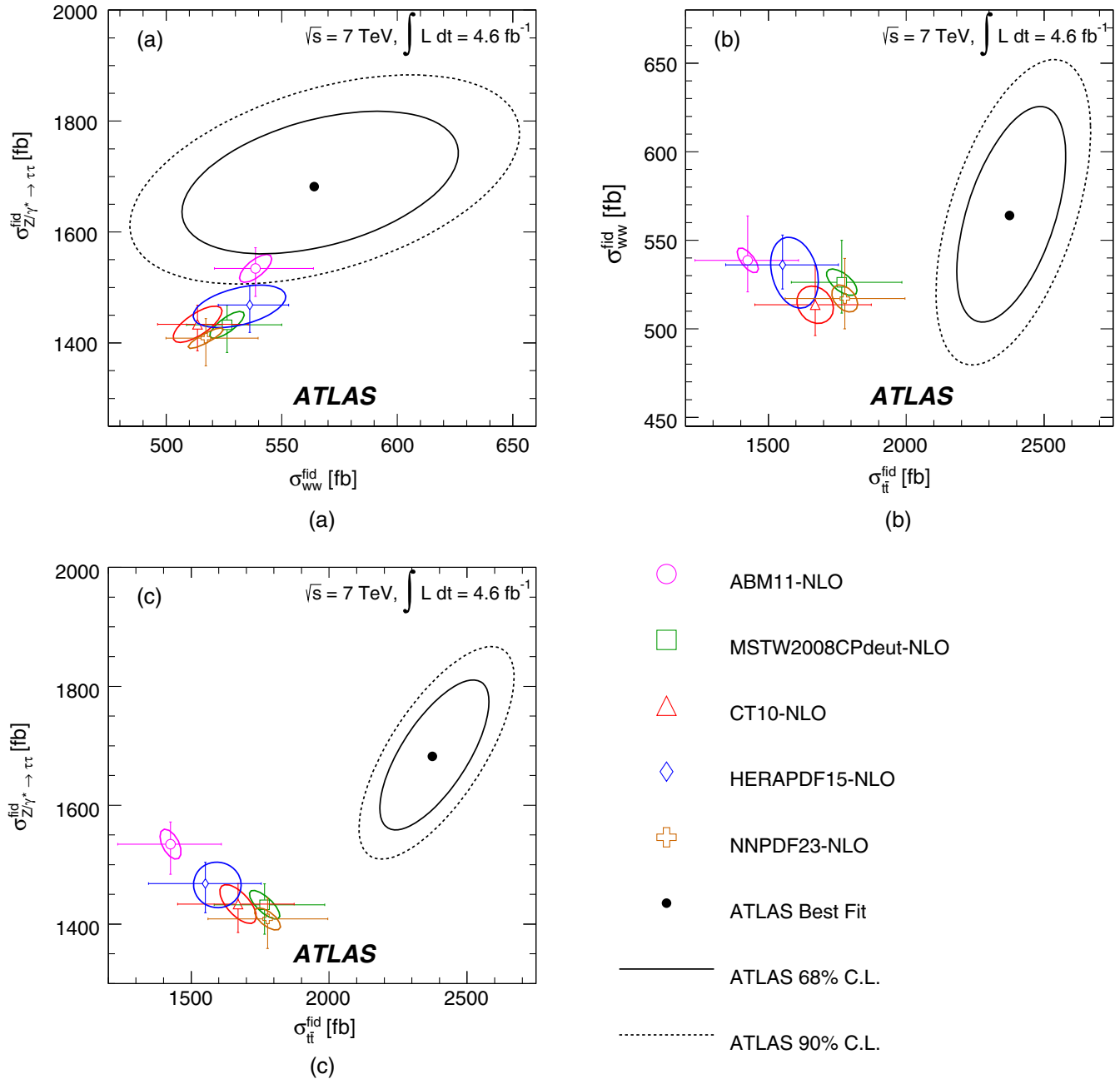

FIG. 6 (color online). Contours of the likelihood function as a function of two fiducial production cross-sections of interest: (a) $\sigma^{\mathrm{fid}}_{Z/\gamma^{*}\to\tau\tau}$ versus $\sigma^{\mathrm{fid}}_{WW}$, (b) $\sigma^{\mathrm{fid}}_{WW}$ versus $\sigma^{\mathrm{fid}}_{t\bar{t}}$, (c) $\sigma^{\mathrm{fid}}_{Z/\gamma^{*}\to\tau\tau}$ versus $\sigma^{\mathrm{fid}}_{t\bar{t}}$. The contours obtained from the data (full circle) represent the 68 (full line) and 90% C.L. (dashed line) areas accounting for the full set of systematic uncertainties described in Table II. The fiducial cross-sections for WW and $t\bar{t}$ exclude contributions from tau-lepton decays. The theoretical WW cross-section does not include contributions from $gg \to H \to WW$. The theoretical fiducial cross-section predictions are shown at NLO in QCD for different PDF sets (open symbols) with the ellipse contours corresponding to the 68% C.L. uncertainties on each PDF set. Also shown as horizontal and vertical error bars around each prediction are the uncertainties due to the choice of QCD factorization and renormalization scales (see text).

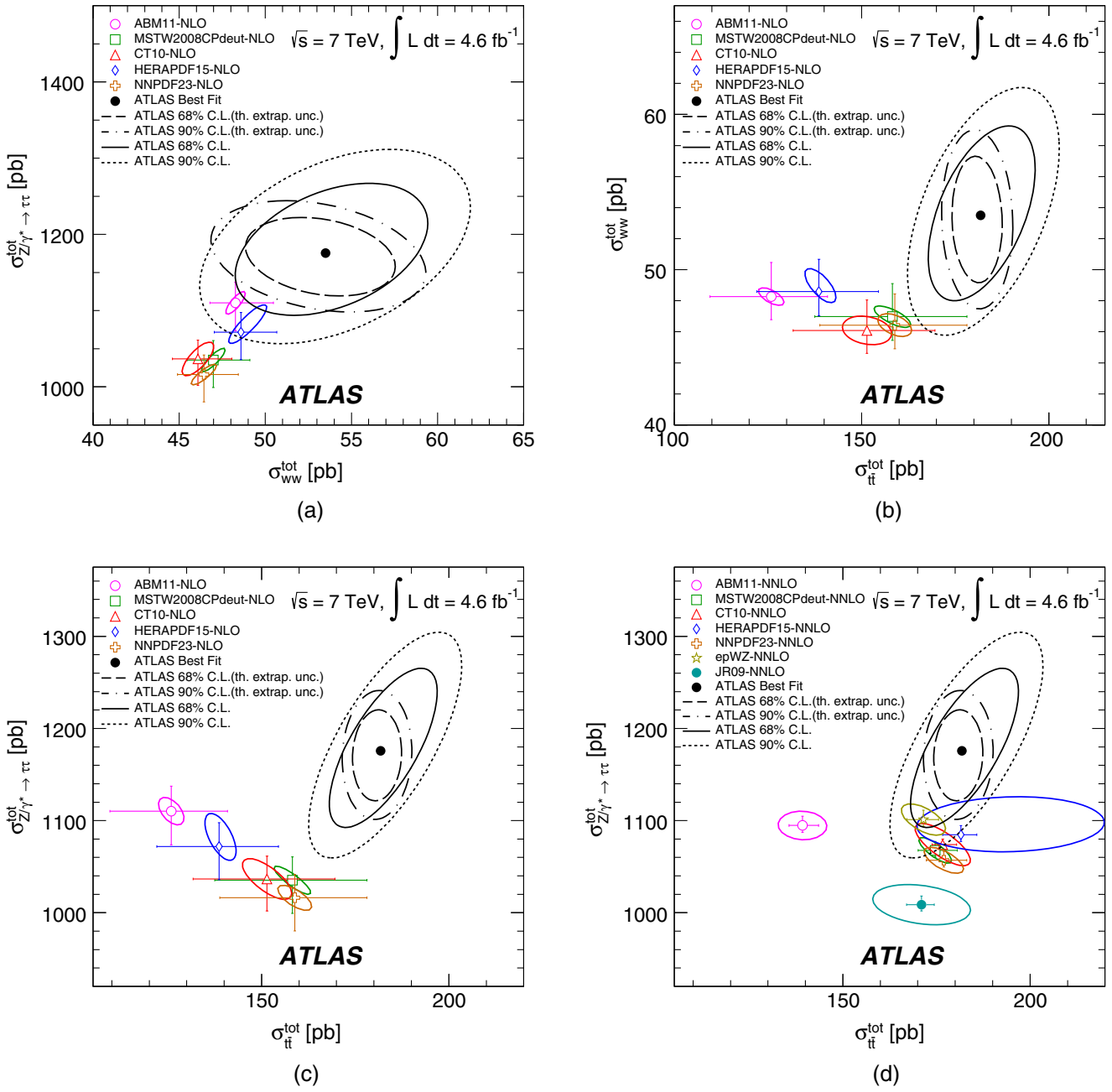

FIG. 7 (color online). Contours of the likelihood function as a function of two full production cross-sections of interest: (a) $\sigma^{\mathrm{tot}}_{Z/\gamma^* \to \tau\tau}$ versus $\sigma^{\mathrm{tot}}_{WW}$ compared to NLO predictions; (b) $\sigma^{\mathrm{tot}}_{WW}$ versus $\sigma^{\mathrm{tot}}_{t\bar{t}}$ compared to NLO predictions; (c,d) $\sigma^{\mathrm{tot}}_{Z/\gamma^* \to \tau\tau}$ versus $\sigma^{\mathrm{tot}}_{t\bar{t}}$ compared to NLO, NNLO predictions. The contours obtained from the data (full circle) represent the 68 (full line) and 90% C.L. (dashed line) areas accounting for the full set of systematic uncertainties described in Table II. Contours labeled "th. extrap. uncertainty" depict the theoretical uncertainties on extrapolating the fiducial cross-section to the full phase space and are obtained by constructing a likelihood function with only theoretical uncertainties. The theoretical WW cross-section does not include contributions from $gg \to H \to WW$. The theoretical cross-section predictions are shown at NLO (a, b, and c) or NNLO (d) in QCD for different PDF sets (open symbols) with the ellipse contours corresponding to the 68% C.L. uncertainties on each PDF set. Also shown as horizontal and vertical error bars around each prediction are the uncertainties due to the choice of QCD factorization and renormalization scales (see text).

TABLE VII. Correlation factors of the fitted yields for measured signal processes. These values give the correlations between the numbers of fitted events in the fiducial region which includes leptons from τ decays.

Processes	Correlation
$Z/\gamma^* \to \tau\tau$ versus WW	0.37
WW versus $t\bar{t}$	0.53
$Z/\gamma^* \to \tau\tau$ versus $t\bar{t}$	0.61

VIII. CONCLUSION

Simultaneous measurements of the $t\bar{t}$, WW and $Z/\gamma^* \to \tau\tau$ fiducial and total production cross-sections using 4.6 fb^{-1} of data collected with the ATLAS detector from pp collisions at $\sqrt{s} = 7$ TeV at the LHC are presented. Exactly two high transverse momentum isolated leptons are selected, and are required to be one electron and one muon of opposite charge. The number of signal events is extracted using a template fit to the distribution of missing transverse momentum and jet multiplicity observed in the data. The measurements are consistent with the previously published dedicated ATLAS cross-section measurements and with the predicted theoretical cross-sections within their uncertainties. This simultaneous extraction of the cross-sections for these processes at the LHC provides a broader test of the SM predictions than individual measurements by unifying the fiducial region, object and event requirements, and background estimations. The uncertainty bands of the measured fiducial cross-sections of $t\bar{t}$ and $Z/\gamma^* \to \tau\tau$ suggest that the NLO predictions underestimate the data, while comparisons to NNLO calculations indicate that MSTW2008, CT10, HERAPDF, NNPDF, and epWZ PDF sets describe the data well.

ACKNOWLEDGMENTS

We thank CERN for the very successful operation of the LHC, as well as the support staff from our institutions without whom ATLAS could not be operated efficiently. We acknowledge the support of ANPCyT, Argentina; YerPhI, Armenia; ARC, Australia; BMWF and FWF, Austria; ANAS, Azerbaijan; SSTC, Belarus; CNPq and FAPESP, Brazil; NSERC, NRC and CFI, Canada; CERN; CONICYT, Chile; CAS, MOST and NSFC, China; COLCIENCIAS, Colombia; MSMT CR, MPO CR and VSC CR, Czech Republic; DNRF, DNSRC and Lundbeck Foundation, Denmark; EPLANET, ERC and NSRF, European Union; IN2P3-CNRS, CEA-DSM/IRFU, France; GNSF, Georgia; BMBF, DFG, HGF, MPG and AvH Foundation, Germany; GSRT and NSRF, Greece; ISF, MINERVA, GIF, I-CORE and Benoziyo Center, Israel; INFN, Italy; MEXT and JSPS, Japan; CNRST, Morocco; FOM and NWO, Netherlands; BRF and RCN, Norway; MNiSW and NCN, Poland; GRICES and FCT, Portugal; MNE/IFA, Romania; MES of Russia and ROSATOM, Russian Federation; JINR; MSTD, Serbia; MSSR, Slovakia; ARRS and MIZŠ, Slovenia; DST/NRF, South Africa; MINECO, Spain; SRC and Wallenberg Foundation, Sweden; SER, SNSF and Cantons of Bern and Geneva, Switzerland; NSC, Taiwan; TAEK, Turkey; STFC, the Royal Society and Leverhulme Trust, United Kingdom; DOE and NSF, USA. The crucial computing support from all WLCG partners is acknowledged gratefully, in particular from CERN and the ATLAS Tier-1 facilities at TRIUMF (Canada), NDGF (Denmark, Norway, Sweden), CC-IN2P3 (France), KIT/GridKA (Germany), INFN-CNAF (Italy), NL-T1 (Netherlands), PIC (Spain), ASGC (Taiwan), RAL (UK) and BNL (USA) and in the Tier-2 facilities worldwide.

[1] A. Abulencia *et al.* (CDF Collaboration), Phys. Rev. D **78**, 012003 (2008).
[2] ATLAS Collaboration, JINST **3**, S08003 (2008).
[3] ATLAS Collaboration, Eur. Phys. J. C **73**, 2518 (2013).
[4] ATLAS Collaboration, Eur. Phys. J. C **74**, 3109 (2014).
[5] ATLAS Collaboration, Phys. Rev. D **87**, 112001 (2013).
[6] ATLAS Collaboration, Phys. Rev. D **84**, 112006 (2011).
[7] CMS Collaboration, J. High Energy Phys. 11 (2012) 067.
[8] CMS Collaboration, Eur. Phys. J. C **73**, 2610 (2013).
[9] CMS Collaboration, J. High Energy Phys. 08 (2011) 117.
[10] The ATLAS reference system is a right-hand Cartesian coordinate system, with the nominal collision point at the origin. The anticlockwise beam direction defines the positive z axis, while the positive x axis is defined as pointing from the collision point to the center of the LHC ring and the positive y axis points upwards. The azimuthal angle, ϕ, is measured around the beam axis, and the polar angle, θ, is the angle measured with respect to the z axis. The pseudorapidity is given by $-\ln\tan(\theta/2)$. Transverse momentum and energy are defined as $p_{\mathrm{T}} = p\sin\theta$ and $E_{\mathrm{T}} = E\sin\theta$, respectively.
[11] ATLAS Collaboration, Eur. Phys. J. C **70**, 823 (2010).
[12] S. Agostinelli *et al.* (GEANT4 Collaboration), Nucl. Instrum. Methods Phys. Res., Sect. A **506**, 250 (2003).
[13] K. Nakamura *et al.* (Particle Data Group Collaboration), J. Phys. G **37**, 075021 (2010).
[14] T. Sjostrand, S. Mrenna, and P. Z. Skands, J. High Energy Phys. 05 (2006) 026.
[15] J. Butterworth, J. R. Forshaw, and M. Seymour, Z. Phys. C **72**, 637 (1996).

[16] G. Corcella, I. G. Knowles, G. Marchesini, S. Moretti, K. Odagiri, P. Richardson, M. H. Seymour, and B. R. Webber, J. High Energy Phys. 01 (2001) 010.
[17] H.-L. Lai, M. Guzzi, J. Huston, Z. Li, P. M. Nadolsky, J. Pumplin, and C.-P. Yuan, Phys. Rev. D **82**, 074024 (2010).
[18] M. L. Mangano, M. Moretti, F. Piccinini, R. Pittau, and A. D. Polosa, J. High Energy Phys. 07 (2003) 001.
[19] D. Stump, J. Huston, J. Pumplin, W.-K. Tung, H.-L. Lai, S. Kuhlmann, and J. F. Owens, J. High Energy Phys. 10 (2003) 046.
[20] S. Frixione and B. R. Webber, J. High Energy Phys. 06 (2002) 029.
[21] M. Cacciari, M. Czakon, M. Mangano, A. Mitov, and P. Nason, Phys. Lett. B **710**, 612 (2012).
[22] P. Bärnreuther, M. Czakon, and A. Mitov, Phys. Rev. Lett. **109**, 132001 (2012).
[23] M. Czakon and A. Mitov, J. High Energy Phys. 12 (2012) 054.
[24] M. Czakon and A. Mitov, J. High Energy Phys. 01 (2013) 080.
[25] M. Czakon, P. Fiedler, and A. Mitov, Phys. Rev. Lett. **110**, 252004 (2013).
[26] M. Czakon and A. Mitov, Comput. Phys. Commun. **185**, 2930 (2014).
[27] T. A. Aaltonen *et al.* (Tevatron Electroweak Working Group, CDF Collaboration, D0 Collaboration), arXiv:0808.1089.
[28] M. Botje, J. Butterworth, A. Cooper-Sarkar, A. de Roeck, J. Feltesse *et al.*, arXiv:1101.0538.
[29] A. Martin, W. Stirling, R. Thorne, and G. Watt, Eur. Phys. J. C **63**, 189 (2009).
[30] A. Martin, W. Stirling, R. Thorne, and G. Watt, Eur. Phys. J. C **64**, 653 (2009).
[31] J. Gao, M. Guzzi, J. Huston, H.-L. Lai, Z. Li, P. Nadolsky, J. Pumplin, D. Stump, and C.-P. Yuan, Phys. Rev. D **89**, 033009 (2014).
[32] R. D. Ball, V. Bertone, S. Carrazza, C. S. Deans, L. Del Debbio *et al.*, Nucl. Phys. **B867**, 244 (2013).
[33] S. Alioli, P. Nason, C. Oleari, and E. Re, J. High Energy Phys. 06 (2010) 043.
[34] T. Binoth, M. Ciccolini, N. Kauer, and M. Kramer, J. High Energy Phys. 12 (2006) 046.
[35] J. Campbell, E. Castaneda-Miranda, Y. Fang, N. Kauer, B. Mellado, and S. Wu, Phys. Rev. D **80**, 054023 (2009).
[36] S. Heinemeyer *et al.* (LHC Higgs Cross Section Working Group Collaboration), arXiv:1307.1347.
[37] T. Gleisberg, S. Höche, F. Krauss, M. Schönherr, S. Schumann, F. Siegert, and J. Winter, J. High Energy Phys. 02 (2009) 007.
[38] R. Gavin, Y. Li, F. Petriello, and S. Quackenbush, Comput. Phys. Commun. **182**, 2388 (2011).
[39] S. Frixione, E. Laenen, P. Motylinski, and B. R. Webber, J. High Energy Phys. 03 (2006) 092.
[40] S. Frixione, E. Laenen, P. Motylinski, B. R. Webber, and C. D. White, J. High Energy Phys. 07 (2008) 029.
[41] N. Kidonakis, Phys. Rev. D **82**, 054018 (2010).
[42] J. M. Campbell, R. K. Ellis, and D. L. Rainwater, Phys. Rev. D **68**, 094021 (2003).
[43] ATLAS Collaboration, Eur. Phys. J. C **74**, 2941 (2014).
[44] ATLAS Collaboration, Report No. ATLAS-CONF-2010-036.
[45] ATLAS Collaboration, Report No. ATLAS-CONF-2010-064.
[46] M. Cacciari, G. P. Salam, and G. Soyez, J. High Energy Phys. 04 (2008) 063.
[47] ATLAS Collaboration, Eur. Phys. J. C **73**, 2304 (2013).
[48] ATLAS Collaboration, JINST **9**, P07024 (2014).
[49] ATLAS Collaboration, Eur. Phys. J. C **70**, 1193 (2010).
[50] ATLAS Collaboration, Eur. Phys. J. C **75**, 17 (2015).
[51] ATLAS Collaboration, Eur. Phys. J. C **72**, 1844 (2012).
[52] ATLAS Collaboration, Eur. Phys. J. C **71**, 1577 (2011).
[53] J. Wenninger, Report No. CERN-ATS-2013-40, 2013.
[54] ATLAS Collaboration, Report No. ATLAS-CONF-2011-032.
[55] ATLAS Collaboration, Eur. Phys. J. C **73**, 2306 (2013).
[56] J. Beringer *et al.* (Particle Data Group Collaboration), Phys. Rev. D **86**, 010001 (2012).
[57] S. Alekhin, J. Blumlein, and S. Moch, Phys. Rev. D **86**, 054009 (2012).
[58] A. D. Martin, A. J. Th. M. Mathijssen, W. J. Stirling, R. S. Thorne, B. J. A. Watt, and G. Watt, Eur. Phys. J. C **73**, 2318 (2013).
[59] V. Radescu (H1, ZEUS Collaboration), *Proc. Sci.*, ICHEP2010 (2010) 168, http://pos.sissa.it/archive/conferences/120/168/ICHEP%202010_168.pdf.
[60] P. Jimenez-Delgado and E. Reya, Phys. Rev. D **80**, 114011 (2009).
[61] ATLAS Collaboration, Phys. Rev. Lett. **109**, 012001 (2012).

G. Aad,[84] B. Abbott,[112] J. Abdallah,[152] S. Abdel Khalek,[116] O. Abdinov,[11] R. Aben,[106] B. Abi,[113] M. Abolins,[89] O. S. AbouZeid,[159] H. Abramowicz,[154] H. Abreu,[153] R. Abreu,[30] Y. Abulaiti,[147a,147b] B. S. Acharya,[165a,165b,b] L. Adamczyk,[38a] D. L. Adams,[25] J. Adelman,[177] S. Adomeit,[99] T. Adye,[130] T. Agatonovic-Jovin,[13a] J. A. Aguilar-Saavedra,[125a,125f] M. Agustoni,[17] S. P. Ahlen,[22] F. Ahmadov,[64,c] G. Aielli,[134a,134b] H. Akerstedt,[147a,147b] T. P. A. Åkesson,[80] G. Akimoto,[156] A. V. Akimov,[95] G. L. Alberghi,[20a,20b] J. Albert,[170] S. Albrand,[55] M. J. Alconada Verzini,[70] M. Aleksa,[30] I. N. Aleksandrov,[64] C. Alexa,[26a] G. Alexander,[154] G. Alexandre,[49] T. Alexopoulos,[10] M. Alhroob,[165a,165c] G. Alimonti,[90a] L. Alio,[84] J. Alison,[31] B. M. M. Allbrooke,[18] L. J. Allison,[71] P. P. Allport,[73] J. Almond,[83] A. Aloisio,[103a,103b] A. Alonso,[36] F. Alonso,[70] C. Alpigiani,[75] A. Altheimer,[35] B. Alvarez Gonzalez,[89] M. G. Alviggi,[103a,103b] K. Amako,[65] Y. Amaral Coutinho,[24a] C. Amelung,[23] D. Amidei,[88] S. P. Amor Dos Santos,[125a,125c] A. Amorim,[125a,125b] S. Amoroso,[48] N. Amram,[154] G. Amundsen,[23] C. Anastopoulos,[140] L. S. Ancu,[49] N. Andari,[30] T. Andeen,[35] C. F. Anders,[58b]

G. Anders,[30] K. J. Anderson,[31] A. Andreazza,[90a,90b] V. Andrei,[58a] X. S. Anduaga,[70] S. Angelidakis,[9] I. Angelozzi,[106] P. Anger,[44] A. Angerami,[35] F. Anghinolfi,[30] A. V. Anisenkov,[108] N. Anjos,[125a] A. Annovi,[47] A. Antonaki,[9] M. Antonelli,[47] A. Antonov,[97] J. Antos,[145b] F. Anulli,[133a] M. Aoki,[65] L. Aperio Bella,[18] R. Apolle,[119,d] G. Arabidze,[89] I. Aracena,[144] Y. Arai,[65] J. P. Araque,[125a] A. T. H. Arce,[45] J-F. Arguin,[94] S. Argyropoulos,[42] M. Arik,[19a] A. J. Armbruster,[30] O. Arnaez,[30] V. Arnal,[81] H. Arnold,[48] M. Arratia,[28] O. Arslan,[21] A. Artamonov,[96] G. Artoni,[23] S. Asai,[156] N. Asbah,[42] A. Ashkenazi,[154] B. Åsman,[147a,147b] L. Asquith,[6] K. Assamagan,[25] R. Astalos,[145a] M. Atkinson,[166] N. B. Atlay,[142] B. Auerbach,[6] K. Augsten,[127] M. Aurousseau,[146b] G. Avolio,[30] G. Azuelos,[94,e] Y. Azuma,[156] M. A. Baak,[30] A. Baas,[58a] C. Bacci,[135a,135b] H. Bachacou,[137] K. Bachas,[155] M. Backes,[30] M. Backhaus,[30] J. Backus Mayes,[144] E. Badescu,[26a] P. Bagiacchi,[133a,133b] P. Bagnaia,[133a,133b] Y. Bai,[33a] T. Bain,[35] J. T. Baines,[130] O. K. Baker,[177] P. Balek,[128] F. Balli,[137] E. Banas,[39] Sw. Banerjee,[174] A. A. E. Bannoura,[176] V. Bansal,[170] H. S. Bansil,[18] L. Barak,[173] S. P. Baranov,[95] E. L. Barberio,[87] D. Barberis,[50a,50b] M. Barbero,[84] T. Barillari,[100] M. Barisonzi,[176] T. Barklow,[144] N. Barlow,[28] B. M. Barnett,[130] R. M. Barnett,[15] Z. Barnovska,[5] A. Baroncelli,[135a] G. Barone,[49] A. J. Barr,[119] F. Barreiro,[81] J. Barreiro Guimarães da Costa,[57] R. Bartoldus,[144] A. E. Barton,[71] P. Bartos,[145a] V. Bartsch,[150] A. Bassalat,[116] A. Basye,[166] R. L. Bates,[53] L. Batkova,[145a] J. R. Batley,[28] M. Battaglia,[138] M. Battistin,[30] F. Bauer,[137] H. S. Bawa,[144,f] T. Beau,[79] P. H. Beauchemin,[162] R. Beccherle,[123a,123b] P. Bechtle,[21] H. P. Beck,[17] K. Becker,[176] S. Becker,[99] M. Beckingham,[171] C. Becot,[116] A. J. Beddall,[19c] A. Beddall,[19c] S. Bedikian,[177] V. A. Bednyakov,[64] C. P. Bee,[149] L. J. Beemster,[106] T. A. Beermann,[176] M. Begel,[25] K. Behr,[119] C. Belanger-Champagne,[86] P. J. Bell,[49] W. H. Bell,[49] G. Bella,[154] L. Bellagamba,[20a] A. Bellerive,[29] M. Bellomo,[85] K. Belotskiy,[97] O. Beltramello,[30] O. Benary,[154] D. Benchekroun,[136a] K. Bendtz,[147a,147b] N. Benekos,[166] Y. Benhammou,[154] E. Benhar Noccioli,[49] J. A. Benitez Garcia,[160b] D. P. Benjamin,[45] J. R. Bensinger,[23] K. Benslama,[131] S. Bentvelsen,[106] D. Berge,[106] E. Bergeaas Kuutmann,[16] N. Berger,[5] F. Berghaus,[170] J. Beringer,[15] C. Bernard,[22] P. Bernat,[77] C. Bernius,[78] F. U. Bernlochner,[170] T. Berry,[76] P. Berta,[128] C. Bertella,[84] G. Bertoli,[147a,147b] F. Bertolucci,[123a,123b] D. Bertsche,[112] M. I. Besana,[90a] G. J. Besjes,[105] O. Bessidskaia Bylund,[147a,147b] M. F. Bessner,[42] N. Besson,[137] C. Betancourt,[48] S. Bethke,[100] W. Bhimji,[46] R. M. Bianchi,[124] L. Bianchini,[23] M. Bianco,[30] O. Biebel,[99] S. P. Bieniek,[77] K. Bierwagen,[54] J. Biesiada,[15] M. Biglietti,[135a] J. Bilbao De Mendizabal,[49] H. Bilokon,[47] M. Bindi,[54] S. Binet,[116] A. Bingul,[19c] C. Bini,[133a,133b] C. W. Black,[151] J. E. Black,[144] K. M. Black,[22] D. Blackburn,[139] R. E. Blair,[6] J.-B. Blanchard,[137] T. Blazek,[145a] I. Bloch,[42] C. Blocker,[23] W. Blum,[82,a] U. Blumenschein,[54] G. J. Bobbink,[106] V. S. Bobrovnikov,[108] S. S. Bocchetta,[80] A. Bocci,[45] C. Bock,[99] C. R. Boddy,[119] M. Boehler,[48] T. T. Boek,[176] J. A. Bogaerts,[30] A. G. Bogdanchikov,[108] A. Bogouch,[91,a] C. Bohm,[147a] J. Bohm,[126] V. Boisvert,[76] T. Bold,[38a] V. Boldea,[26a] A. S. Boldyrev,[98] M. Bomben,[79] M. Bona,[75] M. Boonekamp,[137] A. Borisov,[129] G. Borissov,[71] M. Borri,[83] S. Borroni,[42] J. Bortfeldt,[99] V. Bortolotto,[135a,135b] K. Bos,[106] D. Boscherini,[20a] M. Bosman,[12] H. Boterenbrood,[106] J. Boudreau,[124] J. Bouffard,[2] E. V. Bouhova-Thacker,[71] D. Boumediene,[34] C. Bourdarios,[116] N. Bousson,[113] S. Boutouil,[136d] A. Boveia,[31] J. Boyd,[30] I. R. Boyko,[64] J. Bracinik,[18] A. Brandt,[8] G. Brandt,[15] O. Brandt,[58a] U. Bratzler,[157] B. Brau,[85] J. E. Brau,[115] H. M. Braun,[176,a] S. F. Brazzale,[165a,165c] B. Brelier,[159] K. Brendlinger,[121] A. J. Brennan,[87] R. Brenner,[167] S. Bressler,[173] K. Bristow,[146c] T. M. Bristow,[46] D. Britton,[53] F. M. Brochu,[28] I. Brock,[21] R. Brock,[89] C. Bromberg,[89] J. Bronner,[100] G. Brooijmans,[35] T. Brooks,[76] W. K. Brooks,[32b] J. Brosamer,[15] E. Brost,[115] J. Brown,[55] P. A. Bruckman de Renstrom,[39] D. Bruncko,[145b] R. Bruneliere,[48] S. Brunet,[60] A. Bruni,[20a] G. Bruni,[20a] M. Bruschi,[20a] L. Bryngemark,[80] T. Buanes,[14] Q. Buat,[143] F. Bucci,[49] P. Buchholz,[142] R. M. Buckingham,[119] A. G. Buckley,[53] S. I. Buda,[26a] I. A. Budagov,[64] F. Buehrer,[48] L. Bugge,[118] M. K. Bugge,[118] O. Bulekov,[97] A. C. Bundock,[73] H. Burckhart,[30] S. Burdin,[73] B. Burghgrave,[107] S. Burke,[130] I. Burmeister,[43] E. Busato,[34] D. Büscher,[48] V. Büscher,[82] P. Bussey,[53] C. P. Buszello,[167] B. Butler,[57] J. M. Butler,[22] A. I. Butt,[3] C. M. Buttar,[53] J. M. Butterworth,[77] P. Butti,[106] W. Buttinger,[28] A. Buzatu,[53] M. Byszewski,[10] S. Cabrera Urbán,[168] D. Caforio,[20a,20b] O. Cakir,[4a] P. Calafiura,[15] A. Calandri,[137] G. Calderini,[79] P. Calfayan,[99] R. Calkins,[107] L. P. Caloba,[24a] D. Calvet,[34] S. Calvet,[34] R. Camacho Toro,[49] S. Camarda,[42] D. Cameron,[118] L. M. Caminada,[15] R. Caminal Armadans,[12] S. Campana,[30] M. Campanelli,[77] A. Campoverde,[149] V. Canale,[103a,103b] A. Canepa,[160a] M. Cano Bret,[75] J. Cantero,[81] R. Cantrill,[76] T. Cao,[40] M. D. M. Capeans Garrido,[30] I. Caprini,[26a] M. Caprini,[26a] M. Capua,[37a,37b] R. Caputo,[82] R. Cardarelli,[134a] T. Carli,[30] G. Carlino,[103a] L. Carminati,[90a,90b] S. Caron,[105] E. Carquin,[32a] G. D. Carrillo-Montoya,[146c] J. R. Carter,[28] J. Carvalho,[125a,125c] D. Casadei,[77] M. P. Casado,[12] M. Casolino,[12] E. Castaneda-Miranda,[146b] A. Castelli,[106] V. Castillo Gimenez,[168] N. F. Castro,[125a] P. Catastini,[57] A. Catinaccio,[30] J. R. Catmore,[118] A. Cattai,[30] G. Cattani,[134a,134b] S. Caughron,[89] V. Cavaliere,[166] D. Cavalli,[90a] M. Cavalli-Sforza,[12] V. Cavasinni,[123a,123b] F. Ceradini,[135a,135b] B. Cerio,[45] K. Cerny,[128] A. S. Cerqueira,[24b] A. Cerri,[150] L. Cerrito,[75] F. Cerutti,[15] M. Cerv,[30] A. Cervelli,[17] S. A. Cetin,[19b] A. Chafaq,[136a]

D. Chakraborty,[107] I. Chalupkova,[128] P. Chang,[166] B. Chapleau,[86] J. D. Chapman,[28] D. Charfeddine,[116] D. G. Charlton,[18] C. C. Chau,[159] C. A. Chavez Barajas,[150] S. Cheatham,[86] A. Chegwidden,[89] S. Chekanov,[6] S. V. Chekulaev,[160a] G. A. Chelkov,[64,g] M. A. Chelstowska,[88] C. Chen,[63] H. Chen,[25] K. Chen,[149] L. Chen,[33d,h] S. Chen,[33c] X. Chen,[146c] Y. Chen,[35] H. C. Cheng,[88] Y. Cheng,[31] A. Cheplakov,[64] R. Cherkaoui El Moursli,[136e] V. Chernyatin,[25,a] E. Cheu,[7] L. Chevalier,[137] V. Chiarella,[47] G. Chiefari,[103a,103b] J. T. Childers,[6] A. Chilingarov,[71] G. Chiodini,[72a] A. S. Chisholm,[18] R. T. Chislett,[77] A. Chitan,[26a] M. V. Chizhov,[64] S. Chouridou,[9] B. K. B. Chow,[99] D. Chromek-Burckhart,[30] M. L. Chu,[152] J. Chudoba,[126] J. J. Chwastowski,[39] L. Chytka,[114] G. Ciapetti,[133a,133b] A. K. Ciftci,[4a] R. Ciftci,[4a] D. Cinca,[53] V. Cindro,[74] A. Ciocio,[15] P. Cirkovic,[13b] Z. H. Citron,[173] M. Citterio,[90a] M. Ciubancan,[26a] A. Clark,[49] P. J. Clark,[46] R. N. Clarke,[15] W. Cleland,[124] J. C. Clemens,[84] C. Clement,[147a,147b] Y. Coadou,[84] M. Cobal,[165a,165c] A. Coccaro,[139] J. Cochran,[63] L. Coffey,[23] J. G. Cogan,[144] J. Coggeshall,[166] B. Cole,[35] S. Cole,[107] A. P. Colijn,[106] J. Collot,[55] T. Colombo,[58c] G. Colon,[85] G. Compostella,[100] P. Conde Muiño,[125a,125b] E. Coniavitis,[48] M. C. Conidi,[12] S. H. Connell,[146b] I. A. Connelly,[76] S. M. Consonni,[90a,90b] V. Consorti,[48] S. Constantinescu,[26a] C. Conta,[120a,120b] G. Conti,[57] F. Conventi,[103a,i] M. Cooke,[15] B. D. Cooper,[77] A. M. Cooper-Sarkar,[119] N. J. Cooper-Smith,[76] K. Copic,[15] T. Cornelissen,[176] M. Corradi,[20a] F. Corriveau,[86,j] A. Corso-Radu,[164] A. Cortes-Gonzalez,[12] G. Cortiana,[100] G. Costa,[90a] M. J. Costa,[168] D. Costanzo,[140] D. Côté,[8] G. Cottin,[28] G. Cowan,[76] B. E. Cox,[83] K. Cranmer,[109] G. Cree,[29] S. Crépé-Renaudin,[55] F. Crescioli,[79] W. A. Cribbs,[147a,147b] M. Crispin Ortuzar,[119] M. Cristinziani,[21] V. Croft,[105] G. Crosetti,[37a,37b] C.-M. Cuciuc,[26a] T. Cuhadar Donszelmann,[140] J. Cummings,[177] M. Curatolo,[47] C. Cuthbert,[151] H. Czirr,[142] P. Czodrowski,[3] Z. Czyczula,[177] S. D'Auria,[53] M. D'Onofrio,[73] M. J. Da Cunha Sargedas De Sousa,[125a,125b] C. Da Via,[83] W. Dabrowski,[38a] A. Dafinca,[119] T. Dai,[88] O. Dale,[14] F. Dallaire,[94] C. Dallapiccola,[85] M. Dam,[36] A. C. Daniells,[18] M. Dano Hoffmann,[137] V. Dao,[105] G. Darbo,[50a] S. Darmora,[8] J. A. Dassoulas,[42] A. Dattagupta,[60] W. Davey,[21] C. David,[170] T. Davidek,[128] E. Davies,[119,d] M. Davies,[154] O. Davignon,[79] A. R. Davison,[77] P. Davison,[77] Y. Davygora,[58a] E. Dawe,[143] I. Dawson,[140] R. K. Daya-Ishmukhametova,[85] K. De,[8] R. de Asmundis,[103a] S. De Castro,[20a,20b] S. De Cecco,[79] N. De Groot,[105] P. de Jong,[106] H. De la Torre,[81] F. De Lorenzi,[63] L. De Nooij,[106] D. De Pedis,[133a] A. De Salvo,[133a] U. De Sanctis,[165a,165b] A. De Santo,[150] J. B. De Vivie De Regie,[116] W. J. Dearnaley,[71] R. Debbe,[25] C. Debenedetti,[138] B. Dechenaux,[55] D. V. Dedovich,[64] I. Deigaard,[106] J. Del Peso,[81] T. Del Prete,[123a,123b] F. Deliot,[137] C. M. Delitzsch,[49] M. Deliyergiyev,[74] A. Dell'Acqua,[30] L. Dell'Asta,[22] M. Dell'Orso,[123a,123b] M. Della Pietra,[103a,i] D. della Volpe,[49] M. Delmastro,[5] P. A. Delsart,[55] C. Deluca,[106] S. Demers,[177] M. Demichev,[64] A. Demilly,[79] S. P. Denisov,[129] D. Derendarz,[39] J. E. Derkaoui,[136d] F. Derue,[79] P. Dervan,[73] K. Desch,[21] C. Deterre,[42] P. O. Deviveiros,[106] A. Dewhurst,[130] S. Dhaliwal,[106] A. Di Ciaccio,[134a,134b] L. Di Ciaccio,[5] A. Di Domenico,[133a,133b] C. Di Donato,[103a,103b] A. Di Girolamo,[30] B. Di Girolamo,[30] A. Di Mattia,[153] B. Di Micco,[135a,135b] R. Di Nardo,[47] A. Di Simone,[48] R. Di Sipio,[20a,20b] D. Di Valentino,[29] F. A. Dias,[46] M. A. Diaz,[32a] E. B. Diehl,[88] J. Dietrich,[42] T. A. Dietzsch,[58a] S. Diglio,[84] A. Dimitrievska,[13a] J. Dingfelder,[21] C. Dionisi,[133a,133b] P. Dita,[26a] S. Dita,[26a] F. Dittus,[30] F. Djama,[84] T. Djobava,[51b] M. A. B. do Vale,[24c] A. Do Valle Wemans,[125a,125g] T. K. O. Doan,[5] D. Dobos,[30] C. Doglioni,[49] T. Doherty,[53] T. Dohmae,[156] J. Dolejsi,[128] Z. Dolezal,[128] B. A. Dolgoshein,[97,a] M. Donadelli,[24d] S. Donati,[123a,123b] P. Dondero,[120a,120b] J. Donini,[34] J. Dopke,[130] A. Doria,[103a] M. T. Dova,[70] A. T. Doyle,[53] M. Dris,[10] J. Dubbert,[88] S. Dube,[15] E. Dubreuil,[34] E. Duchovni,[173] G. Duckeck,[99] O. A. Ducu,[26a] D. Duda,[176] A. Dudarev,[30] F. Dudziak,[63] L. Duflot,[116] L. Duguid,[76] M. Dührssen,[30] M. Dunford,[58a] H. Duran Yildiz,[4a] M. Düren,[52] A. Durglishvili,[51b] M. Dwuznik,[38a] M. Dyndal,[38a] J. Ebke,[99] W. Edson,[2] N. C. Edwards,[46] W. Ehrenfeld,[21] T. Eifert,[144] G. Eigen,[14] K. Einsweiler,[15] T. Ekelof,[167] M. El Kacimi,[136c] M. Ellert,[167] S. Elles,[5] F. Ellinghaus,[82] N. Ellis,[30] J. Elmsheuser,[99] M. Elsing,[30] D. Emeliyanov,[130] Y. Enari,[156] O. C. Endner,[82] M. Endo,[117] R. Engelmann,[149] J. Erdmann,[177] A. Ereditato,[17] D. Eriksson,[147a] G. Ernis,[176] J. Ernst,[2] M. Ernst,[25] J. Ernwein,[137] D. Errede,[166] S. Errede,[166] E. Ertel,[82] M. Escalier,[116] H. Esch,[43] C. Escobar,[124] B. Esposito,[47] A. I. Etienvre,[137] E. Etzion,[154] H. Evans,[60] A. Ezhilov,[122] L. Fabbri,[20a,20b] G. Facini,[31] R. M. Fakhrutdinov,[129] S. Falciano,[133a] R. J. Falla,[77] J. Faltova,[128] Y. Fang,[33a] M. Fanti,[90a,90b] A. Farbin,[8] A. Farilla,[135a] T. Farooque,[12] S. Farrell,[164] S. M. Farrington,[171] P. Farthouat,[30] F. Fassi,[136e] P. Fassnacht,[30] D. Fassouliotis,[9] A. Favareto,[50a,50b] L. Fayard,[116] P. Federic,[145a] O. L. Fedin,[122,k] W. Fedorko,[169] M. Fehling-Kaschek,[48] S. Feigl,[30] L. Feligioni,[84] C. Feng,[33d] E. J. Feng,[6] H. Feng,[88] A. B. Fenyuk,[129] S. Fernandez Perez,[30] S. Ferrag,[53] J. Ferrando,[53] A. Ferrari,[167] P. Ferrari,[106] R. Ferrari,[120a] D. E. Ferreira de Lima,[53] A. Ferrer,[168] D. Ferrere,[49] C. Ferretti,[88] A. Ferretto Parodi,[50a,50b] M. Fiascaris,[31] F. Fiedler,[82] A. Filipčič,[74] M. Filipuzzi,[42] F. Filthaut,[105] M. Fincke-Keeler,[170] K. D. Finelli,[151] M. C. N. Fiolhais,[125a,125c] L. Fiorini,[168] A. Firan,[40] A. Fischer,[2] J. Fischer,[176] W. C. Fisher,[89] E. A. Fitzgerald,[23] M. Flechl,[48] I. Fleck,[142] P. Fleischmann,[88] S. Fleischmann,[176] G. T. Fletcher,[140] G. Fletcher,[75] T. Flick,[176]

A. Floderus,[80] L. R. Flores Castillo,[174,l] A. C. Florez Bustos,[160b] M. J. Flowerdew,[100] A. Formica,[137] A. Forti,[83] D. Fortin,[160a] D. Fournier,[116] H. Fox,[71] S. Fracchia,[12] P. Francavilla,[79] M. Franchini,[20a,20b] S. Franchino,[30] D. Francis,[30] M. Franklin,[57] S. Franz,[61] M. Fraternali,[120a,120b] S. T. French,[28] C. Friedrich,[42] F. Friedrich,[44] D. Froidevaux,[30] J. A. Frost,[28] C. Fukunaga,[157] E. Fullana Torregrosa,[82] B. G. Fulsom,[144] J. Fuster,[168] C. Gabaldon,[55] O. Gabizon,[173] A. Gabrielli,[20a,20b] A. Gabrielli,[133a,133b] S. Gadatsch,[106] S. Gadomski,[49] G. Gagliardi,[50a,50b] P. Gagnon,[60] C. Galea,[105] B. Galhardo,[125a,125c] E. J. Gallas,[119] V. Gallo,[17] B. J. Gallop,[130] P. Gallus,[127] G. Galster,[36] K. K. Gan,[110] R. P. Gandrajula,[62] J. Gao,[33b,h] Y. S. Gao,[144,f] F. M. Garay Walls,[46] F. Garberson,[177] C. García,[168] J. E. García Navarro,[168] M. Garcia-Sciveres,[15] R. W. Gardner,[31] N. Garelli,[144] V. Garonne,[30] C. Gatti,[47] G. Gaudio,[120a] B. Gaur,[142] L. Gauthier,[94] P. Gauzzi,[133a,133b] I. L. Gavrilenko,[95] C. Gay,[169] G. Gaycken,[21] E. N. Gazis,[10] P. Ge,[33d] Z. Gecse,[169] C. N. P. Gee,[130] D. A. A. Geerts,[106] Ch. Geich-Gimbel,[21] K. Gellerstedt,[147a,147b] C. Gemme,[50a] A. Gemmell,[53] M. H. Genest,[55] S. Gentile,[133a,133b] M. George,[54] S. George,[76] D. Gerbaudo,[164] A. Gershon,[154] H. Ghazlane,[136b] N. Ghodbane,[34] B. Giacobbe,[20a] S. Giagu,[133a,133b] V. Giangiobbe,[12] P. Giannetti,[123a,123b] F. Gianotti,[30] B. Gibbard,[25] S. M. Gibson,[76] M. Gilchriese,[15] T. P. S. Gillam,[28] D. Gillberg,[30] G. Gilles,[34] D. M. Gingrich,[3,e] N. Giokaris,[9] M. P. Giordani,[165a,165c] R. Giordano,[103a,103b] F. M. Giorgi,[20a] F. M. Giorgi,[16] P. F. Giraud,[137] D. Giugni,[90a] C. Giuliani,[48] M. Giulini,[58b] B. K. Gjelsten,[118] S. Gkaitatzis,[155] I. Gkialas,[155,m] L. K. Gladilin,[98] C. Glasman,[81] J. Glatzer,[30] P. C. F. Glaysher,[46] A. Glazov,[42] G. L. Glonti,[64] M. Goblirsch-Kolb,[100] J. R. Goddard,[75] J. Godfrey,[143] J. Godlewski,[30] C. Goeringer,[82] S. Goldfarb,[88] T. Golling,[177] D. Golubkov,[129] A. Gomes,[125a,125b,125d] L. S. Gomez Fajardo,[42] R. Gonçalo,[125a] J. Goncalves Pinto Firmino Da Costa,[137] L. Gonella,[21] S. González de la Hoz,[168] G. Gonzalez Parra,[12] S. Gonzalez-Sevilla,[49] L. Goossens,[30] P. A. Gorbounov,[96] H. A. Gordon,[25] I. Gorelov,[104] B. Gorini,[30] E. Gorini,[72a,72b] A. Gorišek,[74] E. Gornicki,[39] A. T. Goshaw,[6] C. Gössling,[43] M. I. Gostkin,[64] M. Gouighri,[136a] D. Goujdami,[136c] M. P. Goulette,[49] A. G. Goussiou,[139] C. Goy,[5] S. Gozpinar,[23] H. M. X. Grabas,[137] L. Graber,[54] I. Grabowska-Bold,[38a] P. Grafström,[20a,20b] K-J. Grahn,[42] J. Gramling,[49] E. Gramstad,[118] S. Grancagnolo,[16] V. Grassi,[149] V. Gratchev,[122] H. M. Gray,[30] E. Graziani,[135a] O. G. Grebenyuk,[122] Z. D. Greenwood,[78,n] K. Gregersen,[77] I. M. Gregor,[42] P. Grenier,[144] J. Griffiths,[8] A. A. Grillo,[138] K. Grimm,[71] S. Grinstein,[12,o] Ph. Gris,[34] Y. V. Grishkevich,[98] J.-F. Grivaz,[116] J. P. Grohs,[44] A. Grohsjean,[42] E. Gross,[173] J. Grosse-Knetter,[54] G. C. Grossi,[134a,134b] J. Groth-Jensen,[173] Z. J. Grout,[150] L. Guan,[33b] F. Guescini,[49] D. Guest,[177] O. Gueta,[154] C. Guicheney,[34] E. Guido,[50a,50b] T. Guillemin,[116] S. Guindon,[2] U. Gul,[53] C. Gumpert,[44] J. Gunther,[127] J. Guo,[35] S. Gupta,[119] P. Gutierrez,[112] N. G. Gutierrez Ortiz,[53] C. Gutschow,[77] N. Guttman,[154] C. Guyot,[137] C. Gwenlan,[119] C. B. Gwilliam,[73] A. Haas,[109] C. Haber,[15] H. K. Hadavand,[8] N. Haddad,[136e] P. Haefner,[21] S. Hageböck,[21] Z. Hajduk,[39] H. Hakobyan,[178] M. Haleem,[42] D. Hall,[119] G. Halladjian,[89] K. Hamacher,[176] P. Hamal,[114] K. Hamano,[170] M. Hamer,[54] A. Hamilton,[146a] S. Hamilton,[162] P. G. Hamnett,[42] L. Han,[33b] K. Hanagaki,[117] K. Hanawa,[156] M. Hance,[15] P. Hanke,[58a] R. Hanna,[137] J. B. Hansen,[36] J. D. Hansen,[36] P. H. Hansen,[36] K. Hara,[161] A. S. Hard,[174] T. Harenberg,[176] F. Hariri,[116] S. Harkusha,[91] D. Harper,[88] R. D. Harrington,[46] O. M. Harris,[139] P. F. Harrison,[171] F. Hartjes,[106] S. Hasegawa,[102] Y. Hasegawa,[141] A. Hasib,[112] S. Hassani,[137] S. Haug,[17] M. Hauschild,[30] R. Hauser,[89] M. Havranek,[126] C. M. Hawkes,[18] R. J. Hawkings,[30] A. D. Hawkins,[80] T. Hayashi,[161] D. Hayden,[89] C. P. Hays,[119] H. S. Hayward,[73] S. J. Haywood,[130] S. J. Head,[18] T. Heck,[82] V. Hedberg,[80] L. Heelan,[8] S. Heim,[121] T. Heim,[176] B. Heinemann,[15] L. Heinrich,[109] J. Hejbal,[126] L. Helary,[22] C. Heller,[99] M. Heller,[30] S. Hellman,[147a,147b] D. Hellmich,[21] C. Helsens,[30] J. Henderson,[119] R. C. W. Henderson,[71] Y. Heng,[174] C. Hengler,[42] A. Henrichs,[177] A. M. Henriques Correia,[30] S. Henrot-Versille,[116] C. Hensel,[54] G. H. Herbert,[16] Y. Hernández Jiménez,[168] R. Herrberg-Schubert,[16] G. Herten,[48] R. Hertenberger,[99] L. Hervas,[30] G. G. Hesketh,[77] N. P. Hessey,[106] R. Hickling,[75] E. Higón-Rodriguez,[168] E. Hill,[170] J. C. Hill,[28] K. H. Hiller,[42] S. Hillert,[21] S. J. Hillier,[18] I. Hinchliffe,[15] E. Hines,[121] M. Hirose,[158] D. Hirschbuehl,[176] J. Hobbs,[149] N. Hod,[106] M. C. Hodgkinson,[140] P. Hodgson,[140] A. Hoecker,[30] M. R. Hoeferkamp,[104] J. Hoffman,[40] D. Hoffmann,[84] J. I. Hofmann,[58a] M. Hohlfeld,[82] T. R. Holmes,[15] T. M. Hong,[121] L. Hooft van Huysduynen,[109] J-Y. Hostachy,[55] S. Hou,[152] A. Hoummada,[136a] J. Howard,[119] J. Howarth,[42] M. Hrabovsky,[114] I. Hristova,[16] J. Hrivnac,[116] T. Hryn'ova,[5] C. Hsu,[146c] P. J. Hsu,[82] S.-C. Hsu,[139] D. Hu,[35] X. Hu,[25] Y. Huang,[42] Z. Hubacek,[30] F. Hubaut,[84] F. Huegging,[21] T. B. Huffman,[119] E. W. Hughes,[35] G. Hughes,[71] M. Huhtinen,[30] T. A. Hülsing,[82] M. Hurwitz,[15] N. Huseynov,[64,c] J. Huston,[89] J. Huth,[57] G. Iacobucci,[49] G. Iakovidis,[10] I. Ibragimov,[142] L. Iconomidou-Fayard,[116] E. Ideal,[177] P. Iengo,[103a] O. Igonkina,[106] T. Iizawa,[172] Y. Ikegami,[65] K. Ikematsu,[142] M. Ikeno,[65] Y. Ilchenko,[31,p] D. Iliadis,[155] N. Ilic,[159] Y. Inamaru,[66] T. Ince,[100] P. Ioannou,[9] M. Iodice,[135a] K. Iordanidou,[9] V. Ippolito,[57] A. Irles Quiles,[168] C. Isaksson,[167] M. Ishino,[67] M. Ishitsuka,[158] R. Ishmukhametov,[110] C. Issever,[119] S. Istin,[19a] J. M. Iturbe Ponce,[83] R. Iuppa,[134a,134b] J. Ivarsson,[80] W. Iwanski,[39] H. Iwasaki,[65] J. M. Izen,[41] V. Izzo,[103a] B. Jackson,[121] M. Jackson,[73] P. Jackson,[1] M. R. Jaekel,[30] V. Jain,[2] K. Jakobs,[48] S. Jakobsen,[30] T. Jakoubek,[126]

J. Jakubek,[127] D. O. Jamin,[152] D. K. Jana,[78] E. Jansen,[77] H. Jansen,[30] J. Janssen,[21] M. Janus,[171] G. Jarlskog,[80] N. Javadov,[64,c] T. Javůrek,[48] L. Jeanty,[15] J. Jejelava,[51a,q] G.-Y. Jeng,[151] D. Jennens,[87] P. Jenni,[48,r] J. Jentzsch,[43] C. Jeske,[171] S. Jézéquel,[5] H. Ji,[174] W. Ji,[82] J. Jia,[149] Y. Jiang,[33b] M. Jimenez Belenguer,[42] S. Jin,[33a] A. Jinaru,[26a] O. Jinnouchi,[158] M. D. Joergensen,[36] K. E. Johansson,[147a,147b] P. Johansson,[140] K. A. Johns,[7] K. Jon-And,[147a,147b] G. Jones,[171] R. W. L. Jones,[71] T. J. Jones,[73] J. Jongmanns,[58a] P. M. Jorge,[125a,125b] K. D. Joshi,[83] J. Jovicevic,[148] X. Ju,[174] C. A. Jung,[43] R. M. Jungst,[30] P. Jussel,[61] A. Juste Rozas,[12,o] M. Kaci,[168] A. Kaczmarska,[39] M. Kado,[116] H. Kagan,[110] M. Kagan,[144] E. Kajomovitz,[45] C. W. Kalderon,[119] S. Kama,[40] A. Kamenshchikov,[129] N. Kanaya,[156] M. Kaneda,[30] S. Kaneti,[28] V. A. Kantserov,[97] J. Kanzaki,[65] B. Kaplan,[109] A. Kapliy,[31] D. Kar,[53] K. Karakostas,[10] N. Karastathis,[10] M. Karnevskiy,[82] S. N. Karpov,[64] Z. M. Karpova,[64] K. Karthik,[109] V. Kartvelishvili,[71] A. N. Karyukhin,[129] L. Kashif,[174] G. Kasieczka,[58b] R. D. Kass,[110] A. Kastanas,[14] Y. Kataoka,[156] A. Katre,[49] J. Katzy,[42] V. Kaushik,[7] K. Kawagoe,[69] T. Kawamoto,[156] G. Kawamura,[54] S. Kazama,[156] V. F. Kazanin,[108] M. Y. Kazarinov,[64] R. Keeler,[170] R. Kehoe,[40] M. Keil,[54] J. S. Keller,[42] J. J. Kempster,[76] H. Keoshkerian,[5] O. Kepka,[126] B. P. Kerševan,[74] S. Kersten,[176] K. Kessoku,[156] J. Keung,[159] F. Khalil-zada,[11] H. Khandanyan,[147a,147b] A. Khanov,[113] A. Khodinov,[97] A. Khomich,[58a] T. J. Khoo,[28] G. Khoriauli,[21] A. Khoroshilov,[176] V. Khovanskiy,[96] E. Khramov,[64] J. Khubua,[51b] H. Y. Kim,[8] H. Kim,[147a,147b] S. H. Kim,[161] N. Kimura,[172] O. Kind,[16] B. T. King,[73] M. King,[168] R. S. B. King,[119] S. B. King,[169] J. Kirk,[130] A. E. Kiryunin,[100] T. Kishimoto,[66] D. Kisielewska,[38a] F. Kiss,[48] T. Kittelmann,[124] K. Kiuchi,[161] E. Kladiva,[145b] M. Klein,[73] U. Klein,[73] K. Kleinknecht,[82] P. Klimek,[147a,147b] A. Klimentov,[25] R. Klingenberg,[43] J. A. Klinger,[83] T. Klioutchnikova,[30] P. F. Klok,[105] E.-E. Kluge,[58a] P. Kluit,[106] S. Kluth,[100] E. Kneringer,[61] E. B. F. G. Knoops,[84] A. Knue,[53] D. Kobayashi,[158] T. Kobayashi,[156] M. Kobel,[44] M. Kocian,[144] P. Kodys,[128] P. Koevesarki,[21] T. Koffas,[29] E. Koffeman,[106] L. A. Kogan,[119] S. Kohlmann,[176] Z. Kohout,[127] T. Kohriki,[65] T. Koi,[144] H. Kolanoski,[16] I. Koletsou,[5] J. Koll,[89] A. A. Komar,[95,a] Y. Komori,[156] T. Kondo,[65] N. Kondrashova,[42] K. Köneke,[48] A. C. König,[105] S. König,[82] T. Kono,[65,s] R. Konoplich,[109,t] N. Konstantinidis,[77] R. Kopeliansky,[153] S. Koperny,[38a] L. Köpke,[82] A. K. Kopp,[48] K. Korcyl,[39] K. Kordas,[155] A. Korn,[77] A. A. Korol,[108,u] I. Korolkov,[12] E. V. Korolkova,[140] V. A. Korotkov,[129] O. Kortner,[100] S. Kortner,[100] V. V. Kostyukhin,[21] V. M. Kotov,[64] A. Kotwal,[45] C. Kourkoumelis,[9] V. Kouskoura,[155] A. Koutsman,[160a] R. Kowalewski,[170] T. Z. Kowalski,[38a] W. Kozanecki,[137] A. S. Kozhin,[129] V. Kral,[127] V. A. Kramarenko,[98] G. Kramberger,[74] D. Krasnopevtsev,[97] M. W. Krasny,[79] A. Krasznahorkay,[30] J. K. Kraus,[21] A. Kravchenko,[25] S. Kreiss,[109] M. Kretz,[58c] J. Kretzschmar,[73] K. Kreutzfeldt,[52] P. Krieger,[159] K. Kroeninger,[54] H. Kroha,[100] J. Kroll,[121] J. Kroseberg,[21] J. Krstic,[13a] U. Kruchonak,[64] H. Krüger,[21] T. Kruker,[17] N. Krumnack,[63] Z. V. Krumshteyn,[64] A. Kruse,[174] M. C. Kruse,[45] M. Kruskal,[22] T. Kubota,[87] S. Kuday,[4a] S. Kuehn,[48] A. Kugel,[58c] A. Kuhl,[138] T. Kuhl,[42] V. Kukhtin,[64] Y. Kulchitsky,[91] S. Kuleshov,[32b] M. Kuna,[133a,133b] J. Kunkle,[121] A. Kupco,[126] H. Kurashige,[66] Y. A. Kurochkin,[91] R. Kurumida,[66] V. Kus,[126] E. S. Kuwertz,[148] M. Kuze,[158] J. Kvita,[114] A. La Rosa,[49] L. La Rotonda,[37a,37b] C. Lacasta,[168] F. Lacava,[133a,133b] J. Lacey,[29] H. Lacker,[16] D. Lacour,[79] V. R. Lacuesta,[168] E. Ladygin,[64] R. Lafaye,[5] B. Laforge,[79] T. Lagouri,[177] S. Lai,[48] H. Laier,[58a] L. Lambourne,[77] S. Lammers,[60] C. L. Lampen,[7] W. Lampl,[7] E. Lançon,[137] U. Landgraf,[48] M. P. J. Landon,[75] V. S. Lang,[58a] A. J. Lankford,[164] F. Lanni,[25] K. Lantzsch,[30] S. Laplace,[79] C. Lapoire,[21] J. F. Laporte,[137] T. Lari,[90a] M. Lassnig,[30] P. Laurelli,[47] W. Lavrijsen,[15] A. T. Law,[138] P. Laycock,[73] B. T. Le,[55] O. Le Dortz,[79] E. Le Guirriec,[84] E. Le Menedeu,[12] T. LeCompte,[6] F. Ledroit-Guillon,[55] C. A. Lee,[152] H. Lee,[106] J. S. H. Lee,[117] S. C. Lee,[152] L. Lee,[177] G. Lefebvre,[79] M. Lefebvre,[170] F. Legger,[99] C. Leggett,[15] A. Lehan,[73] M. Lehmacher,[21] G. Lehmann Miotto,[30] X. Lei,[7] W. A. Leight,[29] A. Leisos,[155] A. G. Leister,[177] M. A. L. Leite,[24d] R. Leitner,[128] D. Lellouch,[173] B. Lemmer,[54] K. J. C. Leney,[77] T. Lenz,[106] G. Lenzen,[176] B. Lenzi,[30] R. Leone,[7] S. Leone,[123a,123b] K. Leonhardt,[44] C. Leonidopoulos,[46] S. Leontsinis,[10] C. Leroy,[94] C. G. Lester,[28] C. M. Lester,[121] M. Levchenko,[122] J. Levêque,[5] D. Levin,[88] L. J. Levinson,[173] M. Levy,[18] A. Lewis,[119] G. H. Lewis,[109] A. M. Leyko,[21] M. Leyton,[41] B. Li,[33b,v] B. Li,[84] H. Li,[149] H. L. Li,[31] L. Li,[45] L. Li,[33e] S. Li,[45] Y. Li,[33c,w] Z. Liang,[138] H. Liao,[34] B. Liberti,[134a] P. Lichard,[30] K. Lie,[166] J. Liebal,[21] W. Liebig,[14] C. Limbach,[21] A. Limosani,[87] S. C. Lin,[152,x] T. H. Lin,[82] F. Linde,[106] B. E. Lindquist,[149] J. T. Linnemann,[89] E. Lipeles,[121] A. Lipniacka,[14] M. Lisovyi,[42] T. M. Liss,[166] D. Lissauer,[25] A. Lister,[169] A. M. Litke,[138] B. Liu,[152] D. Liu,[152] J. B. Liu,[33b] K. Liu,[33b,y] L. Liu,[88] M. Liu,[45] M. Liu,[33b] Y. Liu,[33b] M. Livan,[120a,120b] S. S. A. Livermore,[119] A. Lleres,[55] J. Llorente Merino,[81] S. L. Lloyd,[75] F. Lo Sterzo,[152] E. Lobodzinska,[42] P. Loch,[7] W. S. Lockman,[138] T. Loddenkoetter,[21] F. K. Loebinger,[83] A. E. Loevschall-Jensen,[36] A. Loginov,[177] C. W. Loh,[169] T. Lohse,[16] K. Lohwasser,[42] M. Lokajicek,[126] V. P. Lombardo,[5] B. A. Long,[22] J. D. Long,[88] R. E. Long,[71] L. Lopes,[125a] D. Lopez Mateos,[57] B. Lopez Paredes,[140] I. Lopez Paz,[12] J. Lorenz,[99] N. Lorenzo Martinez,[60] M. Losada,[163] P. Loscutoff,[15] X. Lou,[41] A. Lounis,[116] J. Love,[6] P. A. Love,[71] A. J. Lowe,[144,f] F. Lu,[33a] H. J. Lubatti,[139] C. Luci,[133a,133b] A. Lucotte,[55] F. Luehring,[60] W. Lukas,[61] L. Luminari,[133a] O. Lundberg,[147a,147b]

B. Lund-Jensen,[148] M. Lungwitz,[82] D. Lynn,[25] R. Lysak,[126] E. Lytken,[80] H. Ma,[25] L. L. Ma,[33d] G. Maccarrone,[47] A. Macchiolo,[100] J. Machado Miguens,[125a,125b] D. Macina,[30] D. Madaffari,[84] R. Madar,[48] H. J. Maddocks,[71] W. F. Mader,[44] A. Madsen,[167] M. Maeno,[8] T. Maeno,[25] E. Magradze,[54] K. Mahboubi,[48] J. Mahlstedt,[106] S. Mahmoud,[73] C. Maiani,[137] C. Maidantchik,[24a] A. A. Maier,[100] A. Maio,[125a,125b,125d] S. Majewski,[115] Y. Makida,[65] N. Makovec,[116] P. Mal,[137,z] B. Malaescu,[79] Pa. Malecki,[39] V. P. Maleev,[122] F. Malek,[55] U. Mallik,[62] D. Malon,[6] C. Malone,[144] S. Maltezos,[10] V. M. Malyshev,[108] S. Malyukov,[30] J. Mamuzic,[13b] B. Mandelli,[30] L. Mandelli,[90a] I. Mandić,[74] R. Mandrysch,[62] J. Maneira,[125a,125b] A. Manfredini,[100] L. Manhaes de Andrade Filho,[24b] J. A. Manjarres Ramos,[160b] A. Mann,[99] P. M. Manning,[138] A. Manousakis-Katsikakis,[9] B. Mansoulie,[137] R. Mantifel,[86] L. Mapelli,[30] L. March,[168] J. F. Marchand,[29] G. Marchiori,[79] M. Marcisovsky,[126] C. P. Marino,[170] M. Marjanovic,[13a] C. N. Marques,[125a] F. Marroquim,[24a] S. P. Marsden,[83] Z. Marshall,[15] L. F. Marti,[17] S. Marti-Garcia,[168] B. Martin,[30] B. Martin,[89] T. A. Martin,[171] V. J. Martin,[46] B. Martin dit Latour,[14] H. Martinez,[137] M. Martinez,[12,o] S. Martin-Haugh,[130] A. C. Martyniuk,[77] M. Marx,[139] F. Marzano,[133a] A. Marzin,[30] L. Masetti,[82] T. Mashimo,[156] R. Mashinistov,[95] J. Masik,[83] A. L. Maslennikov,[108] I. Massa,[20a,20b] N. Massol,[5] P. Mastrandrea,[149] A. Mastroberardino,[37a,37b] T. Masubuchi,[156] P. Mättig,[176] J. Mattmann,[82] J. Maurer,[26a] S. J. Maxfield,[73] D. A. Maximov,[108,u] R. Mazini,[152] L. Mazzaferro,[134a,134b] G. Mc Goldrick,[159] S. P. Mc Kee,[88] A. McCarn,[88] R. L. McCarthy,[149] T. G. McCarthy,[29] N. A. McCubbin,[130] K. W. McFarlane,[56,a] J. A. Mcfayden,[77] G. Mchedlidze,[54] S. J. McMahon,[130] R. A. McPherson,[170,j] A. Meade,[85] J. Mechnich,[106] M. Medinnis,[42] S. Meehan,[31] S. Mehlhase,[99] A. Mehta,[73] K. Meier,[58a] C. Meineck,[99] B. Meirose,[80] C. Melachrinos,[31] B. R. Mellado Garcia,[146c] F. Meloni,[17] A. Mengarelli,[20a,20b] S. Menke,[100] E. Meoni,[162] K. M. Mercurio,[57] S. Mergelmeyer,[21] N. Meric,[137] P. Mermod,[49] L. Merola,[103a,103b] C. Meroni,[90a] F. S. Merritt,[31] H. Merritt,[110] A. Messina,[30,aa] J. Metcalfe,[25] A. S. Mete,[164] C. Meyer,[82] C. Meyer,[31] J-P. Meyer,[137] J. Meyer,[30] R. P. Middleton,[130] S. Migas,[73] L. Mijović,[21] G. Mikenberg,[173] M. Mikestikova,[126] M. Mikuž,[74] A. Milic,[30] D. W. Miller,[31] C. Mills,[46] A. Milov,[173] D. A. Milstead,[147a,147b] D. Milstein,[173] A. A. Minaenko,[129] I. A. Minashvili,[64] A. I. Mincer,[109] B. Mindur,[38a] M. Mineev,[64] Y. Ming,[174] L. M. Mir,[12] G. Mirabelli,[133a] T. Mitani,[172] J. Mitrevski,[99] V. A. Mitsou,[168] S. Mitsui,[65] A. Miucci,[49] P. S. Miyagawa,[140] J. U. Mjörnmark,[80] T. Moa,[147a,147b] K. Mochizuki,[84] S. Mohapatra,[35] W. Mohr,[48] S. Molander,[147a,147b] R. Moles-Valls,[168] K. Mönig,[42] C. Monini,[55] J. Monk,[36] E. Monnier,[84] J. Montejo Berlingen,[12] F. Monticelli,[70] S. Monzani,[133a,133b] R. W. Moore,[3] A. Moraes,[53] N. Morange,[62] D. Moreno,[82] M. Moreno Llácer,[54] P. Morettini,[50a] M. Morgenstern,[44] M. Morii,[57] S. Moritz,[82] A. K. Morley,[148] G. Mornacchi,[30] J. D. Morris,[75] L. Morvaj,[102] H. G. Moser,[100] M. Mosidze,[51b] J. Moss,[110] K. Motohashi,[158] R. Mount,[144] E. Mountricha,[25] S. V. Mouraviev,[95,a] E. J. W. Moyse,[85] S. Muanza,[84] R. D. Mudd,[18] F. Mueller,[58a] J. Mueller,[124] K. Mueller,[21] T. Mueller,[28] T. Mueller,[82] D. Muenstermann,[49] Y. Munwes,[154] J. A. Murillo Quijada,[18] W. J. Murray,[171,130] H. Musheghyan,[54] E. Musto,[153] A. G. Myagkov,[129,bb] M. Myska,[127] O. Nackenhorst,[54] J. Nadal,[54] K. Nagai,[61] R. Nagai,[158] Y. Nagai,[84] K. Nagano,[65] A. Nagarkar,[110] Y. Nagasaka,[59] M. Nagel,[100] A. M. Nairz,[30] Y. Nakahama,[30] K. Nakamura,[65] T. Nakamura,[156] I. Nakano,[111] H. Namasivayam,[41] G. Nanava,[21] R. Narayan,[58b] T. Nattermann,[21] T. Naumann,[42] G. Navarro,[163] R. Nayyar,[7] H. A. Neal,[88] P.Yu. Nechaeva,[95] T. J. Neep,[83] P. D. Nef,[144] A. Negri,[120a,120b] G. Negri,[30] M. Negrini,[20a] S. Nektarijevic,[49] A. Nelson,[164] T. K. Nelson,[144] S. Nemecek,[126] P. Nemethy,[109] A. A. Nepomuceno,[24a] M. Nessi,[30,cc] M. S. Neubauer,[166] M. Neumann,[176] R. M. Neves,[109] P. Nevski,[25] P. R. Newman,[18] D. H. Nguyen,[6] R. B. Nickerson,[119] R. Nicolaidou,[137] B. Nicquevert,[30] J. Nielsen,[138] N. Nikiforou,[35] A. Nikiforov,[16] V. Nikolaenko,[129,bb] I. Nikolic-Audit,[79] K. Nikolics,[49] K. Nikolopoulos,[18] P. Nilsson,[8] Y. Ninomiya,[156] A. Nisati,[133a] R. Nisius,[100] T. Nobe,[158] L. Nodulman,[6] M. Nomachi,[117] I. Nomidis,[155] S. Norberg,[112] M. Nordberg,[30] O. Novgorodova,[44] S. Nowak,[100] M. Nozaki,[65] L. Nozka,[114] K. Ntekas,[10] G. Nunes Hanninger,[87] T. Nunnemann,[99] E. Nurse,[77] F. Nuti,[87] B. J. O'Brien,[46] F. O'grady,[7] D. C. O'Neil,[143] V. O'Shea,[53] F. G. Oakham,[29,e] H. Oberlack,[100] T. Obermann,[21] J. Ocariz,[79] A. Ochi,[66] M. I. Ochoa,[77] S. Oda,[69] S. Odaka,[65] H. Ogren,[60] A. Oh,[83] S. H. Oh,[45] C. C. Ohm,[30] H. Ohman,[167] T. Ohshima,[102] W. Okamura,[117] H. Okawa,[25] Y. Okumura,[31] T. Okuyama,[156] A. Olariu,[26a] A. G. Olchevski,[64] S. A. Olivares Pino,[46] D. Oliveira Damazio,[25] E. Oliver Garcia,[168] A. Olszewski,[39] J. Olszowska,[39] A. Onofre,[125a,125e] P. U. E. Onyisi,[31,p] C. J. Oram,[160a] M. J. Oreglia,[31] Y. Oren,[154] D. Orestano,[135a,135b] N. Orlando,[72a,72b] C. Oropeza Barrera,[53] R. S. Orr,[159] B. Osculati,[50a,50b] R. Ospanov,[121] G. Otero y Garzon,[27] H. Otono,[69] M. Ouchrif,[136d] E. A. Ouellette,[170] F. Ould-Saada,[118] A. Ouraou,[137] K. P. Oussoren,[106] Q. Ouyang,[33a] A. Ovcharova,[15] M. Owen,[83] V. E. Ozcan,[19a] N. Ozturk,[8] K. Pachal,[119] A. Pacheco Pages,[12] C. Padilla Aranda,[12] M. Pagáčová,[48] S. Pagan Griso,[15] E. Paganis,[140] C. Pahl,[100] F. Paige,[25] P. Pais,[85] K. Pajchel,[118] G. Palacino,[160b] S. Palestini,[30] M. Palka,[38b] D. Pallin,[34] A. Palma,[125a,125b] J. D. Palmer,[18] Y. B. Pan,[174] E. Panagiotopoulou,[10] J. G. Panduro Vazquez,[76] P. Pani,[106] N. Panikashvili,[88] S. Panitkin,[25] D. Pantea,[26a] L. Paolozzi,[134a,134b]

Th.D. Papadopoulou,[10] K. Papageorgiou,[155,m] A. Paramonov,[6] D. Paredes Hernandez,[34] M. A. Parker,[28] F. Parodi,[50a,50b] J. A. Parsons,[35] U. Parzefall,[48] E. Pasqualucci,[133a] S. Passaggio,[50a] A. Passeri,[135a] F. Pastore,[135a,135b,a] Fr. Pastore,[76] G. Pásztor,[29] S. Pataraia,[176] N. D. Patel,[151] J. R. Pater,[83] S. Patricelli,[103a,103b] T. Pauly,[30] J. Pearce,[170] M. Pedersen,[118] S. Pedraza Lopez,[168] R. Pedro,[125a,125b] S. V. Peleganchuk,[108] D. Pelikan,[167] H. Peng,[33b] B. Penning,[31] J. Penwell,[60] D. V. Perepelitsa,[25] E. Perez Codina,[160a] M. T. Pérez García-Estañ,[168] V. Perez Reale,[35] L. Perini,[90a,90b] H. Pernegger,[30] R. Perrino,[72a] R. Peschke,[42] V. D. Peshekhonov,[64] K. Peters,[30] R. F. Y. Peters,[83] B. A. Petersen,[30] T. C. Petersen,[36] E. Petit,[42] A. Petridis,[147a,147b] C. Petridou,[155] E. Petrolo,[133a] F. Petrucci,[135a,135b] N. E. Pettersson,[158] R. Pezoa,[32b] P. W. Phillips,[130] G. Piacquadio,[144] E. Pianori,[171] A. Picazio,[49] E. Piccaro,[75] M. Piccinini,[20a,20b] R. Piegaia,[27] D. T. Pignotti,[110] J. E. Pilcher,[31] A. D. Pilkington,[77] J. Pina,[125a,125b,125d] M. Pinamonti,[165a,165c,dd] A. Pinder,[119] J. L. Pinfold,[3] A. Pingel,[36] B. Pinto,[125a] S. Pires,[79] M. Pitt,[173] C. Pizio,[90a,90b] L. Plazak,[145a] M.-A. Pleier,[25] V. Pleskot,[128] E. Plotnikova,[64] P. Plucinski,[147a,147b] S. Poddar,[58a] F. Podlyski,[34] R. Poettgen,[82] L. Poggioli,[116] D. Pohl,[21] M. Pohl,[49] G. Polesello,[120a] A. Policicchio,[37a,37b] R. Polifka,[159] A. Polini,[20a] C. S. Pollard,[45] V. Polychronakos,[25] K. Pommès,[30] L. Pontecorvo,[133a] B. G. Pope,[89] G. A. Popeneciu,[26b] D. S. Popovic,[13a] A. Poppleton,[30] X. Portell Bueso,[12] S. Pospisil,[127] K. Potamianos,[15] I. N. Potrap,[64] C. J. Potter,[150] C. T. Potter,[115] G. Poulard,[30] J. Poveda,[60] V. Pozdnyakov,[64] P. Pralavorio,[84] A. Pranko,[15] S. Prasad,[30] R. Pravahan,[8] S. Prell,[63] D. Price,[83] J. Price,[73] L. E. Price,[6] D. Prieur,[124] M. Primavera,[72a] M. Proissl,[46] K. Prokofiev,[47] F. Prokoshin,[32b] E. Protopapadaki,[137] S. Protopopescu,[25] J. Proudfoot,[6] M. Przybycien,[38a] H. Przysiezniak,[5] E. Ptacek,[115] D. Puddu,[135a,135b] E. Pueschel,[85] D. Puldon,[149] M. Purohit,[25,ee] P. Puzo,[116] J. Qian,[88] G. Qin,[53] Y. Qin,[83] A. Quadt,[54] D. R. Quarrie,[15] W. B. Quayle,[165a,165b] M. Queitsch-Maitland,[83] D. Quilty,[53] A. Qureshi,[160b] V. Radeka,[25] V. Radescu,[42] S. K. Radhakrishnan,[149] P. Radloff,[115] P. Rados,[87] F. Ragusa,[90a,90b] G. Rahal,[179] S. Rajagopalan,[25] M. Rammensee,[30] A. S. Randle-Conde,[40] C. Rangel-Smith,[167] K. Rao,[164] F. Rauscher,[99] T. C. Rave,[48] T. Ravenscroft,[53] M. Raymond,[30] A. L. Read,[118] N. P. Readioff,[73] D. M. Rebuzzi,[120a,120b] A. Redelbach,[175] G. Redlinger,[25] R. Reece,[138] K. Reeves,[41] L. Rehnisch,[16] H. Reisin,[27] M. Relich,[164] C. Rembser,[30] H. Ren,[33a] Z. L. Ren,[152] A. Renaud,[116] M. Rescigno,[133a] S. Resconi,[90a] O. L. Rezanova,[108,u] P. Reznicek,[128] R. Rezvani,[94] R. Richter,[100] M. Ridel,[79] P. Rieck,[16] J. Rieger,[54] M. Rijssenbeek,[149] A. Rimoldi,[120a,120b] L. Rinaldi,[20a] E. Ritsch,[61] I. Riu,[12] F. Rizatdinova,[113] E. Rizvi,[75] S. H. Robertson,[86,j] A. Robichaud-Veronneau,[86] D. Robinson,[28] J. E. M. Robinson,[83] A. Robson,[53] C. Roda,[123a,123b] L. Rodrigues,[30] S. Roe,[30] O. Røhne,[118] S. Rolli,[162] A. Romaniouk,[97] M. Romano,[20a,20b] E. Romero Adam,[168] N. Rompotis,[139] L. Roos,[79] E. Ros,[168] S. Rosati,[133a] K. Rosbach,[49] M. Rose,[76] P. L. Rosendahl,[14] O. Rosenthal,[142] V. Rossetti,[147a,147b] E. Rossi,[103a,103b] L. P. Rossi,[50a] R. Rosten,[139] M. Rotaru,[26a] I. Roth,[173] J. Rothberg,[139] D. Rousseau,[116] C. R. Royon,[137] A. Rozanov,[84] Y. Rozen,[153] X. Ruan,[146c] F. Rubbo,[12] I. Rubinskiy,[42] V. I. Rud,[98] C. Rudolph,[44] M. S. Rudolph,[159] F. Rühr,[48] A. Ruiz-Martinez,[30] Z. Rurikova,[48] N. A. Rusakovich,[64] A. Ruschke,[99] J. P. Rutherfoord,[7] N. Ruthmann,[48] Y. F. Ryabov,[122] M. Rybar,[128] G. Rybkin,[116] N. C. Ryder,[119] A. F. Saavedra,[151] S. Sacerdoti,[27] A. Saddique,[3] I. Sadeh,[154] H.F-W. Sadrozinski,[138] R. Sadykov,[64] F. Safai Tehrani,[133a] H. Sakamoto,[156] Y. Sakurai,[172] G. Salamanna,[135a,135b] A. Salamon,[134a] M. Saleem,[112] D. Salek,[106] P. H. Sales De Bruin,[139] D. Salihagic,[100] A. Salnikov,[144] J. Salt,[168] B. M. Salvachua Ferrando,[6] D. Salvatore,[37a,37b] F. Salvatore,[150] A. Salvucci,[105] A. Salzburger,[30] D. Sampsonidis,[155] A. Sanchez,[103a,103b] J. Sánchez,[168] V. Sanchez Martinez,[168] H. Sandaker,[14] R. L. Sandbach,[75] H. G. Sander,[82] M. P. Sanders,[99] M. Sandhoff,[176] T. Sandoval,[28] C. Sandoval,[163] R. Sandstroem,[100] D. P. C. Sankey,[130] A. Sansoni,[47] C. Santoni,[34] R. Santonico,[134a,134b] H. Santos,[125a] I. Santoyo Castillo,[150] K. Sapp,[124] A. Sapronov,[64] J. G. Saraiva,[125a,125d] B. Sarrazin,[21] G. Sartisohn,[176] O. Sasaki,[65] Y. Sasaki,[156] G. Sauvage,[5,a] E. Sauvan,[5] P. Savard,[159,e] D. O. Savu,[30] C. Sawyer,[119] L. Sawyer,[78,n] D. H. Saxon,[53] J. Saxon,[121] C. Sbarra,[20a] A. Sbrizzi,[3] T. Scanlon,[77] D. A. Scannicchio,[164] M. Scarcella,[151] V. Scarfone,[37a,37b] J. Schaarschmidt,[173] P. Schacht,[100] D. Schaefer,[121] R. Schaefer,[42] S. Schaepe,[21] S. Schaetzel,[58b] U. Schäfer,[82] A. C. Schaffer,[116] D. Schaile,[99] R. D. Schamberger,[149] V. Scharf,[58a] V. A. Schegelsky,[122] D. Scheirich,[128] M. Schernau,[164] M. I. Scherzer,[35] C. Schiavi,[50a,50b] J. Schieck,[99] C. Schillo,[48] M. Schioppa,[37a,37b] S. Schlenker,[30] E. Schmidt,[48] K. Schmieden,[30] C. Schmitt,[82] C. Schmitt,[99] S. Schmitt,[58b] B. Schneider,[17] Y. J. Schnellbach,[73] U. Schnoor,[44] L. Schoeffel,[137] A. Schoening,[58b] B. D. Schoenrock,[89] A. L. S. Schorlemmer,[54] M. Schott,[82] D. Schouten,[160a] J. Schovancova,[25] S. Schramm,[159] M. Schreyer,[175] C. Schroeder,[82] N. Schuh,[82] M. J. Schultens,[21] H.-C. Schultz-Coulon,[58a] H. Schulz,[16] M. Schumacher,[48] B. A. Schumm,[138] Ph. Schune,[137] C. Schwanenberger,[83] A. Schwartzman,[144] Ph. Schwegler,[100] Ph. Schwemling,[137] R. Schwienhorst,[89] J. Schwindling,[137] T. Schwindt,[21] M. Schwoerer,[5] F. G. Sciacca,[17] E. Scifo,[116] G. Sciolla,[23] W. G. Scott,[130] F. Scuri,[123a,123b] F. Scutti,[21] J. Searcy,[88] G. Sedov,[42] E. Sedykh,[122] S. C. Seidel,[104] A. Seiden,[138] F. Seifert,[127] J. M. Seixas,[24a] G. Sekhniaidze,[103a] S. J. Sekula,[40] K. E. Selbach,[46] D. M. Seliverstov,[122,a]

G. Sellers,[73] N. Semprini-Cesari,[20a,20b] C. Serfon,[30] L. Serin,[116] L. Serkin,[54] T. Serre,[84] R. Seuster,[160a] H. Severini,[112] T. Sfiligoj,[74] F. Sforza,[100] A. Sfyrla,[30] E. Shabalina,[54] M. Shamim,[115] L. Y. Shan,[33a] R. Shang,[166] J. T. Shank,[22] M. Shapiro,[15] P. B. Shatalov,[96] K. Shaw,[165a,165b] C. Y. Shehu,[150] P. Sherwood,[77] L. Shi,[152,ff] S. Shimizu,[66] C. O. Shimmin,[164] M. Shimojima,[101] M. Shiyakova,[64] A. Shmeleva,[95] M. J. Shochet,[31] D. Short,[119] S. Shrestha,[63] E. Shulga,[97] M. A. Shupe,[7] S. Shushkevich,[42] P. Sicho,[126] O. Sidiropoulou,[155] D. Sidorov,[113] A. Sidoti,[133a] F. Siegert,[44] Dj. Sijacki,[13a] J. Silva,[125a,125d] Y. Silver,[154] D. Silverstein,[144] S. B. Silverstein,[147a] V. Simak,[127] O. Simard,[5] Lj. Simic,[13a] S. Simion,[116] E. Simioni,[82] B. Simmons,[77] R. Simoniello,[90a,90b] M. Simonyan,[36] P. Sinervo,[159] N. B. Sinev,[115] V. Sipica,[142] G. Siragusa,[175] A. Sircar,[78] A. N. Sisakyan,[64,a] S.Yu. Sivoklokov,[98] J. Sjölin,[147a,147b] T. B. Sjursen,[14] H. P. Skottowe,[57] K.Yu. Skovpen,[108] P. Skubic,[112] M. Slater,[18] T. Slavicek,[127] K. Sliwa,[162] V. Smakhtin,[173] B. H. Smart,[46] L. Smestad,[14] S.Yu. Smirnov,[97] Y. Smirnov,[97] L. N. Smirnova,[98,gg] O. Smirnova,[80] K. M. Smith,[53] M. Smizanska,[71] K. Smolek,[127] A. A. Snesarev,[95] G. Snidero,[75] S. Snyder,[25] R. Sobie,[170,j] F. Socher,[44] A. Soffer,[154] D. A. Soh,[152,ff] C. A. Solans,[30] M. Solar,[127] J. Solc,[127] E.Yu. Soldatov,[97] U. Soldevila,[168] E. Solfaroli Camillocci,[133a,133b] A. A. Solodkov,[129] A. Soloshenko,[64] O. V. Solovyanov,[129] V. Solovyev,[122] P. Sommer,[48] H. Y. Song,[33b] N. Soni,[1] A. Sood,[15] A. Sopczak,[127] B. Sopko,[127] V. Sopko,[127] V. Sorin,[12] M. Sosebee,[8] R. Soualah,[165a,165c] P. Soueid,[94] A. M. Soukharev,[108] D. South,[42] S. Spagnolo,[72a,72b] F. Spanò,[76] W. R. Spearman,[57] F. Spettel,[100] R. Spighi,[20a] G. Spigo,[30] M. Spousta,[128] T. Spreitzer,[159] B. Spurlock,[8] R. D. St. Denis,[53,a] S. Staerz,[44] J. Stahlman,[121] R. Stamen,[58a] E. Stanecka,[39] R. W. Stanek,[6] C. Stanescu,[135a] M. Stanescu-Bellu,[42] M. M. Stanitzki,[42] S. Stapnes,[118] E. A. Starchenko,[129] J. Stark,[55] P. Staroba,[126] P. Starovoitov,[42] R. Staszewski,[39] P. Stavina,[145a,a] P. Steinberg,[25] B. Stelzer,[143] H. J. Stelzer,[30] O. Stelzer-Chilton,[160a] H. Stenzel,[52] S. Stern,[100] G. A. Stewart,[53] J. A. Stillings,[21] M. C. Stockton,[86] M. Stoebe,[86] G. Stoicea,[26a] P. Stolte,[54] S. Stonjek,[100] A. R. Stradling,[8] A. Straessner,[44] M. E. Stramaglia,[17] J. Strandberg,[148] S. Strandberg,[147a,147b] A. Strandlie,[118] E. Strauss,[144] M. Strauss,[112] P. Strizenec,[145b] R. Ströhmer,[175] D. M. Strom,[115] R. Stroynowski,[40] S. A. Stucci,[17] B. Stugu,[14] N. A. Styles,[42] D. Su,[144] J. Su,[124] HS. Subramania,[3] R. Subramaniam,[78] A. Succurro,[12] Y. Sugaya,[117] C. Suhr,[107] M. Suk,[127] V. V. Sulin,[95] S. Sultansoy,[4c] T. Sumida,[67] S. Sun,[57] X. Sun,[33a] J. E. Sundermann,[48] K. Suruliz,[140] G. Susinno,[37a,37b] C. Suster,[151] M. R. Sutton,[150] Y. Suzuki,[65] M. Svatos,[126] S. Swedish,[169] M. Swiatlowski,[144] I. Sykora,[145a] T. Sykora,[128] D. Ta,[89] C. Taccini,[135a,135b] K. Tackmann,[42] J. Taenzer,[159] A. Taffard,[164] R. Tafirout,[160a] N. Taiblum,[154] Y. Takahashi,[102] H. Takai,[25] R. Takashima,[68] H. Takeda,[66] T. Takeshita,[141] Y. Takubo,[65] M. Talby,[84] A. A. Talyshev,[108,u] J. Y. C. Tam,[175] K. G. Tan,[87] J. Tanaka,[156] R. Tanaka,[116] S. Tanaka,[132] S. Tanaka,[65] A. J. Tanasijczuk,[143] B. B. Tannenwald,[110] N. Tannoury,[21] S. Tapprogge,[82] S. Tarem,[153] F. Tarrade,[29] G. F. Tartarelli,[90a] P. Tas,[128] M. Tasevsky,[126] T. Tashiro,[67] E. Tassi,[37a,37b] A. Tavares Delgado,[125a,125b] Y. Tayalati,[136d] F. E. Taylor,[93] G. N. Taylor,[87] W. Taylor,[160b] F. A. Teischinger,[30] M. Teixeira Dias Castanheira,[75] P. Teixeira-Dias,[76] K. K. Temming,[48] H. Ten Kate,[30] P. K. Teng,[152] J. J. Teoh,[117] S. Terada,[65] K. Terashi,[156] J. Terron,[81] S. Terzo,[100] M. Testa,[47] R. J. Teuscher,[159,j] J. Therhaag,[21] T. Theveneaux-Pelzer,[34] J. P. Thomas,[18] J. Thomas-Wilsker,[76] E. N. Thompson,[35] P. D. Thompson,[18] P. D. Thompson,[159] A. S. Thompson,[53] L. A. Thomsen,[36] E. Thomson,[121] M. Thomson,[28] W. M. Thong,[87] R. P. Thun,[88,a] F. Tian,[35] M. J. Tibbetts,[15] V. O. Tikhomirov,[95,hh] Yu.A. Tikhonov,[108,u] S. Timoshenko,[97] E. Tiouchichine,[84] P. Tipton,[177] S. Tisserant,[84] T. Todorov,[5] S. Todorova-Nova,[128] B. Toggerson,[7] J. Tojo,[69] S. Tokár,[145a] K. Tokushuku,[65] K. Tollefson,[89] L. Tomlinson,[83] M. Tomoto,[102] L. Tompkins,[31] K. Toms,[104] N. D. Topilin,[64] E. Torrence,[115] H. Torres,[143] E. Torró Pastor,[168] J. Toth,[84,ii] F. Touchard,[84] D. R. Tovey,[140] H. L. Tran,[116] T. Trefzger,[175] L. Tremblet,[30] A. Tricoli,[30] I. M. Trigger,[160a] S. Trincaz-Duvoid,[79] M. F. Tripiana,[12] W. Trischuk,[159] B. Trocmé,[55] C. Troncon,[90a] M. Trottier-McDonald,[143] M. Trovatelli,[135a,135b] P. True,[89] M. Trzebinski,[39] A. Trzupek,[39] C. Tsarouchas,[30] J.C-L. Tseng,[119] P. V. Tsiareshka,[91] D. Tsionou,[137] G. Tsipolitis,[10] N. Tsirintanis,[9] S. Tsiskaridze,[12] V. Tsiskaridze,[48] E. G. Tskhadadze,[51a] I. I. Tsukerman,[96] V. Tsulaia,[15] S. Tsuno,[65] D. Tsybychev,[149] A. Tudorache,[26a] V. Tudorache,[26a] A. N. Tuna,[121] S. A. Tupputi,[20a,20b] S. Turchikhin,[98,gg] D. Turecek,[127] I. Turk Cakir,[4d] R. Turra,[90a,90b] P. M. Tuts,[35] A. Tykhonov,[49] M. Tylmad,[147a,147b] M. Tyndel,[130] K. Uchida,[21] I. Ueda,[156] R. Ueno,[29] M. Ughetto,[84] M. Ugland,[14] M. Uhlenbrock,[21] F. Ukegawa,[161] G. Unal,[30] A. Undrus,[25] G. Unel,[164] F. C. Ungaro,[48] Y. Unno,[65] D. Urbaniec,[35] P. Urquijo,[87] G. Usai,[8] A. Usanova,[61] L. Vacavant,[84] V. Vacek,[127] B. Vachon,[86] N. Valencic,[106] S. Valentinetti,[20a,20b] A. Valero,[168] L. Valery,[34] S. Valkar,[128] E. Valladolid Gallego,[168] S. Vallecorsa,[49] J. A. Valls Ferrer,[168] W. Van Den Wollenberg,[106] P. C. Van Der Deijl,[106] R. van der Geer,[106] H. van der Graaf,[106] R. Van Der Leeuw,[106] D. van der Ster,[30] N. van Eldik,[30] P. van Gemmeren,[6] J. Van Nieuwkoop,[143] I. van Vulpen,[106] M. C. van Woerden,[30] M. Vanadia,[133a,133b] W. Vandelli,[30] R. Vanguri,[121] A. Vaniachine,[6] P. Vankov,[42] F. Vannucci,[79] G. Vardanyan,[178] R. Vari,[133a] E. W. Varnes,[7] T. Varol,[85] D. Varouchas,[79] A. Vartapetian,[8] K. E. Varvell,[151] F. Vazeille,[34] T. Vazquez Schroeder,[54] J. Veatch,[7] F. Veloso,[125a,125c]

S. Veneziano,[133a] A. Ventura,[72a,72b] D. Ventura,[85] M. Venturi,[170] N. Venturi,[159] A. Venturini,[23] V. Vercesi,[120a] M. Verducci,[133a,133b] W. Verkerke,[106] J. C. Vermeulen,[106] A. Vest,[44] M. C. Vetterli,[143,e] O. Viazlo,[80] I. Vichou,[166] T. Vickey,[146c,jj] O. E. Vickey Boeriu,[146c] G. H. A. Viehhauser,[119] S. Viel,[169] R. Vigne,[30] M. Villa,[20a,20b] M. Villaplana Perez,[90a,90b] E. Vilucchi,[47] M. G. Vincter,[29] V. B. Vinogradov,[64] J. Virzi,[15] I. Vivarelli,[150] F. Vives Vaque,[3] S. Vlachos,[10] D. Vladoiu,[99] M. Vlasak,[127] A. Vogel,[21] M. Vogel,[32a] P. Vokac,[127] G. Volpi,[123a,123b] M. Volpi,[87] H. von der Schmitt,[100] H. von Radziewski,[48] E. von Toerne,[21] V. Vorobel,[128] K. Vorobev,[97] M. Vos,[168] R. Voss,[30] J. H. Vossebeld,[73] N. Vranjes,[137] M. Vranjes Milosavljevic,[106] V. Vrba,[126] M. Vreeswijk,[106] T. Vu Anh,[48] R. Vuillermet,[30] I. Vukotic,[31] Z. Vykydal,[127] P. Wagner,[21] W. Wagner,[176] H. Wahlberg,[70] S. Wahrmund,[44] J. Wakabayashi,[102] J. Walder,[71] R. Walker,[99] W. Walkowiak,[142] R. Wall,[177] P. Waller,[73] B. Walsh,[177] C. Wang,[152,kk] C. Wang,[45] F. Wang,[174] H. Wang,[15] H. Wang,[40] J. Wang,[42] J. Wang,[33a] K. Wang,[86] R. Wang,[104] S. M. Wang,[152] T. Wang,[21] X. Wang,[177] C. Wanotayaroj,[115] A. Warburton,[86] C. P. Ward,[28] D. R. Wardrope,[77] M. Warsinsky,[48] A. Washbrook,[46] C. Wasicki,[42] P. M. Watkins,[18] A. T. Watson,[18] I. J. Watson,[151] M. F. Watson,[18] G. Watts,[139] S. Watts,[83] B. M. Waugh,[77] S. Webb,[83] M. S. Weber,[17] S. W. Weber,[175] J. S. Webster,[31] A. R. Weidberg,[119] P. Weigell,[100] B. Weinert,[60] J. Weingarten,[54] C. Weiser,[48] H. Weits,[106] P. S. Wells,[30] T. Wenaus,[25] D. Wendland,[16] Z. Weng,[152,ff] T. Wengler,[30] S. Wenig,[30] N. Wermes,[21] M. Werner,[48] P. Werner,[30] M. Wessels,[58a] J. Wetter,[162] K. Whalen,[29] A. White,[8] M. J. White,[1] R. White,[32b] S. White,[123a,123b] D. Whiteson,[164] D. Wicke,[176] F. J. Wickens,[130] W. Wiedenmann,[174] M. Wielers,[130] P. Wienemann,[21] C. Wiglesworth,[36] L. A. M. Wiik-Fuchs,[21] P. A. Wijeratne,[77] A. Wildauer,[100] M. A. Wildt,[42,ll] H. G. Wilkens,[30] J. Z. Will,[99] H. H. Williams,[121] S. Williams,[28] C. Willis,[89] S. Willocq,[85] A. Wilson,[88] J. A. Wilson,[18] I. Wingerter-Seez,[5] F. Winklmeier,[115] B. T. Winter,[21] M. Wittgen,[144] T. Wittig,[43] J. Wittkowski,[99] S. J. Wollstadt,[82] M. W. Wolter,[39] H. Wolters,[125a,125c] B. K. Wosiek,[39] J. Wotschack,[30] M. J. Woudstra,[83] K. W. Wozniak,[39] M. Wright,[53] M. Wu,[55] S. L. Wu,[174] X. Wu,[49] Y. Wu,[88] E. Wulf,[35] T. R. Wyatt,[83] B. M. Wynne,[46] S. Xella,[36] M. Xiao,[137] D. Xu,[33a] L. Xu,[33b,mm] B. Yabsley,[151] S. Yacoob,[146b,nn] M. Yamada,[65] H. Yamaguchi,[156] Y. Yamaguchi,[117] A. Yamamoto,[65] K. Yamamoto,[63] S. Yamamoto,[156] T. Yamamura,[156] T. Yamanaka,[156] K. Yamauchi,[102] Y. Yamazaki,[66] Z. Yan,[22] H. Yang,[33e] H. Yang,[174] U. K. Yang,[83] Y. Yang,[110] S. Yanush,[92] L. Yao,[33a] W-M. Yao,[15] Y. Yasu,[65] E. Yatsenko,[42] K. H. Yau Wong,[21] J. Ye,[40] S. Ye,[25] A. L. Yen,[57] E. Yildirim,[42] M. Yilmaz,[4b] R. Yoosoofmiya,[124] K. Yorita,[172] R. Yoshida,[6] K. Yoshihara,[156] C. Young,[144] C. J. S. Young,[30] S. Youssef,[22] D. R. Yu,[15] J. Yu,[8] J. M. Yu,[88] J. Yu,[113] L. Yuan,[66] A. Yurkewicz,[107] I. Yusuff,[28,oo] B. Zabinski,[39] R. Zaidan,[62] A. M. Zaitsev,[129,bb] A. Zaman,[149] S. Zambito,[23] L. Zanello,[133a,133b] D. Zanzi,[100] C. Zeitnitz,[176] M. Zeman,[127] A. Zemla,[38a] K. Zengel,[23] O. Zenin,[129] T. Ženiš,[145a] D. Zerwas,[116] G. Zevi della Porta,[57] D. Zhang,[88] F. Zhang,[174] H. Zhang,[89] J. Zhang,[6] L. Zhang,[152] X. Zhang,[33d] Z. Zhang,[116] Z. Zhao,[33b] A. Zhemchugov,[64] J. Zhong,[119] B. Zhou,[88] L. Zhou,[35] N. Zhou,[164] C. G. Zhu,[33d] H. Zhu,[33a] J. Zhu,[88] Y. Zhu,[33b] X. Zhuang,[33a] K. Zhukov,[95] A. Zibell,[175] D. Zieminska,[60] N. I. Zimine,[64] C. Zimmermann,[82] R. Zimmermann,[21] S. Zimmermann,[21] S. Zimmermann,[48] Z. Zinonos,[54] M. Ziolkowski,[142] G. Zobernig,[174] A. Zoccoli,[20a,20b] M. zur Nedden,[16] G. Zurzolo,[103a,103b] V. Zutshi,[107] and L. Zwalinski[30]

(ATLAS Collaboration)

[1]*Department of Physics, University of Adelaide, Adelaide, Australia*
[2]*Physics Department, SUNY Albany, Albany New York, USA*
[3]*Department of Physics, University of Alberta, Edmonton Alberta, Canada*
[4a]*Department of Physics, Ankara University, Ankara, Turkey*
[4b]*Department of Physics, Gazi University, Ankara, Turkey*
[4c]*Division of Physics, TOBB University of Economics and Technology, Ankara, Turkey*
[4d]*Turkish Atomic Energy Authority, Ankara, Turkey*
[5]*LAPP, CNRS/IN2P3 and Université de Savoie, Annecy-le-Vieux, France*
[6]*High Energy Physics Division, Argonne National Laboratory, Argonne, Illinois, USA*
[7]*Department of Physics, University of Arizona, Tucson, Arizona, USA*
[8]*Department of Physics, The University of Texas at Arlington, Arlington, Texas, USA*
[9]*Physics Department, University of Athens, Athens, Greece*
[10]*Physics Department, National Technical University of Athens, Zografou, Greece*
[11]*Institute of Physics, Azerbaijan Academy of Sciences, Baku, Azerbaijan*
[12]*Institut de Física d'Altes Energies and Departament de Física de la Universitat Autònoma de Barcelona, Barcelona, Spain*
[13a]*Institute of Physics, University of Belgrade, Belgrade, Serbia*
[13b]*Vinca Institute of Nuclear Sciences, University of Belgrade, Belgrade, Serbia*

[14]*Department for Physics and Technology, University of Bergen, Bergen, Norway*
[15]*Physics Division, Lawrence Berkeley National Laboratory and University of California, Berkeley, California, USA*
[16]*Department of Physics, Humboldt University, Berlin, Germany*
[17]*Albert Einstein Center for Fundamental Physics and Laboratory for High Energy Physics, University of Bern, Bern, Switzerland*
[18]*School of Physics and Astronomy, University of Birmingham, Birmingham, United Kingdom*
[19a]*Department of Physics, Bogazici University, Istanbul, Turkey*
[19b]*Department of Physics, Dogus University, Istanbul, Turkey*
[19c]*Department of Physics Engineering, Gaziantep University, Gaziantep, Turkey*
[20a]*INFN Sezione di Bologna, Bologna, Italy*
[20b]*Dipartimento di Fisica e Astronomia, Università di Bologna, Bologna, Italy*
[21]*Physikalisches Institut, University of Bonn, Bonn, Germany*
[22]*Department of Physics, Boston University, Boston, Massachusetts, USA*
[23]*Department of Physics, Brandeis University, Waltham, Massachusetts, USA*
[24a]*Universidade Federal do Rio De Janeiro COPPE/EE/IF, Rio de Janeiro, Brazil*
[24b]*Federal University of Juiz de Fora (UFJF), Juiz de Fora, Brazil*
[24c]*Federal University of Sao Joao del Rei (UFSJ), Sao Joao del Rei, Brazil*
[24d]*Instituto de Fisica, Universidade de Sao Paulo, Sao Paulo, Brazil*
[25]*Physics Department, Brookhaven National Laboratory, Upton, New York, USA*
[26a]*National Institute of Physics and Nuclear Engineering, Bucharest, Romania*
[26b]*National Institute for Research and Development of Isotopic and Molecular Technologies, Physics Department, Cluj Napoca, Romania*
[26c]*University Politehnica Bucharest, Bucharest, Romania*
[26d]*West University in Timisoara, Timisoara, Romania*
[27]*Departamento de Física, Universidad de Buenos Aires, Buenos Aires, Argentina*
[28]*Cavendish Laboratory, University of Cambridge, Cambridge, United Kingdom*
[29]*Department of Physics, Carleton University, Ottawa, Ontario, Canada*
[30]*CERN, Geneva, Switzerland*
[31]*Enrico Fermi Institute, University of Chicago, Chicago, Illinois, USA*
[32a]*Departamento de Física, Pontificia Universidad Católica de Chile, Santiago, Chile*
[32b]*Departamento de Física, Universidad Técnica Federico Santa María, Valparaíso, Chile*
[33a]*Institute of High Energy Physics, Chinese Academy of Sciences, Beijing, China*
[33b]*Department of Modern Physics, University of Science and Technology of China, Anhui, China*
[33c]*Department of Physics, Nanjing University, Jiangsu, China*
[33d]*School of Physics, Shandong University, Shandong, China*
[33e]*Physics Department, Shanghai Jiao Tong University, Shanghai, China*
[34]*Laboratoire de Physique Corpusculaire, Clermont Université and Université Blaise Pascal and CNRS/IN2P3, Clermont-Ferrand, France*
[35]*Nevis Laboratory, Columbia University, Irvington, New York, USA*
[36]*Niels Bohr Institute, University of Copenhagen, Kobenhavn, Denmark*
[37a]*INFN Gruppo Collegato di Cosenza, Laboratori Nazionali di Frascati, Italy*
[37b]*Dipartimento di Fisica, Università della Calabria, Rende, Italy*
[38a]*AGH University of Science and Technology, Faculty of Physics and Applied Computer Science, Krakow, Poland*
[38b]*Marian Smoluchowski Institute of Physics, Jagiellonian University, Krakow, Poland*
[39]*The Henryk Niewodniczanski Institute of Nuclear Physics, Polish Academy of Sciences, Krakow, Poland*
[40]*Physics Department, Southern Methodist University, Dallas, Texas, USA*
[41]*Physics Department, University of Texas at Dallas, Richardson, Texas, USA*
[42]*DESY, Hamburg and Zeuthen, Germany*
[43]*Institut für Experimentelle Physik IV, Technische Universität Dortmund, Dortmund, Germany*
[44]*Institut für Kern- und Teilchenphysik, Technische Universität Dresden, Dresden, Germany*
[45]*Department of Physics, Duke University, Durham, North Carolina, USA*
[46]*SUPA - School of Physics and Astronomy, University of Edinburgh, Edinburgh, United Kingdom*
[47]*INFN Laboratori Nazionali di Frascati, Frascati, Italy*
[48]*Fakultät für Mathematik und Physik, Albert-Ludwigs-Universität, Freiburg, Germany*
[49]*Section de Physique, Université de Genève, Geneva, Switzerland*
[50a]*INFN Sezione di Genova, Genova, Italy*
[50b]*Dipartimento di Fisica, Università di Genova, Genova, Italy*
[51a]*E. Andronikashvili Institute of Physics, Iv. Javakhishvili Tbilisi State University, Tbilisi, Georgia*

[51b]High Energy Physics Institute, Tbilisi State University, Tbilisi, Georgia
[52]II Physikalisches Institut, Justus-Liebig-Universität Giessen, Giessen, Germany
[53]SUPA - School of Physics and Astronomy, University of Glasgow, Glasgow, United Kingdom
[54]II Physikalisches Institut, Georg-August-Universität, Göttingen, Germany
[55]Laboratoire de Physique Subatomique et de Cosmologie, Université Grenoble-Alpes, CNRS/IN2P3, Grenoble, France
[56]Department of Physics, Hampton University, Hampton, Virginia, USA
[57]Laboratory for Particle Physics and Cosmology, Harvard University, Cambridge, Massachusetts, USA
[58a]Kirchhoff-Institut für Physik, Ruprecht-Karls-Universität Heidelberg, Heidelberg, Germany
[58b]Physikalisches Institut, Ruprecht-Karls-Universität Heidelberg, Heidelberg, Germany
[58c]ZITI Institut für technische Informatik, Ruprecht-Karls-Universität Heidelberg, Mannheim, Germany
[59]Faculty of Applied Information Science, Hiroshima Institute of Technology, Hiroshima, Japan
[60]Department of Physics, Indiana University, Bloomington, Indiana, USA
[61]Institut für Astro- und Teilchenphysik, Leopold-Franzens-Universität, Innsbruck, Austria
[62]University of Iowa, Iowa City, Iowa, USA
[63]Department of Physics and Astronomy, Iowa State University, Ames, Iowa, USA
[64]Joint Institute for Nuclear Research, JINR Dubna, Dubna, Russia
[65]KEK, High Energy Accelerator Research Organization, Tsukuba, Japan
[66]Graduate School of Science, Kobe University, Kobe, Japan
[67]Faculty of Science, Kyoto University, Kyoto, Japan
[68]Kyoto University of Education, Kyoto, Japan
[69]Department of Physics, Kyushu University, Fukuoka, Japan
[70]Instituto de Física La Plata, Universidad Nacional de La Plata and CONICET, La Plata, Argentina
[71]Physics Department, Lancaster University, Lancaster, United Kingdom
[72a]INFN Sezione di Lecce, Italy
[72b]Dipartimento di Matematica e Fisica, Università del Salento, Lecce, Italy
[73]Oliver Lodge Laboratory, University of Liverpool, Liverpool, United Kingdom
[74]Department of Physics, Jožef Stefan Institute and University of Ljubljana, Ljubljana, Slovenia
[75]School of Physics and Astronomy, Queen Mary University of London, London, United Kingdom
[76]Department of Physics, Royal Holloway University of London, Surrey, United Kingdom
[77]Department of Physics and Astronomy, University College London, London, United Kingdom
[78]Louisiana Tech University, Ruston, Louisiana, USA
[79]Laboratoire de Physique Nucléaire et de Hautes Energies, UPMC and Université Paris-Diderot and CNRS/IN2P3, Paris, France
[80]Fysiska institutionen, Lunds universitet, Lund, Sweden
[81]Departamento de Fisica Teorica C-15, Universidad Autonoma de Madrid, Madrid, Spain
[82]Institut für Physik, Universität Mainz, Mainz, Germany
[83]School of Physics and Astronomy, University of Manchester, Manchester, United Kingdom
[84]CPPM, Aix-Marseille Université and CNRS/IN2P3, Marseille, France
[85]Department of Physics, University of Massachusetts, Amherst, Massachusetts, USA
[86]Department of Physics, McGill University, Montreal, Quebec, Canada
[87]School of Physics, University of Melbourne, Victoria, Australia
[88]Department of Physics, The University of Michigan, Ann Arbor, Michigan, USA
[89]Department of Physics and Astronomy, Michigan State University, East Lansing, Michigan, USA
[90a]INFN Sezione di Milano, Italy
[90b]Dipartimento di Fisica, Università di Milano, Milano, Italy
[91]B.I. Stepanov Institute of Physics, National Academy of Sciences of Belarus, Minsk, Republic of Belarus
[92]National Scientific and Educational Centre for Particle and High Energy Physics, Minsk, Republic of Belarus
[93]Department of Physics, Massachusetts Institute of Technology, Cambridge, Massachusetts, USA
[94]Group of Particle Physics, University of Montreal, Montreal Quebec, Canada
[95]P.N. Lebedev Institute of Physics, Academy of Sciences, Moscow, Russia
[96]Institute for Theoretical and Experimental Physics (ITEP), Moscow, Russia
[97]Moscow Engineering and Physics Institute (MEPhI), Moscow, Russia
[98]D.V. Skobeltsyn Institute of Nuclear Physics, M.V. Lomonosov Moscow State University, Moscow, Russia
[99]Fakultät für Physik, Ludwig-Maximilians-Universität München, München, Germany
[100]Max-Planck-Institut für Physik (Werner-Heisenberg-Institut), München, Germany
[101]Nagasaki Institute of Applied Science, Nagasaki, Japan
[102]Graduate School of Science and Kobayashi-Maskawa Institute, Nagoya University, Nagoya, Japan
[103a]INFN Sezione di Napoli, Italy

[103b]*Dipartimento di Fisica, Università di Napoli, Napoli, Italy*
[104]*Department of Physics and Astronomy, University of New Mexico, Albuquerque, New Mexico, USA*
[105]*Institute for Mathematics, Astrophysics and Particle Physics, Radboud University Nijmegen/Nikhef, Nijmegen, Netherlands*
[106]*Nikhef National Institute for Subatomic Physics and University of Amsterdam, Amsterdam, Netherlands*
[107]*Department of Physics, Northern Illinois University, DeKalb, Illinois, USA*
[108]*Budker Institute of Nuclear Physics, SB RAS, Novosibirsk, Russia*
[109]*Department of Physics, New York University, New York, New York, USA*
[110]*Ohio State University, Columbus, Ohio, USA*
[111]*Faculty of Science, Okayama University, Okayama, Japan*
[112]*Homer L. Dodge Department of Physics and Astronomy, University of Oklahoma, Norman, Oklahoma, USA*
[113]*Department of Physics, Oklahoma State University, Stillwater OK, United States of America*
[114]*Palacký University, RCPTM, Olomouc, Czech Republic*
[115]*Center for High Energy Physics, University of Oregon, Eugene, Oregon, USA*
[116]*LAL, Université Paris-Sud and CNRS/IN2P3, Orsay, France*
[117]*Graduate School of Science, Osaka University, Osaka, Japan*
[118]*Department of Physics, University of Oslo, Oslo, Norway*
[119]*Department of Physics, Oxford University, Oxford, United Kingdom*
[120a]*INFN Sezione di Pavia, Italy*
[120b]*Dipartimento di Fisica, Università di Pavia, Pavia, Italy*
[121]*Department of Physics, University of Pennsylvania, Philadelphia, Pennsylvania, USA*
[122]*Petersburg Nuclear Physics Institute, Gatchina, Russia*
[123a]*INFN Sezione di Pisa, Italy*
[123b]*Dipartimento di Fisica E. Fermi, Università di Pisa, Pisa, Italy*
[124]*Department of Physics and Astronomy, University of Pittsburgh, Pittsburgh, Pennsylvania, USA*
[125a]*Laboratorio de Instrumentacao e Fisica Experimental de Particulas - (LIP), Lisboa, Portugal*
[125b]*Faculdade de Ciências, Universidade de Lisboa, Lisboa, Portugal*
[125c]*Department of Physics, University of Coimbra, Coimbra, Portugal*
[125d]*Centro de Física Nuclear da Universidade de Lisboa, Lisboa, Portugal*
[125e]*Departamento de Fisica, Universidade do Minho, Braga, Portugal*
[125f]*Departamento de Fisica Teorica y del Cosmos and CAFPE, Universidad de Granada, Granada, Spain*
[125g]*Departamento Fisica and CEFITEC of Faculdade de Ciencias e Tecnologia, Universidade Nova de Lisboa, Caparica, Portugal*
[126]*Institute of Physics, Academy of Sciences of the Czech Republic, Praha, Czech Republic*
[127]*Czech Technical University in Prague, Praha, Czech Republic*
[128]*Faculty of Mathematics and Physics, Charles University in Prague, Praha, Czech Republic*
[129]*State Research Center Institute for High Energy Physics, Protvino, Russia*
[130]*Particle Physics Department, Rutherford Appleton Laboratory, Didcot, United Kingdom*
[131]*Physics Department, University of Regina, Regina, Saskatchewan, Canada*
[132]*Ritsumeikan University, Kusatsu, Shiga, Japan*
[133a]*INFN Sezione di Roma, Italy*
[133b]*Dipartimento di Fisica, Sapienza Università di Roma, Roma, Italy*
[134a]*INFN Sezione di Roma Tor Vergata, Italy*
[134b]*Dipartimento di Fisica, Università di Roma Tor Vergata, Roma, Italy*
[135a]*INFN Sezione di Roma Tre, Italy*
[135b]*Dipartimento di Matematica e Fisica, Università Roma Tre, Roma, Italy*
[136a]*Faculté des Sciences Ain Chock, Réseau Universitaire de Physique des Hautes Energies - Université Hassan II, Casablanca, Morocco*
[136b]*Centre National de l'Energie des Sciences Techniques Nucleaires, Rabat, Morocco*
[136c]*Faculté des Sciences Semlalia, Université Cadi Ayyad, LPHEA-Marrakech, Morocco*
[136d]*Faculté des Sciences, Université Mohamed Premier and LPTPM, Oujda, Morocco*
[136e]*Faculté des sciences, Université Mohammed V-Agdal, Rabat, Morocco*
[137]*DSM/IRFU (Institut de Recherches sur les Lois Fondamentales de l'Univers), CEA Saclay (Commissariat à l'Energie Atomique et aux Energies Alternatives), Gif-sur-Yvette, France*
[138]*Santa Cruz Institute for Particle Physics, University of California Santa Cruz, Santa Cruz, California, USA*
[139]*Department of Physics, University of Washington, Seattle, Washington, USA*
[140]*Department of Physics and Astronomy, University of Sheffield, Sheffield, United Kingdom*
[141]*Department of Physics, Shinshu University, Nagano, Japan*

[142]*Fachbereich Physik, Universität Siegen, Siegen, Germany*
[143]*Department of Physics, Simon Fraser University, Burnaby, British Columbia, Canada*
[144]*SLAC National Accelerator Laboratory, Stanford, California, USA*
[145a]*Faculty of Mathematics, Physics & Informatics, Comenius University, Bratislava, Slovak Republic*
[145b]*Department of Subnuclear Physics, Institute of Experimental Physics of the Slovak Academy of Sciences, Kosice, Slovak Republic*
[146a]*Department of Physics, University of Cape Town, Cape Town, South Africa*
[146b]*Department of Physics, University of Johannesburg, Johannesburg, South Africa*
[146c]*School of Physics, University of the Witwatersrand, Johannesburg, South Africa*
[147a]*Department of Physics, Stockholm University, Sweden*
[147b]*The Oskar Klein Centre, Stockholm, Sweden*
[148]*Physics Department, Royal Institute of Technology, Stockholm, Sweden*
[149]*Departments of Physics & Astronomy and Chemistry, Stony Brook University, Stony Brook, New York, USA*
[150]*Department of Physics and Astronomy, University of Sussex, Brighton, United Kingdom*
[151]*School of Physics, University of Sydney, Sydney, Australia*
[152]*Institute of Physics, Academia Sinica, Taipei, Taiwan*
[153]*Department of Physics, Technion: Israel Institute of Technology, Haifa, Israel*
[154]*Raymond and Beverly Sackler School of Physics and Astronomy, Tel Aviv University, Tel Aviv, Israel*
[155]*Department of Physics, Aristotle University of Thessaloniki, Thessaloniki, Greece*
[156]*International Center for Elementary Particle Physics and Department of Physics, The University of Tokyo, Tokyo, Japan*
[157]*Graduate School of Science and Technology, Tokyo Metropolitan University, Tokyo, Japan*
[158]*Department of Physics, Tokyo Institute of Technology, Tokyo, Japan*
[159]*Department of Physics, University of Toronto, Toronto, Ontario, Canada*
[160a]*TRIUMF, Vancouver, British Columbia, Canada*
[160b]*Department of Physics and Astronomy, York University, Toronto, Ontario, Canada*
[161]*Faculty of Pure and Applied Sciences, University of Tsukuba, Tsukuba, Japan*
[162]*Department of Physics and Astronomy, Tufts University, Medford, Massachusetts, USA*
[163]*Centro de Investigaciones, Universidad Antonio Narino, Bogota, Colombia*
[164]*Department of Physics and Astronomy, University of California Irvine, Irvine, California, USA*
[165a]*INFN Gruppo Collegato di Udine, Sezione di Trieste, Udine, Italy*
[165b]*ICTP, Trieste, Italy*
[165c]*Dipartimento di Chimica, Fisica e Ambiente, Università di Udine, Udine, Italy*
[166]*Department of Physics, University of Illinois, Urbana, Illinois, USA*
[167]*Department of Physics and Astronomy, University of Uppsala, Uppsala, Sweden*
[168]*Instituto de Física Corpuscular (IFIC) and Departamento de Física Atómica, Molecular y Nuclear and Departamento de Ingeniería Electrónica and Instituto de Microelectrónica de Barcelona (IMB-CNM), University of Valencia and CSIC, Valencia, Spain*
[169]*Department of Physics, University of British Columbia, Vancouver, British Columbia, Canada*
[170]*Department of Physics and Astronomy, University of Victoria, Victoria, British Columbia, Canada*
[171]*Department of Physics, University of Warwick, Coventry, United Kingdom*
[172]*Waseda University, Tokyo, Japan*
[173]*Department of Particle Physics, The Weizmann Institute of Science, Rehovot, Israel*
[174]*Department of Physics, University of Wisconsin, Madison, Wisconsin, USA*
[175]*Fakultät für Physik und Astronomie, Julius-Maximilians-Universität, Würzburg, Germany*
[176]*Fachbereich C Physik, Bergische Universität Wuppertal, Wuppertal, Germany*
[177]*Department of Physics, Yale University, New Haven, Connecticut, USA*
[178]*Yerevan Physics Institute, Yerevan, Armenia*
[179]*Centre de Calcul de l'Institut National de Physique Nucléaire et de Physique des Particules (IN2P3), Villeurbanne, France*

[a]Deceased.
[b]Also at Department of Physics, King's College London, London, United Kingdom.
[c]Also at Institute of Physics, Azerbaijan Academy of Sciences, Baku, Azerbaijan.
[d]Also at Particle Physics Department, Rutherford Appleton Laboratory, Didcot, United Kingdom.
[e]Also at TRIUMF, Vancouver, British Columbia, Canada.
[f]Also at Department of Physics, California State University, Fresno, California, USA.
[g]Also at Tomsk State University, Tomsk, Russia.
[h]Also at CPPM, Aix-Marseille Université and CNRS/IN2P3, Marseille, France.

[i]Also at Università di Napoli Parthenope, Napoli, Italy.
[j]Also at Institute of Particle Physics (IPP), Canada.
[k]Also at Department of Physics, St. Petersburg State Polytechnical University, St. Petersburg, Russia.
[l]Also at Chinese University of Hong Kong, China.
[m]Also at Department of Financial and Management Engineering, University of the Aegean, Chios, Greece.
[n]Also at Louisiana Tech University, Ruston, Louisiana, USA.
[o]Also at Institucio Catalana de Recerca i Estudis Avancats, ICREA, Barcelona, Spain.
[p]Also at Department of Physics, The University of Texas at Austin, Austin, Texas, USA.
[q]Also at Institute of Theoretical Physics, Ilia State University, Tbilisi, Georgia.
[r]Also at CERN, Geneva, Switzerland.
[s]Also at Ochadai Academic Production, Ochanomizu University, Tokyo, Japan.
[t]Also at Manhattan College, New York, New York, USA.
[u]Also at Novosibirsk State University, Novosibirsk, Russia.
[v]Also at Institute of Physics, Academia Sinica, Taipei, Taiwan.
[w]Also at LAL, Université Paris-Sud and CNRS/IN2P3, Orsay, France.
[x]Also at Academia Sinica Grid Computing, Institute of Physics, Academia Sinica, Taipei, Taiwan.
[y]Also at Laboratoire de Physique Nucléaire et de Hautes Energies, UPMC and Université Paris-Diderot and CNRS/IN2P3, Paris, France.
[z]Also at School of Physical Sciences, National Institute of Science Education and Research, Bhubaneswar, India.
[aa]Also at Dipartimento di Fisica, Sapienza Università di Roma, Roma, Italy.
[bb]Also at Moscow Institute of Physics and Technology State University, Dolgoprudny, Russia.
[cc]Also at Section de Physique, Université de Genève, Geneva, Switzerland.
[dd]Also at International School for Advanced Studies (SISSA), Trieste, Italy.
[ee]Also at Department of Physics and Astronomy, University of South Carolina, Columbia, South Carolina, USA.
[ff]Also at School of Physics and Engineering, Sun Yat-sen University, Guangzhou, China.
[gg]Also at Faculty of Physics, M.V. Lomonosov Moscow State University, Moscow, Russia.
[hh]Also at Moscow Engineering and Physics Institute (MEPhI), Moscow, Russia.
[ii]Also at Institute for Particle and Nuclear Physics, Wigner Research Centre for Physics, Budapest, Hungary.
[jj]Also at Department of Physics, Oxford University, Oxford, United Kingdom.
[kk]Also at Department of Physics, Nanjing University, Jiangsu, China.
[ll]Also at Institut für Experimentalphysik, Universität Hamburg, Hamburg, Germany.
[mm]Also at Department of Physics, The University of Michigan, Ann Arbor, Michigan, USA.
[nn]Also at Discipline of Physics, University of KwaZulu-Natal, Durban, South Africa.
[oo]Also at University of Malaya, Department of Physics, Kuala Lumpur, Malaysia.